International

WOCE

Newsletter

Number 32 ISSN 1029-1725 September 1998

IN THIS ISSUE

Published by the WOCE International Project Office at Southampton Oceanography Centre, UK

Personal Impressions of the WOCE Conference – Laying the Foundation for Major Applications

Hartmut Grassl, Director of World Climate Research Programme, WMO.
grassl_h@gateway.wmo.ch

Attending the WOCE International Conference on Oceanography and Climate in Halifax, Nova Scotia, Canada, 25–29 May 1998, was fun: it highlighted the probability that WOCE will achieve its goals and, I feel, opened the door to major, but still remote, goals of the World Climate Research Programme (WCRP). The Conference also reminded me of the intrinsic time-scale of global change research projects: roughly a decade of proper planning (decision for WOCE was taken in 1979), nearly another decade of field work (1990 to 1998) and at least 5 years for evaluation and synthesis (until 2002 and beyond). Thus, the initiators of a project are often not the principal investigators and some beneficiaries were still only school children during WOCE's planning phase. For the success of projects with such long time-scales, one must have far-sighted planners, but also flexible executors and governing bodies.

Why can we already speak of the major success of WOCE, only months after the formal end of the field phase? Because WOCE has already made new discoveries through observations of deep ocean structure, because major technological advances were stimulated by WOCE (e.g., satellite sensors for precise ocean topography, automatic profilers and drifters) and because computing capacity has increased by two orders of magnitude since the inception of WOCE.

As an atmospheric physicist with a remote sensing background (and contacts to oceanographic research since 1965) the Conference showed me that:

- the ocean responds strongly to continuous atmospheric forcing on interannual and decadal time-scales, i.e., shows a remarkable degree of variability;
- the Atlantic Ocean really transports heat from the southern to the northern hemisphere;
- mixing in the interior ocean is a strong function of bottom topography;
- new estimates of the magnitude of the net freshwater balance of major ocean basins are smaller than earlier ones, making the global thermohaline circulation an even more delicate feature of our planet;
- the WOCE field phase years were characterised by rather abnormal conditions with respect to atmospheric forcing;
- transports in some deep ocean basins are still largely unknown;
- tracer concentration measurements add information mainly about time-scales of oceanic transport;
- the conveyor belt as a simplified but acceptable sketch of global ocean circulation has survived despite evidence of growing complexity;
- ocean models with high spatial resolution are realistic enough to be used to test coarse resolution models;
- assimilation of ocean data into global models to get a consistent ocean structure in the 1990s is in its infancy;
- data management and dissemination has reached a unique level for oceanography;
- the oceanographic science community accepts the important stimulating effect of climate research for its own discipline;
- remote sensing from space gives global data sets for many ocean surface parameters including energy fluxes with unprecedented spatial and temporal resolution and rapidly improving accuracy;
- WOCE sections have helped the Joint Global Ocean Flux Study of IGBP to get enough data to estimate carbon uptake rate for certain basins.

The successes of TOGA and WOCE have shown that we really need a real-time ocean observing system for a multitude of new applications:

- Climate variability predictions (for seasonal to inter-annual time-scales)
- Ocean weather forecasting (for days to weeks)
- Climate change detection (consistent global ocean structure)
- Climate change projections (consistent global ocean structure)
- Coastal zone modelling and management (correct boundary conditions).

Thus, most of the research observation systems built up by the scientific community should become part of GCOS or GOOS, as recently happened for the USA contribution to the TOGA-TAO array. Maybe a mix of operational and research observation networks is the best way to guarantee the proper use of all information.

I congratulate the WOCE community on its achievements and I hope that the legacy of WOCE will stimulate CLIVAR to become as focused as WOCE in achieving the goals set out in its initial implementation plan.

The WOCE Data Resource: Providing Access to Data and Products

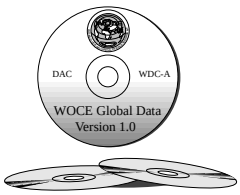

Eric J. Lindstrom, NASA, USA; and N. Penny Holliday, SOC, UK.
penny.holliday@soc.soton.ac.uk

A priority area for work by the WOCE data facilities and WOCE Data Products Committee is to provide better and more comprehensive access to WOCE data of all kinds. One concept that is assisting in this direction is that of a WOCE "Data Resource". The idea is that the seeker of WOCE data should begin to see the highly distributed WOCE data system more as a single entity (despite the fact that the data assembly, quality control, distribution and documentation functions will remain highly distributed). The distributed system continues to allow the value-adding processes of quality control, collation of metadata and establishment of common data formats for each data type. However the Data Resource is rubric for more natural arrangement of the WOCE data for the analysis, modelling, data assimilation and interpretation. The development of a "virtual" WOCE Data Resource that logically combines access to all of the WOCE data streams (including metadata, modelling results and data products) may better satisfy a range of generic user needs during the WOCE AIMS phase.

The Data Resource concept

The aim of the Data Resource is to provide researchers with an interface through which a wide range of WOCE data and data products may be accessed without concern for the complex internal structure and distributed nature of the WOCE data infrastructure. The WOCE Data Resource idea, if successfully implemented by the facilities participating in WOCE, will allow integrated data products to be developed more easily and transparently from available data.

A rich variety of data and products

A unique aspect of WOCE is the richness of data types and variety of products being generated. The WOCE hydrographic data are the core measurements of the observational programme, and include CTD and discrete bottle data from one-time and repeated sections and time series stations. Almost all WOCE Hydrographic Programme (WHP) data sets include discrete salinity sampling, and those from the one-time survey also include oxygen, nutrients, and a range of other tracers including chlorofluorocarbons, tritium, helium-3, carbon-14 and several CO_2 parameters. The WHP Special Analysis Centre has generated standard vertical sections and property plots from many data sets, and are carrying out comprehensive studies of cruise data intercomparison as part of their quality control procedures. Printed and online atlases of WHP data are presently being planned and generated.

WOCE Lagrangian observations include those from surface drifters (typically drogued at 15 m) and subsurface neutrally buoyant floats. The basic drifter data set contains position, time and temperature, and sometimes additional parameters such as salinity and atmospheric pressure. The Drifter Data Assembly Centre (DAC) generates a krigged file (interpolated to 6-hour intervals) from the raw data. The subsurface float data set includes positions, times and float pressure, and there are an increasing number of associated temperature and salinity data from the profiling floats. Many floats have nominal depths of around 1000 m, but some have been deployed much deeper (up to 4000 m) and some at 200 m.

WOCE Data Information Unit

"... information, tracking data, gateway to the WOCE Data Resource... "
http://diu.cms.udel.edu/woce/oceanic.html

WOCE Data Assembly Centres

"... assembly, quality control, data products..."

WOCE Special Analysis Centres

"... analysis, synthesis, derived data sets..."

Moored current meter arrays have been deployed for WOCE in narrow passages and strong currents. The data set consists of velocity, time and position for each current meter, and may also include temperature, salinity and pressure. The Current Meter DAC has generated mean flow statistics for each array, and has acquired and quality controlled a large set of relevant historical data. Further direct current measurements are made by acoustic Doppler current profilers (ADCPs) operated as hull-mounted instruments sampling the upper 300 m and as lowered ADCPs sampling the full water column at stations. The ADCP DAC at present assembles the shipboard data and can provide the full resolution data set and an averaged set with hourly time spans and 10 m depth intervals.

WOCE in-situ sea level data are received from a global network of tide gauges and the data are treated in two different modes. The fast delivery DAC obtains data in real-time from over 100 stations globally, and provides hourly, daily and monthly data sets within a month of collection. The delayed mode centre assembles and quality controls data from 160 stations, and provides original resolution and hourly data, station metadata, summary

statistics, plots of low frequency variations, and analysis of tidal constants.

During the WOCE observation period research vessels and moored buoys collected marine meteorology data including surface winds, air and sea temperature, humidity, atmospheric pressure, precipitation and other variables. The Surface Meteorology DAC assembles, extensively quality controls and documents these data. Air-sea flux values for momentum, turbulent heat, and moisture can be estimated from the data using bulk formulae. The Air-Sea Fluxes SAC is one of a number of groups that produce near-global fields of atmospheric variables and fluxes as well as uncertainties.

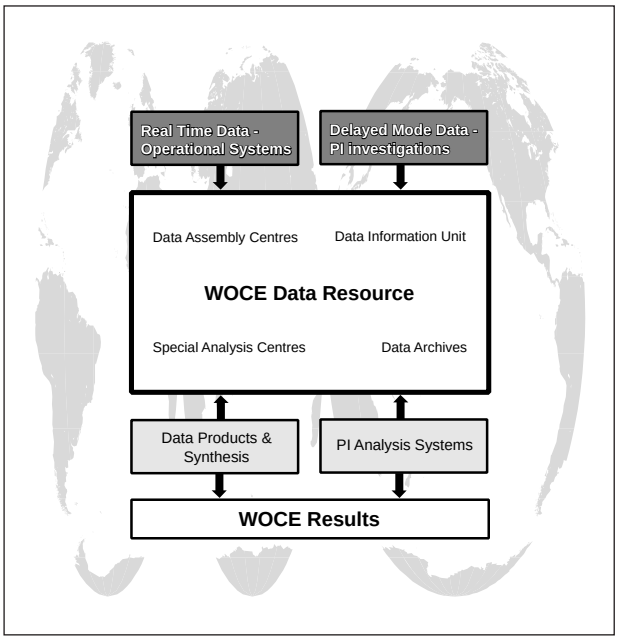

Upper ocean thermal data are collected mainly from XBTs deployed by voluntary observing ships in two modes; broadscale with relatively low along-track resolution, and a limited number of sections with high along track resolution. The temperature profiles are sent to data centres in real-time (with relatively low vertical resolution) and most are eventually replaced by their high vertical resolution equivalents in delayed mode. The quality control of the data occurs in two stages; the data centres perform initial checks and three science centres perform a more rigorous scientific quality control. The profiles are managed in a database which ensures users have access to the highest vertical resolution and most rigorously tested profiles available. Products such as gridded temperature fields at several depths have been generated for some ocean basins.

Satellite altimetry data have been collected from the ERS-1, ERS-2 and TOPEX/POSEIDON platforms, providing unprecedented observations of sea level variability and wave height. Also of interest to WOCE are measurements of wind speed from scatterometers, sea-surface temperature from radiometers, and water vapour content. The satellite agencies distribute data and a variety of gridded fields and other products from their online data centres.

The WOCE Data Information Unit (DIU) is a comprehensive guide to the WOCE programme and is the gateway to the online WOCE Data Resource. Links to WOCE data and products, information about data status, and details of all the field activities can be found at the DIU. The centre supports a bibliography of WOCE publications and links to online abstracts relating to WOCE.

Implementing the WOCE Data Resource

The WOCE Data Resource is being built upon the already existing data streams. All DACs have established interfaces that allow the selection and search of their own individual data streams. These data streams will be linked in a more systematic way to create one cross-linked searchable data set. This is being accomplished in several stages, the initial phase of which has already been achieved. The World Wide Web has enabled the creation of an embryonic virtual data resource through which the DACs offer access to data and products. The Data Products Committee in conjunction with US-NODC produced a set of CD-ROMs for the WOCE Conference in May 1998, containing the WOCE Global Data, products and metadata.

The second phase of implementation of the WOCE Data Resource will be the integration of the data sets, documentation and products from the individual data streams into a single logical virtual site that can be accessed and searched by individual investigators. This will be achieved through the combined efforts of the DACs and the US-NODC which is providing the final archive of WOCE data. The final phase of the project is incorporation of final "complete" data streams into the WOCE Data Resource thereby becoming the legacy of the WOCE field programme.

WOCE Global Data on CD-ROMs

A major step towards the WOCE Data Resource has been the recent production of version 1.0 of the WOCE Global Data on CD-ROMs. These platform-independent CD-ROMs can be read with free software (Web browsers) and contain all available data, metadata and products at the DACs in February 1998. However the CD-ROMs do not represent the complete WOCE Data Resource since it is continually expanding as more data become available through completion of quality control or public release by investigators. Data products are evolving as scientific issues are addressed and as synthesis proceeds, and many initial products could become redundant as new data are added and new ideas for forming products are developed. So further issues of the WOCE Global Data on CD-ROM (or appropriate media of the time) are envisaged. Version 2 will represent the second phase of the implementation of the WOCE Data Resource by allowing the user to search and access data through a single interface, and version 3 will contain the "complete" WOCE data set (the WOCE legacy).

Offsets of the IAPSO Standard Seawater Through the Batch P129 and its Application to Pacific WHP Crossovers

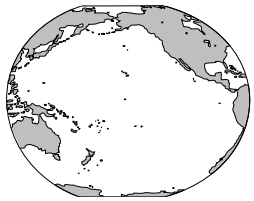

Michio Aoyama, Meteorological Research Institute, Japan; Terrence M. Joyce, Woods Hole Oceanographic Institution, USA; Takeshi Kawano, Japan Marine Science and Technology Center, Japan; Yasushi Takatsuki, Japan Meteorological Agency, Japan.
maoyama@mri-jma.go.jp

Offsets of IAPSO Standard Seawater (SSW) batches P103 to P129 referenced to reproducible KCl standard solution are examined. Several comparison experiments were carried out during the period from 1991 to 1997. Since the reference SSW batch varies from experiment to experiment, a method needs to be defined by which one can combine recent results with the previously presented offsets up to P112 (Mantyla, 1980, 1987, 1994; Takatsuki et al., 1991). Mantyla (1987) used the mean of offsets from P91 through P102 as the absolute reference to establish SSW batch to batch offsets. Takatsuki et al. (1991) also adjusted their offsets with the mean of SSW batches P91–P102. We use the previously determined offsets of P94 and P110 as the keys for relating to the recent comparisons. Therefore offsets for SSW batches P103–P129 proposed by this study could be relative to the mean of SSW batches P91–P102. Then offsets of SSW from P29 through P129 became available relative to the same reference, the mean of SSW batches P91–P102, after Mantyla (1987). The KCl labelled batches generally follow well within PSS with reproducible KCl standard solution. Batch to batch differences, however, should be corrected when adjusting the salinity within 0.002 PSS in accuracy for the existing salinity data sets. For example, the SSW batch numbers varied from P96 to P124 for salinity measurements of the Pacific WHP observations. The salinity differences at 42 Pacific WHP crossovers are reduced by 0.5×10^{-3} PSS after applying these offsets. We present offsets of P103 through P129 excluding P113, P115, P117, P125 and P126 together with previously published offsets for P29–P102, so that one may make adjustments to most of the historical hydrographic data sets in the world.

Comparison experiments

We have 11 comparison experiments for the period from 1991 through 1997. Six of the 11 experiments were comparisons of two target batches while five comparisons, two at Japan Meteorological Agency (JMA), two at Woods Hole Oceanographic Institution (WHOI) and the latest one at the Japan Marine Science and Technology Center (JAMSTEC), include several target batches which varied from relatively old ones, such as P94, P110, to the present batches (detail in Aoyama et al., sub.) Since we could not get ampoules or comparison results for P113, P115, P117, P125 and P126, the offsets for these batches are not presented in this article. Culkin and Ridout (sub.) also carried out the comparison of recent 10 batches (P120–P129) against the defined KCl standard, however, they show the results in the unit of 0.00001 in K15 (equivalent to ca. 0.4×10^{-3} PSS). A systematic bias seems to be exist between the offsets

Table 1. Offsets from P91 through P129.

Batch	Prep. Date	K15	Salinity x 103 PSS	Offset
P91	10 May 1980	1.00007	35.0027	-1.0*
P92	29 Oct. 1981	0.99988	34.9953	-1.5*
P93	31 Oct. 1981	0.99990	34.9961	-0.4*
P94	18 Nov. 1981	0.99992	34.9969	-0.2*
P95	8 Mar. 1983	0.99997	34.9988	0.9*
P96	3 Mar. 1983	1.00006	35.0023	1.2*
P97	3 Mar. 1983	1.00002	35.0008	0.8*
P98	3 Mar. 1983	0.99993	34.9973	0.8*
P99	27 July 1984	0.99997	34.9988	-0.4*
P100	29 Nov. 1984	1.00003	35.0012	-0.3*
P101	4 June 1985	1.00002	35.0008	0.5*
P102	29 Nov. 1984	1.00001	35.0004	0.2*
P103	11 Oct. 1985	0.99987	34.9949	-0.3
P104	21 Feb. 1986	0.99994	34.9976	-0.2
P105	21 Feb. 1986	0.99988	34.9953	0.8
P106	8 June 1987	0.99989	34.9957	-0.8
P107	11 Nov. 1987	0.99991	34.9965	-0.2
P108	7 Apr. 1988	0.99980	34.9921	0.4
P109	7 Apr. 1988	0.99976	34.9905	0.9
P110	20 July 1988	0.99999	34.9996	0.6
P111	7 Feb. 1989	0.99982	34.9929	0.8
P112	4 July 1989	0.99984	34.9937	0.6
P113	not available now			
P114	30 July 1990	0.99986	34.9945	0.7
P115	not available now			
P116	10 July 1991	0.99981	34.9925	0.1
P117	not available now			
P118	12 Nov. 1991	0.99994	34.9976	-0.2
P119	28 Feb. 1992	0.99990	34.9961	-1.3
P120	6 Apr. 1992	0.99985	34.9941	-2.2
P121	8 Sep. 1992	0.99985	34.9941	-0.9
P122	21 Jan. 1993	0.99991	34.9965	-0.9
P123	10 June 1993	0.99994	34.9977	-0.6
P124	18 Jan. 1994	0.99990	34.9961	-0.7
P125	not available now			
P126	not available now			
P127	14 Feb. 1995	0.99990	34.9961	-0.5
P128	18 July 1995	0.99986	34.9945	0.1
P129	22 Nov. 1995	0.99996	34.9980	-0.9

*Offset for P91 through P102 from Mantyla (1987).

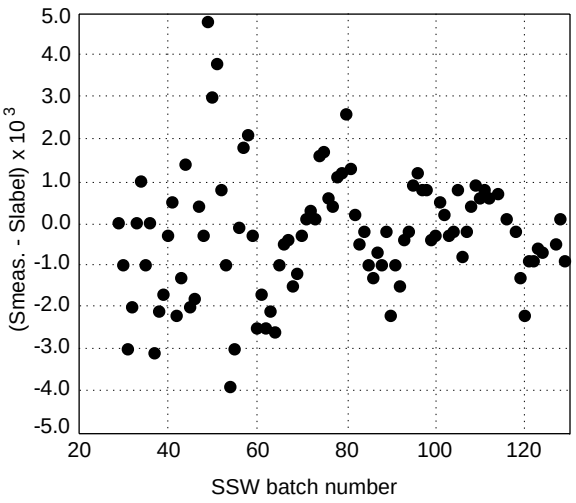

Figure 1. Batch to batch differences for P29 through P129 except P113, P115, P117, P125 and P126.

proposed by our study and offsets by Culkin and Ridout (sub.). This means that our proposed offsets may have some bias against the difference defined KCl standard, however, the traceability between the previously published offsets and the offsets of recent SSW batches is much important in practical purpose. We do not discuss this bias in this article.

Batch to batch differences for P29–P129

Table 1 summarises the proposed offsets as well as the batch number, preparation date, label K15, label-derived salinity and adjusted offsets together with the previously presented offsets (Mantyla, 1987). Label derived salinity for P91 through P129 was calculated from the labelled K15 conductivity ratios using the PSS78 equations (UNESCO, 1981). The adjusted offsets of 11 experiments are, with some exceptions, in excellent agreement considering the modern measurement precision (0.2×10^{-3} PSS) and within-batch differences ($0.1-0.3\times10^{-3}$ PSS) between P103 and P129. Since relatively large within-batch differences of $0.6-0.9\times10^{-3}$ (1σ) PSS for P114 are observed (Nakano, pers. comm.; Aoyama et al., sub.; Kawano, sub.), this might cause the larger difference among the offsets obtained from five comparison experiments. Although we do not know the obvious reason for relatively larger offsets for P119 and P120, larger than PSS, relatively larger within-batch differences might be one of the reasons. Another possibility for relatively larger offsets for a batch might be attributed to measurement precision. The offsets for the KCl labelled batches (P91 through P129 except P113, P115, P117, P125 and P126), range from -2.2×10^{-3} (P120) to 1.2×10^{-3} (P96) PSS with an average of -0.1×10^{-3} PSS. The disagreement between the KCl labelled batches (P91 through P129 except P113, P115, P117, P125 and P126) is still greater (1σ of 0.8×10^{-3}) than the modern measurement precision of 0.2×10^{-3} PSS. Inaccuracy of the proposed offsets basically depends on the within-batch differences and measurement precision of each experiment. Inaccuracy of proposed offsets are $0.1-0.3\times10^{-3}$ PSS for most of the batches, while those might be up to $0.5-0.9\times10^{-3}$ PSS for P104, P114, P116, P119, P120 and P127. Offsets for P29 through P129 except P113, P115, P117, P125 and P126 are shown in Fig. 1 and ranged from 4.8×10^{-3} (P49) to -3.9×10^{-3} (P54) with an average of -0.3×10^{-3}. The disagreement for P29 through P129 is 1.5×10^{-3} (1σ). It is clear that the offsets tend to decrease gradually with time (batch number) from ca. 5.0×10^{-3} to 2.0×10^{-3} during these 40 years. However, the greatest discrepancy between batches of SSW is 8.7×10^{-3} between P49 and P54 among P29 through P129. This means that the uncorrected salinity may have the inaccuracy of ca. 5.0×10^{-3} in maximum relative to KCl

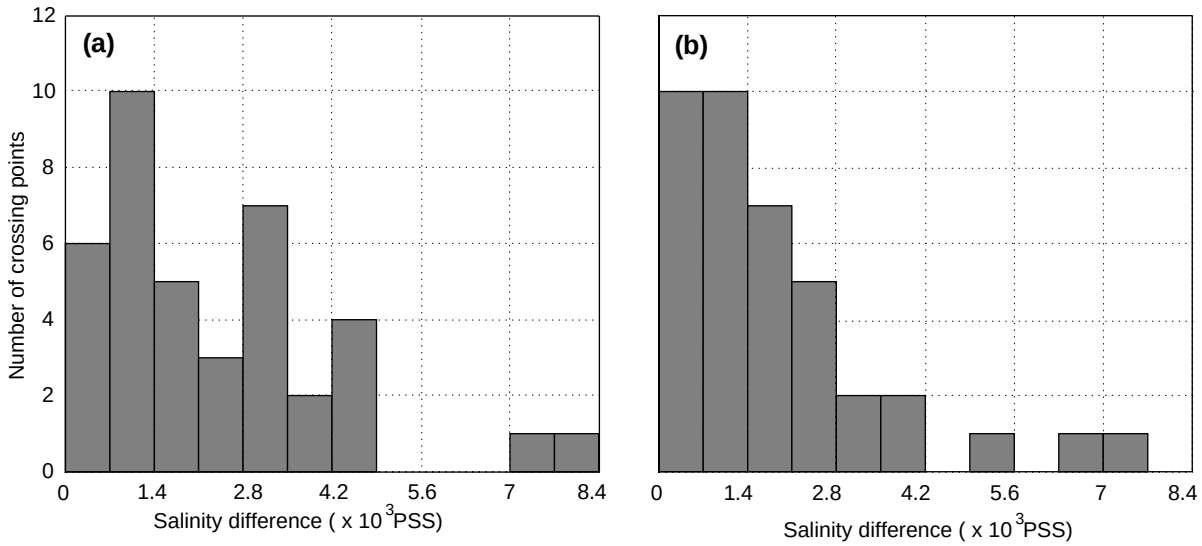

Figure 2.(a) Absolute salinity differences at 39 crossover points in the Pacific Ocean without SSW offsets correction. (b) Same as (a), but with SSW offsets correction.

solution and may also have relative error of ca. 9×10^{-3} between the perceived salinity standardised with different SSW batches among P29 through P129 except P113, P115, P117, P125 and P126.

Application of the SSW offsets to WHP crossover points

The salinity differences at the WHP crossover points at the Pacific are examined and the proposed SSW offsets shown in Table 1 are applied to them. Water sample salinity are interpolated on the θ surfaces ranging from 1.0°C to 1.6°C with the interval of 0.05°C. The salinity comparison are done at the crossing among the one-time survey lines. When the distance between the stations from each line is close enough, within several nautical miles, the comparison was directly carried out for these overlaying stations. Otherwise when the overlaying stations are not available, comparisons were made using 2 or 3 stations along each line closest to the intersection. The absolute value of the salinity differences at 39 crossover points, crossovers among P1, P1W, P2, P3, P4, P6C, P8S, P9, P10, P13, P13JC, P14N, P15N, P16NC, P17NCSE, P19C, P24 and S4P cruises, ranged from 0.0×10^{-3} PSS to 7.8×10^{-3} PSS with an average of 2.38×10^{-3} PSS. Then the adjusted salinity differences generally became smaller than before, 28 cases among the 39 crossover points, and ranged from 0.1×10^{-3} PSS to 7.2×10^{-3} PSS with an average of 1.84×10^{-3} PSS. The histograms with SSW offsets correction and without correction are shown in Fig. 2a and 2b. Less scattered histogram, Fig. 2b, clearly shows that SSW offsets correction reduce the salinity differences in general and make the distribution of the inter-cruise salinity differences much statistically reasonable. In the Atlantic Ocean, the salinity differences at 32 cases among 52 crossover points were also reduced from 2.29×10^{-3} PSS to 1.86×10^{-3} PSS (Gouretski and Jancke, 1998). Taking account of the offsets of SSW batches allows to reduce relative salinity differences by $0.4-0.5\times10^{-3}$ PSS in both Pacific and Atlantic Oceans.

Conclusions

Table of offsets of IAPSO SSW are presented from P103 through P129 from several comparison experiments together with the previously presented offset of P29 through P102. Offsets for the KCl labelled batches (P91 through P129 except P113, P115, P117, P125 and P126) ranged from -2.2×10^{-3} (P120) to 1.2×10^{-3} PSS (P96) with an average of -0.1×10^{-3} PSS. Offsets for P29 through P129 except P113, P115, P117, P125 and P126 ranged from 4.8×10^{-3} (P49) to -3.9×10^{-3} (P54) with an average of -0.3×10^{-3}. Thus, the KCl labelled batches generally follow well within 1.0×10^{-3} PSS with the reproducible KCl standard solution. This implies that batch to batch differences should be corrected when adjusting the salinity within 0.002 PSS in accuracy for the existing salinity data sets. Taking account the offsets of SSW batches allows to reduce relative salinity differences by $0.4-0.5\times10^{-3}$ PSS at the WOCE one-time cruises crossover points in both Pacific and Atlantic Oceans.

References

Aoyama, M., T. M. Joyce, T. Kawano, and Y. Takatsuki. Offsets of the IAPSO Standard Seawater for P103 through P129. Deep-Sea Res., sub.

Culkin, F., and P. S. Ridout: Stability of IAPSO Standard Seawater. J. Atmos. and Oceanic Tech., sub.

Gouretski, V., and K. Jancke, 1998: Deep water property comparison for WOCE cruises in the Atlantic Ocean. WHP Special Analysis Centre, Hamburg, 17pp.

Kawano, T.: Comparison of some recent batches of IAPSO Standard Seawater. Deep-Sea Res., sub.

Mantyla, A. W., 1980: Electric conductivity comparisons of Standard Seawater batches P29 to P84. Deep-Sea Res., 27A, 837–846.

Mantyla, A. W., 1987: Standard Seawater comparison updated. Phys. Oceanogr., 17, 543–548.

Mantyla, A. W., 1994: The treatment of inconsistencies in Atlantic deep water salinity data. Deep-Sea Res., 41, 1387–1405.

Takatsuki, Y., M. Aoyama, T. Nakano, H. Miyagi, T. Ishihara, and T. Tsutsumida, 1991: Standard seawater comparison of some recent batches. J. Atmos. and Oceanic Tech., 8, 895–897

UNESCO, 1981: Tenth report of the Joint Panel on Oceanographic Tables and Standards. UNESCO Tech. Paper in Mar. Sci., 36, 25pp.

Deep Water Property Comparison for the Atlantic WOCE Cruises

Victor Gouretski and Kai Jancke, WHP Special Analysis Centre, Germany.
gouretski@bsh.d400.de

Assessment of the magnitude and time-spatial scales of inter-annual variability in the ocean is an important issue of physical oceanography. However, accurate measuring of the characteristics in the deep ocean has proved to be a difficult task, and it was not until WOCE that the first consistent high quality global hydrographic data has become a reality. Such a data set is expected to be able to answer the question of how variable the deep ocean is on a decadal time scale.

A direct assessment of the variability in the ocean can be made by comparing the data from different cruises in the same geographical area. However changes revealed by the measurements are not only due to natural variability, but also due to random and systematic errors in the data. Whereas random measurement errors are relatively easy to handle and their net effect is reduced when a large number of samples is taken, the problem of systematic errors in the data still remains.

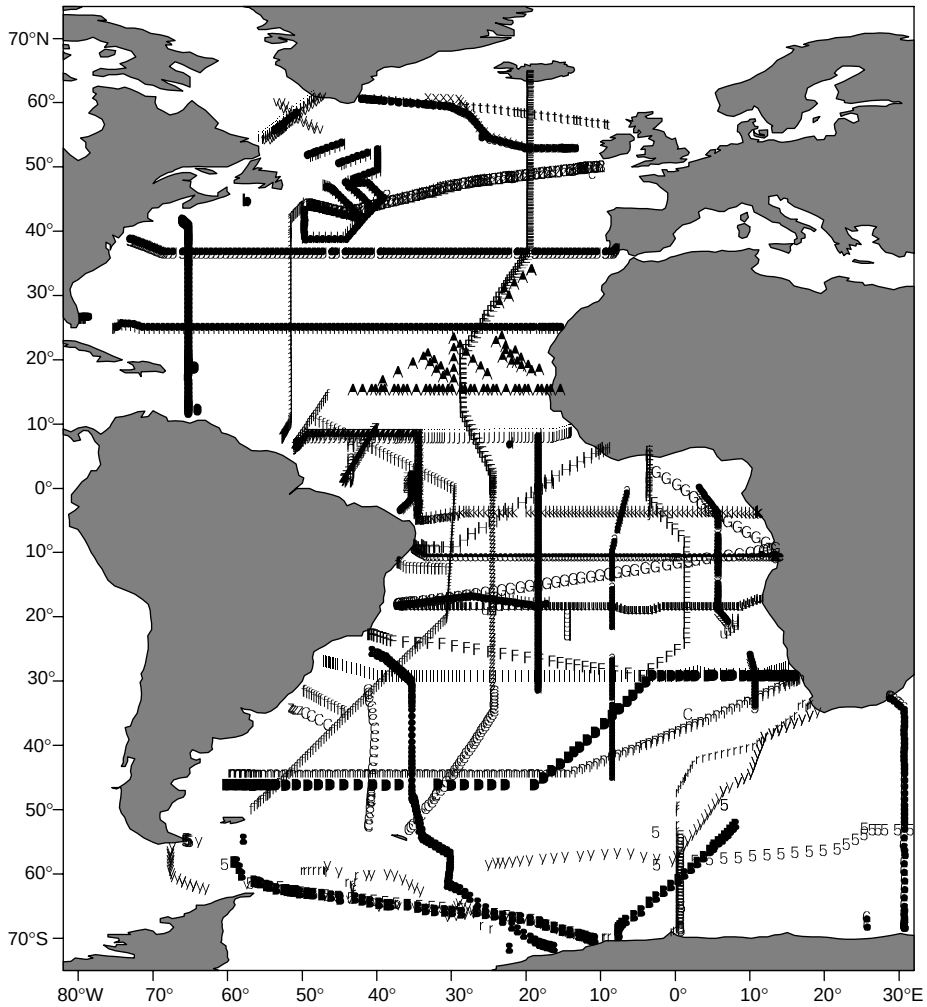

EXPOCODE		DATE
0	A22_316N151/4	9708-9709
1	A20_316N151/3	9707-9708
2	A2_MT039/3	9706-9706
3	AR19_GA276/1	9605-9606
4	ETAMBOT2/2AR15	9604-9605
5	SR4_ANT13/4	9603-9605
6	I6	9602-9603
7	LETAMBOT1/2AR04	9509-9510
8	A23_JC10/1	9503-9505
9	A13_CITHER_3	9503-9503
a	A14_CITHER_3	9501-9502
b	AR13_HU94030	9410-9411
c	A2_MT030/2	9410-9411
d	AR15_316N142/3	9404-9405
e	A8_MT28/1	9404-9405
f	A17_CITHER_2	9401-9403
g	A3_9310	9309-9310
h	AR19_GA226/2	9307-9307
i	AR7W_HU93019-1	9306-9306
j	A6_A3CITHER	9302-9303
k	A7_A3CITHER	9301-9302
l	A10_MT22/5	9212-9301
m	A11_9212-9301	9212-9301
n	AR4E/AR4W/AR15	9210-9211
o	AR7E_AZ129-1	9209-9209
p	A5_HE06/1	9207-9208
q	AR7_HU92014-1	9205-9206
r	SR2/SR4_ANTX/4	9205-9207
s	A1E_MT18/1	9109-9109
t	AR7E_TR91-1	9104-9104
u	A9_MT15/3	9102-9103
v	SR4_ANT9	9011-9012
w	AR7W_DA90120012	9007-9007
x	AR7E_TR90-3	9007-9007
y	A21/S4/SR2_MT11	9001-9003
z	A16C_8903-8904	8903-8904
A	METEOR_9	8901-8904
B	SR4/SR2/A12ANT8	8901-8930
C	SAVE5_8901-8903	8901-8903
D	SAVE4_8812-8901	8812-8901
E	A16N_8807-8808	8807-8808
F	SAVE3_8801-8803	8801-8803
G	SAVE2_8712-8801	8712-8801
H	SAVE1_8711-8712	8711-8712

Figure 1. WOCE Atlantic data set (including Meteor-9 and SAVE cruises).

Systematic offsets between the cruises have been addressed in the literature. For example, Gordon and Molinelli (1982) discuss systematic differences in the nutrient data for the Southern Ocean. Wyrtki (1971) presented a table of cruises discarded due to unacceptably large offsets, and Mantyla (1994) made a detailed study of salinity offsets between a number of pre-WOCE cruises in the Atlantic Ocean. Gouretski and Jancke (1996) determined parameter offsets for the cruises in the South Pacific and Aoyama and Joyce (1996) presented a study of deep water property offsets between the WOCE Pacific cruises at the cross-over points.

Differences in techniques and methods between laboratories analysing water samples on different cruises inevitably result in systematic offsets. One cause for systematic offsets for oxygen, silicate, phosphate and nitrates is the absence of a standard similar to the IAPSO Standard Sea Water (SSW). However, as pointed out by Mantyla (1994) the calibration using SSW does not protect against inter-cruise salinity differences because of salinometer response shift, sensor hysteresis problems and offsets between SSW batches.

Data

In this study we analyse deep-water parameter offsets for the WOCE Atlantic cruises (Fig. 1). Most of the WOCE data were obtained from the WHP Office, but some are courtesy of principal investigators (see acknowledgements). The only non-WOCE data is that obtained during the South Atlantic Ventilation Experiment (SAVE) and during the RV Meteor cruise 9. Both SAVE and Meteor-9 were occupied immediately before the start of WOCE and covered a considerable part of the tropical and south Atlantic. The quality of the SAVE and Meteor-9 data seems to meet WOCE standards. Only bottle data were taken for the analysis, and offsets were determined for salinity, oxygen, silicate, nitrate and phosphate. The data set spans a ten year period from November 1987 (SAVE1) to September 1997 (A22).

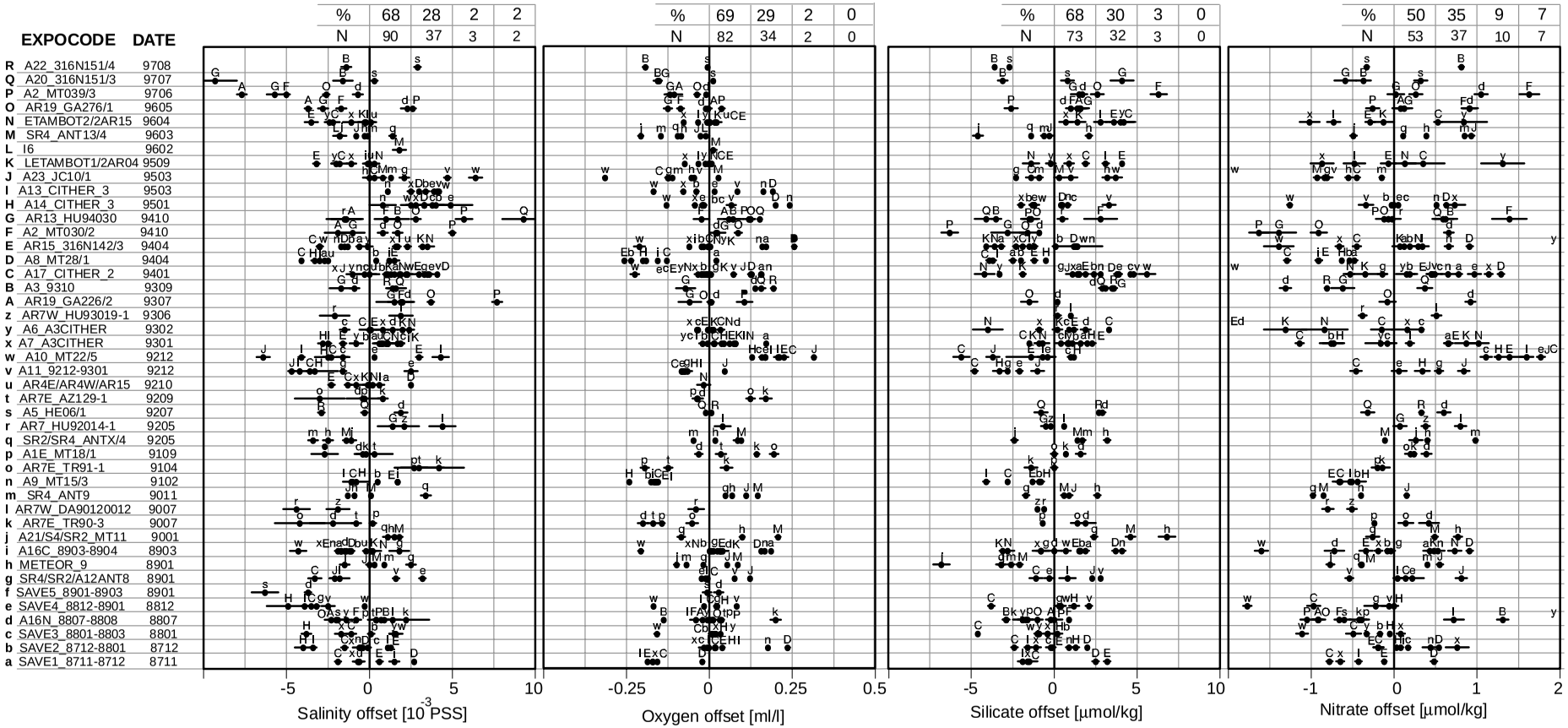

Figure 2. Inter-cruise offsets for salinity,oxygen, silicate and nitrate. For each horizontal line large dots give offsets relative to the cruise designated by a letter in the leftmost column. For instance, SAVE4 (e) has systematically lower salinities (negative offset) relative to A10 (w), A11(v), SAVE5 (g), A17 (C), A13 (I) and A14 (H). Figures above each plots show % and number of offsets laying within ±1, 2, 3 or 4 graph divisions.

Method of the offset determination

Table 1. *Summary of the inter-cruise parameter offsets*

	Parameter				
	Salinity	Oxygen	Silicate	Nitrate	Phosphate
Number of pairs	135	126	111	112	103
Min	0.0000	0.100	0.10	0.02	0.000
Max	0.0064	0.315	5.60	2.17	0.179
Aver	0.0019	0.087	1.89	0.57	0.049
Stand_dev	0.0014	0.079	1.29	0.45	0.043
Accuracy (~reproducibility)	0.0020	~0.070	~2.50	~0.50	~0.060

Cruise tracks shown in Fig. 1 yield a total of 135 cross-over, junction or overlapping areas, so that an automated procedure for the offset determination was required and developed. Our method of determining inter-cruise offsets is based on the experimental fact of the uniformity of potential temperature-parameter relationships in the deepest levels, and thus follows the idea of Saunders (1986) to use deep water pools as natural validation baths. Data from different cruises are compared in parameter-temperature space under the assumption that both random and systematic errors in temperature are negligible. To exclude possible effects of seasonal variability and to restrict the analysis to the range of narrow temperature-parameter envelopes, samples with depth less than 1000 metres and potential temperatures greater than 3°C were never included. In general deeper and cooler limits were employed. The maximum station separation for cross-over analysis was 250 km.

A net of cruise tracks (Fig. 1) with most of the cruises having intersections with several other cruises allows an estimate of systematic errors. Each measurement of the parameter *F* at potential temperature θ may be decomposed into the sum of the true value F_o, systematic error (bias) δ and random error ε:

$$F(\theta) = F_o(\theta) + \delta + \varepsilon(\theta), \qquad (1)$$

where the bias δ is assumed to be constant within each cruise. A *direct* estimate of the offset between two cruises *i* and *j* is:

$$\Delta F_{ij} = D_{ij} + \{< \varepsilon_i(\theta) - \varepsilon_j(\theta) - \gamma_{ij}(\theta) >\} = D_{ij} + \alpha_{ij} \qquad (2)$$

where $D_{ij} = \delta_i - \delta_j$, $< >$ and $\{ \}$ denote average over $\theta < \theta_{max}$ and over distinct station pairs respectively. The term γ_{ij} is the difference between true parameter values for cruise *i* and *j* caused by time and space variability of F_o within the cross-over area. If both cruises have intersections with another cruise *n*, an indirect estimate Δf_{ijn} of the offset between cruises *i* and *j* is possible:

$$\Delta f_{ijn} = \Delta F_{in} - \Delta F_{jn} = D_{ij} + \alpha_{in} - \alpha_{jn} = D_{ij} + \beta_{ijn} \qquad (3)$$

Results

Relative inter-cruise offsets for individual cruises are shown in Fig. 2. Our calculations reveal a high-degree of consistency of the WOCE Atlantic data set: 68% of salinity offsets are smaller than 0.0025, 69% of oxygen offsets are smaller than 0.125 ml/l, 68% of silicate offsets are smaller than 2.5 μmol/kg and 50% of nitrate offsets are smaller than 0.5 μmol/kg. Offset statistics are given in Table 1 along with the WHP one-time survey quality standards (WOCE Operations Manual, 1994). For all parameters mean offset values are close to or smaller than accuracy standards for one-time hydrography (WOCE Operations Manual, 1994). Some cruises exhibit obvious systematic deviations. For instance, SAVE4, A11, A2, SR2 are characterised by systematically lower salinities, whereas A13, A14, A23, AR19 have systematically higher salinities. No significant correlation was found between the offset magnitudes and the time interval between the cruises. Our calculations do not show any geographical dependence of the offset magnitude and the offsets for different parameters appear to be uncorrelated.

Using corrections to IAPSO SSW as reported by Aoyama et al. (1998) we calculated salinity offsets with and without corrections for 52 cruise pairs having different batches. Accounting for SSW corrections decreases the mean absolute offset value from 2.29×10^{-3} to 1.86×10^{-3} with the absolute offsets increased in 20 cases and decreased in 32 cases.

Formulae (2) and (3) give direct and indirect estimates of the true inter-cruise offsets *D* with uncertainties α and β representing the combined effect of random errors ε and time-spacial variability γ. If α and β are negligible, direct and indirect estimates are identical and perfectly correlated. Both α and β are independent of *D* and ε and γ are independent of each other. Cross-over areas for a typical cruise are distributed over a large oceanic region, often being situated in relatively isolated oceanic basins. Tem-

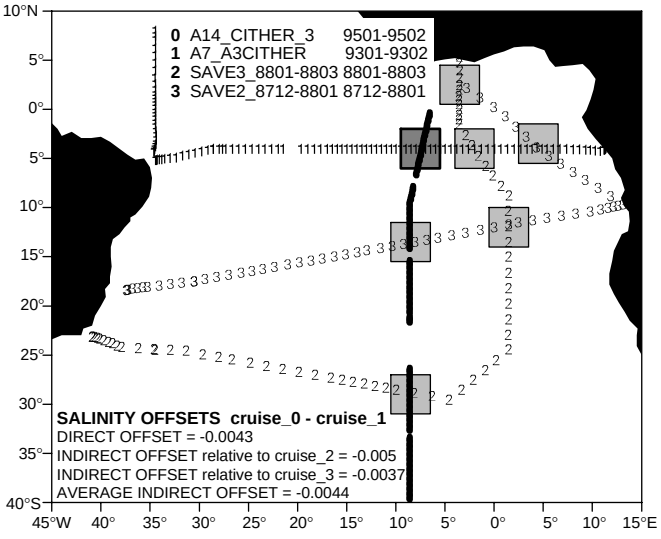

Figure 3. Example of direct and indirect offset estimates for two WOCE cruises in the tropical Atlantic A14 and A7.

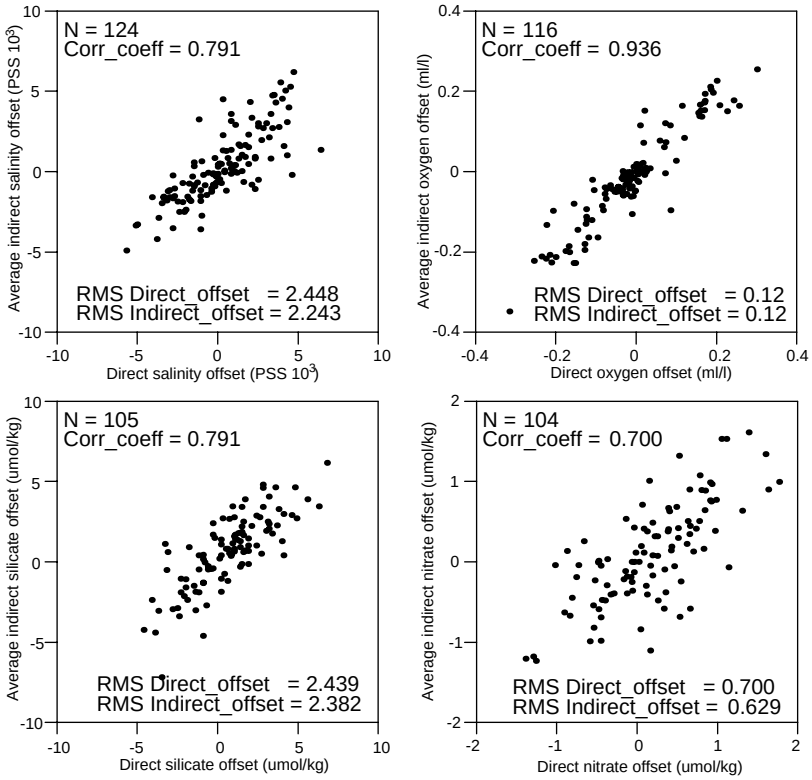

Figure 4. Correlations between directly and indirectly calculated offsets.

perature ranges ($\theta < \theta_{max}$) and time intervals between cruise occupations are different for each cross-over area, so that it seems reasonable to assume, that parameter changes γ due to the space-time variability for different cross-over areas (cruise pairs) are also independent of each other. Under this assumption variables α and β are independent. The correlation coefficient between ΔF and Δf will then depend on the variances of the true offsets *D* and of the variances of ε and γ. High values of the correlation coefficient would indicate that the combined effect of random errors and time-spatial variability is small compared to that of systematic offsets.

The geometry of the WOCE Atlantic cruise lines is such that on average 4 indirect offset estimates are available for each direct estimate. Fig. 3 gives an example of direct and indirect offset calculation for a pair of WOCE cruises (A14 and A7) in the tropical Atlantic. Both cruises have crossings with two SAVE cruises, and the direct salinity offset estimate (0.0043) is in a good agreement with indirect estimates (0.0037 and 0.0050). Shown in Fig. 4 are correlations between direct and average indirect offset estimates for the whole data set. For all parameters correlations exceed 0.7, so that the apparent deep water variability may be explained mostly by the presence of systematic errors (offsets) in the data. Correlation is highest for oxygen (0.936). According to Fig. 2a about 70% of cruise pairs have oxygen offsets less than 0.125 ml/l. A number of data subsets show remarkable consistency with mean relative offsets less than 0.05 ml/l (SAVE2, SAVE3, SAVE4; A6–A7; AR15–AR4). Thus, methods of measuring dissolved oxygen seem to be still ahead of other parameters in quality in agreement with an earlier assessment of oxygen measurement quality by J. Reid (see introduction to the Climatological Atlas of the World Ocean, 1982). The diagram for nitrate is characterised by the largest scattering around the perfect fit line ($\Delta F = \Delta f$) and the correlation coefficient is the lowest (0.700). We note that some data with relatively high nitrate offsets (for instance, A10 data) are still preliminary.

Conclusion

Our analysis confirms a high consistency of the WOCE Atlantic hydrographic data set. On average, inter-cruise parameter differences are smaller or close to the quality standards set for the WOCE hydrographic programme. However, systematic differences between the cruises exist. Analysis of directly and indirectly estimated inter-cruise property offsets shows that the inter-cruise offsets are caused mostly by the systematic errors in the data, and not by the natural variability.

Acknowledgements

The authors are indebted to E. Fahrbach, B. King, H. Mercier, T. Müller, C. Oudot, Y.-H. Park, W. Smethie and B. Tereschenkov for making their non-public hydrographic data available for the offset analysis. We extend our thanks to S. Diggs who prepared for us some of the datasets. We are thankful to M. Aoyama for the table of corrections for IAPSO SSW.

References

Aoyama, M., and T. M. Joyce, 1996: WHP Property comparisons from crossing lines in the North Pacific. WOCE Pacific Workshop, 19–23 August 1996, Newport Beach, CA, USA.

Aoyama, M., T. M. Joyce, T. Kawano, and Y. Takatsuki, 1998: Offsets of the IAPSO standard seawater for P103 through P129. (Submitted)

Gordon, A. L., and E. J. Molinelli, 1982: Southern Ocean Atlas. Part I, Thermohaline and chemical distributions and Atlas data set. Columbia University Press, New York, USA.

Wyrtki, K., 1971: Oceanographic Atlas of the International Indian Ocean Expedition. NSF, US Government Printing Office, Washington, DC, USA.

Saunders, P. M., 1986: The accuracy of measurements of salinity, oxygen, and temperature in the deep ocean. J. Phys. Oceanogr., 16, 189–195.

Mantyla, A., 1994: The treatment of inconsistencies in Atlantic deep water salinity data. Deep-Sea Res., 41, 1387–1405.

Gouretski, V., and K. Jancke, 1996: A new hydrographic data set for the South Pacific: synthesis of WOCE and historical data, WOCE Report No. 143/96.

WOCE Operations Manual, 1994: Woods Hole, MA, USA.

Large Scale Oceanic Nutrient and Oxygen Fluxes

Alexandre Ganachaud and Carl Wunsch, Department of Earth, Atmospheric and Planetary Sciences, MIT, USA. ganacho@mit.edu

Much of the motivation for the WOCE hydrographic programme was the need to be able to compute global budgets of scalar fields important to climate, including heat and freshwater. Also important to climate (and oceanic biology and chemistry generally) are the fluxes and flux divergences of nutrients (phosphate, nitrate, etc., and oxygen) as these are intimately related to the oceanic carbon cycle and fluxes.

We have calculated preliminary global estimates from the WOCE hydrographic data of the nutrients and oxygen using the box geostrophic inverse method, similar to the calculation of Macdonald and Wunsch (1996). The physical properties – mass, heat and freshwater fluxes – have also been computed, but these will not be described here, except for the mass flux, which is central to all the other properties.

Nutrients are consumed and converted to particulate and organic matter in the surface layers of the ocean. After going through the food chain, some particles are recycled in the euphotic zone, while the remainder (3 to 80%, depending upon location, time and author) is exported towards the deep oceanic layers where it is mostly remineralised. Because of the confinement to the surface of production of organic matter and the constant loss to the deep ocean, 98% of the nutrients are permanently in the dissolved inorganic phase.

Oceanic currents consequently carry huge quantities of dissolved nutrients. The rate at which these are carried toward the euphotic zone often controls primary production. Direct measurements of production and dissolution rates are sparse and difficult to interpret, but it is possible – in principle – to base estimates of them on an accurate dissolved nutrient budget in the deep ocean.

Here we seek a global circulation scheme that is consistent with both dynamical and biogeochemical principles. The benefits are two-fold: on the one hand, the dynamics provide information about the nutrient fluxes; on the other hand, the nutrient fluxes are able to provide constraints on the circulation.

The inverse model

Macdonald and Wunsch (1996) used pre-WOCE hydrographic lines; here we shift to the WOCE hydrography itself, but with some limited pre-WOCE data along with the so-called JADE hydrographic section (Fig. 1). The result is an estimate of the average circulation during the 1985–1996 period (except for the 1981 section at 36°N in the North Atlantic, the earliest section used was from 1985). Across each section relative geostrophic transports are computed relative to a reference level. The top layer includes the Ekman transport from the NCEP wind stress re-analysis. Reference level velocities are then adjusted so that mass, salt and some nutrients or nutrient combinations are conserved within estimated errors. Within the oceanic boxes enclosed by the hydrographic sections and the continent, we defined a set of layers bounded by neutral surfaces (McDougall, 1987). Near-conservation is required top-to-bottom and in individual layers. A cross-isoneutral transfer is permitted between layers. The model is linear – no change is permitted in the density field. An underlying assumption is the ergodic one – that trans-oceanic integrals are equivalent to long-term time averages.

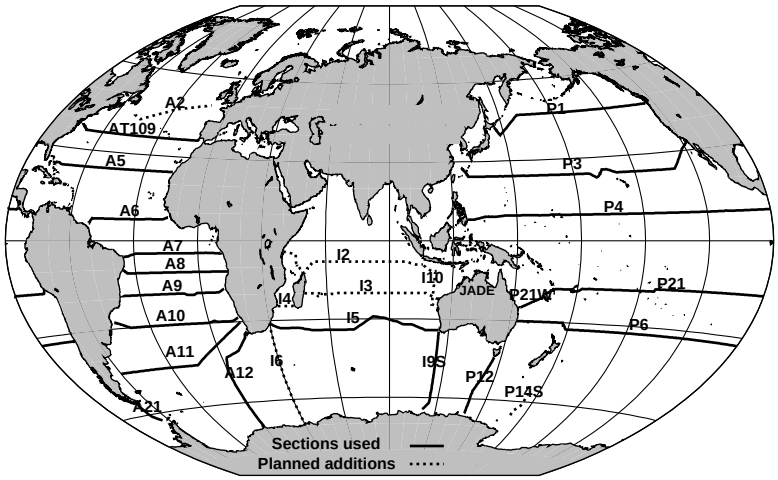

Figure 1. Hydrographic sections used in the model (mainly from WOCE). Each section consists of high-density measurements of temperature, salinity, oxygen, nutrients and in some cases total carbon and alkalinity. Our preliminary inversion here uses the solid line sections. The dotted line sections will be included in the near future.

Constraints and a priori errors

Geostrophy and Ekman dynamics are imposed by construction. The flow is required to nearly conserve mass and salt top-to-bottom and in individual layers. The total silica is conserved only top-to-bottom, allowing a residual in individual layers to accommodate and quantify the source from siliceous shell dissolution or the sink from biological consumption. Oxidation of soft organic tissues are taken into account by requiring conservation of the nitrate-oxygen "NO" combination $9.1[NO_3]+[O_2]$ (Broecker, 1974) in individual layers. In addition, the

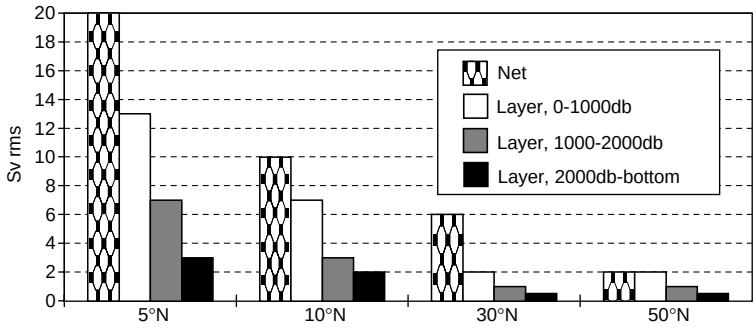

Figure 2. A priori errors due to the baroclinic variability in the mass equations, as obtained from the Semtner and Chervin (1992) ¼° general circulation model. Values were computed in the North Atlantic and extrapolated to low latitudes and other oceans.

phosphate-oxygen "PO138" tracer $138[PO_4]+[O_2]$ was verified, a posteriori, as conserved.

The weights given to each constraint are derived from the expected noise in the equation. To produce realistic uncertainties, we made an error budget for the mass and silica, accounting for the different assumptions of the model (geostrophy, steady state, etc.) and for the measurement noise. Fig. 2 summarises the a priori noise expected in the mass conservation equation for a single section. The dominant error comes from the variability in the density field (baroclinic variability) and was estimated with the help of an eddy-permitting general circulation model (Semtner and Chervin, 1992). Typically, for a mid-latitude box enclosed by two sections, mass conservation is imposed to within 10 Sv for the total mass and to within 0.7 to 2 Sv in individual layers, depending on the depth. Salt conservation was given the same relative weight as mass conservation. We also estimated, with the GCM output, the effect of the baroclinic variability on the silica flux variability using an empirical relationship between temperature, salinity and silica. In the North Atlantic mid-latitudes a flux variability (model error) of $\pm 50\ \mathrm{kmol\,Si\,s^{-1}}$ was found. In general, these errors are larger than previously believed realistic. They are also a strong function of latitude.

Global inversion

The inversion provides a consistent estimate of the fluxes and residuals of mass, salt, heat, oxygen, nitrate, phosphate and silicate with full uncertainty estimates. We present here only our preliminary estimate of the mass, nitrate and oxygen budgets (Figs. 3 to 4); the heat fluxes (not shown) are generally consistent with our previous estimates. The mass and salt residuals are consistent with the a priori noise and are indistinguishable from zero in most layers. The graphs on the left of each section in Fig. 3 give the vertical structure of the flow across the section (positive is northward or eastward). The North Atlantic Deep Water transport varies from 16±3 Sv at 36°N to 21±2 Sv at 30°S while Circumpolar Deep Water plus Antarctic Bottom Water flow ranges from 5.6±1.2 Sv at 30°S to 2.5±1.5 Sv at 24°N. The circumpolar waters feed the Indian Ocean at a rate of 10±7 Sv and the Pacific Ocean at 18±5 Sv, consistent with current meter observations and other estimates. The graphics on the right columns between the sections, give the cross-neutral surface transfer rates required by the geostrophic circulation.

The net fluxes of nitrate (Fig. 4, arrows) are significantly non-zero only across a few sections at relatively high latitudes. The residuals are indicated in terms of utilisation rates (graphs) and integrated over several layers (boxed numbers) where significant. They are considered "dubious" when associated with a marginally significant mass divergence. The Atlantic Ocean appears as a source of nitrate, which is exported towards both poles. In the subtropical North Atlantic, we recover the nitrate influx found by Rintoul and Wunsch (1991). However, mass is not properly balanced at 24°N (the WOCE line at 36°N was made available to us by Dr Terechenkov, but because it had calibration problems we were forced to use the 1981 pre-WOCE line there). The Southern Ocean surface layers show nitrate utilisation values between 0.1 and $0.4\ \mathrm{mol\,NO_3\,yr^{-1}\,m^{-2}}$, consistent in magnitude with other new production estimates (e.g., Jenkins, 1988; Berger et al., 1989). In the North Pacific there is a marginal indication of northward export, too. Whether the apparent nitrate loss in the equatorial Pacific is due to leakage in the Pacific-Indian Throughflow or to surface utilisation should become clearer when we incorporate the JADE section from Timor to Australia.

A net equatorward transport of oxygen is found in the North Atlantic (Fig. 5). The South Atlantic does not show any significant flux while the equatorial Pacific imports oxygen. The residuals, indicated as oxygen utilisation rates (OUR), are of the same magnitude as expected from tracer measurements (Spitzer and Jenkins, 1989). The Southern Oceans show sources of oxygen in the surface layers and sinks in the intermediate and deep layers, in agreement with the classical view of photosynthesis-remineralisation.

The net silica fluxes (not shown) are mostly indistinguishable from zero by construction. The residuals indicate siliceous particulate exports in the range 0.2–0.9 mol $\mathrm{SiO_2\,yr^{-1}\,m^{-2}}$ in the Southern Ocean.

Future improvements and changes

These results are all preliminary. In particular, the model is being changed to include more of the WOCE hydrographic lines. The final results will include global estimates of the flux and flux divergence of mass, salt, heat, freshwater, silica, nitrate, phosphate and oxygen and are part of an MIT/WHOI PhD thesis (Ganachaud, in preparation).

Acknowledgements

We are grateful to all the oceanographers, PIs and scientists who collected and let us use the data, either directly or by

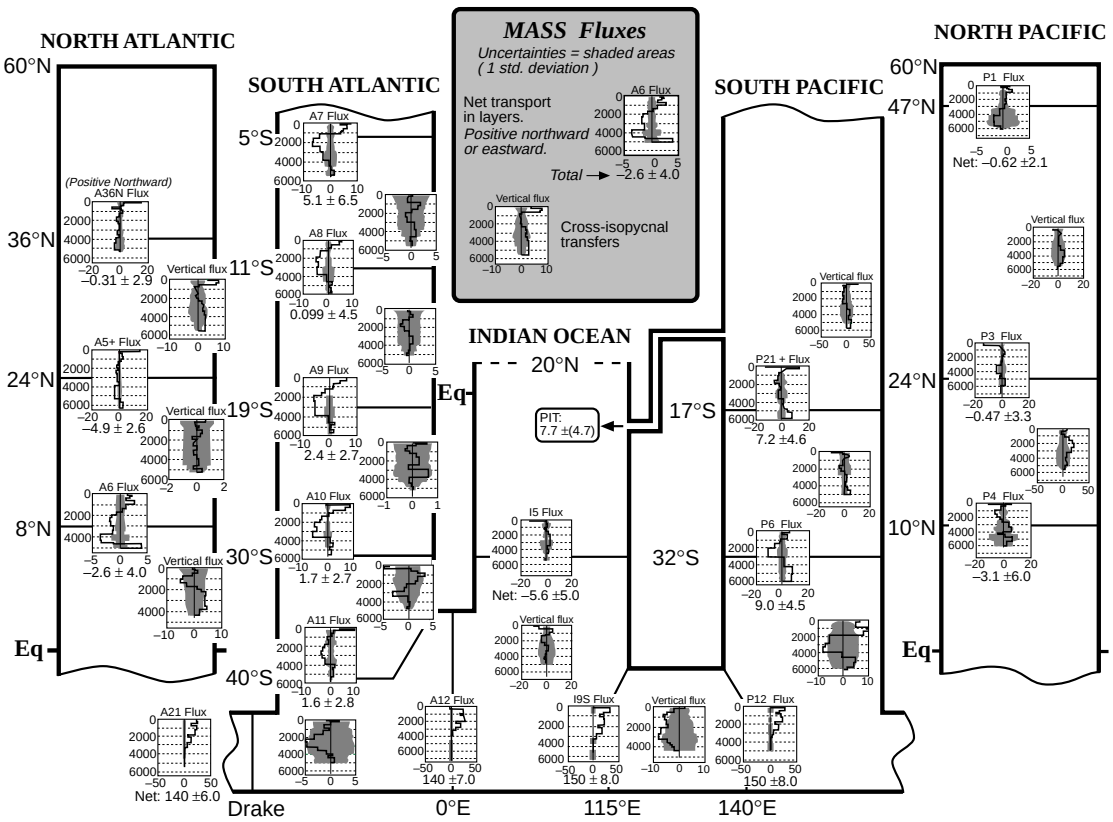

Figure 3. Estimated mass fluxes. The Atlantic and Pacific Oceans have been split at the equator for clarity. The net transports by layer across each section are given by the graphs on left of each section. The cross-isoneutral transports (labelled as "cross-isopycnal" or "vertical") with the boxes between the sections are indicated by the graphs on the right columns, between the sections. PIT is the Pacific-Indian Throughflow.

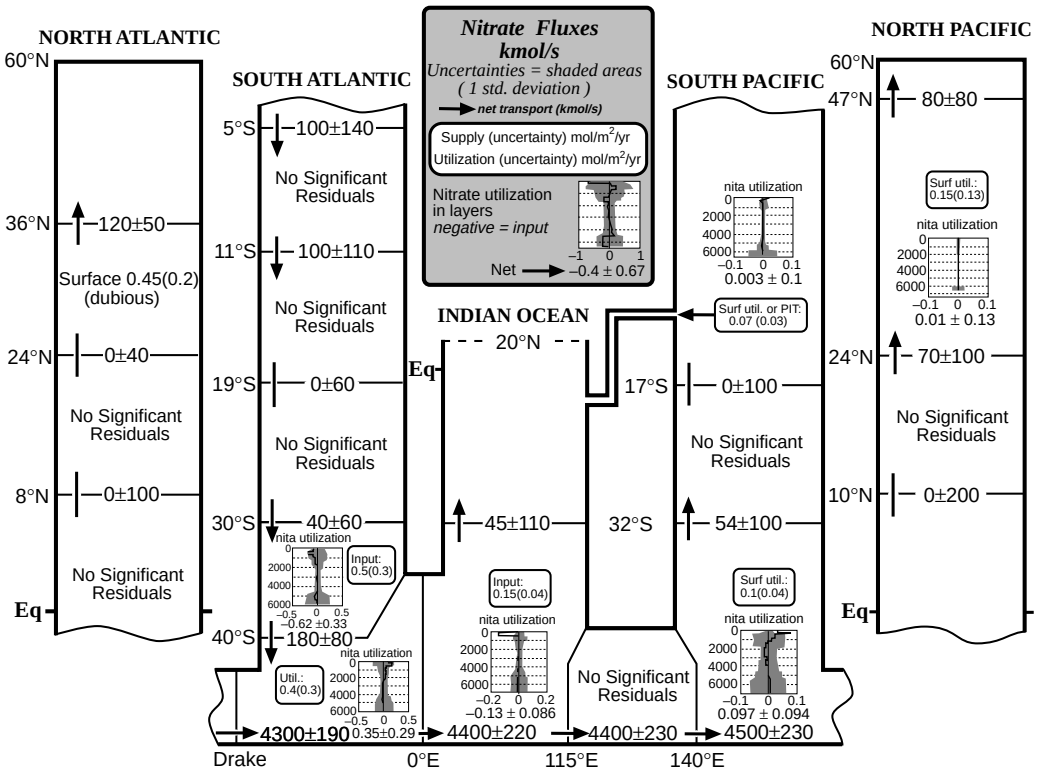

Figure 4. Nitrate circulation: the net transport across each section is indicated to the right of each arrow (kmol NO_3 s^{-1}). Nitrate utilisation is indicated, when significant, by the graphs. The boxed numbers indicate either the utilisation or the input integrated over several layers. "Surface" indicates an utilisation/input in the surface layers.

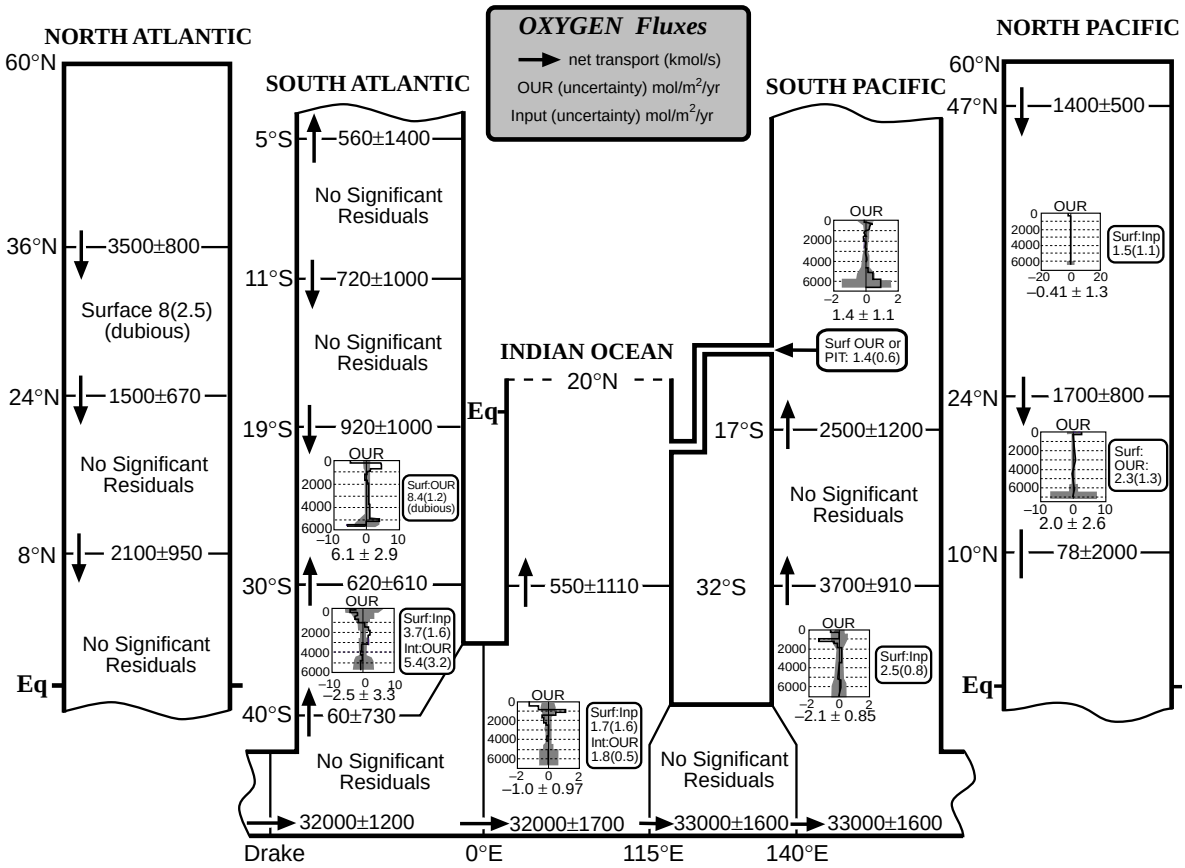

Figure 5. Oxygen circulation; same convention as for nitrate. The residuals are given in terms of Oxygen Utilisation Rate (OUR, mol/m^2 yr). Negative OUR indicates dissolved oxygen input (Inp). The boxed numbers give the OUR or input integrated over surface or interior layers.

making them publicly available: P. Koltermann (Section A2), G. Parrilla and R. Millard (A5), M. Arhan, C. Oudot, A. Morlière and C. Colin (A6, A7), G. Siedler, R. Onken and D. Mueller (A8, A9, A10), P. Saunders (A11), W. Roether (A12), P. Lemke (A21), B. Warren, G. Johnson and W. Nowlin (I2, I3), J. Toole (I4, I5), Y-H. Park, C. Jeandel and N. Metzl (I6), M. McCartney (I9S), N. Bray and G. Packard (I10), M. Fieux, A. G. Ilahude, R. Molcard and B. Coste (JADE), L. Talley (P1), J. Swift and D. Roemmich (P3), J. Toole, E. Brady and H. Bryden (P4), M. McCartney, H. Bryden and J. Toole (P6, P21), S. Rintoul (P12), J. Bullister and G. Johnson (P14S), M. McCartney and H. Bryden (P21). The A6 and A7 initial reference levels were provided by M. Lux (Lux, 1998). J. Toole provided the I5 ones (Robbins and Toole, 1996 and S. Wijffels the P10 ones (i.e. Macdonald, 1995, Table A3). Thanks to S. Diggs and J. Swift of the WHP Office who transmitted to us most of the data. Thanks to Alison Macdonald for her useful advice about the model. S. Jayne and R. Tokmakian provided the GCM fields for our error analysis. D. Spiegel helped with the data treatment; B. Brown helped with the graphics. This research is supported by the MIT Climate Modeling Initiative and the NSF grant OCE-9529545.

A colour version of the figures is available on **http://puddle.mit.edu/~ganacho/WIN/index.html**.

References

Berger, W., V. S. Smetacek, and G. Wefer, 1989: Ocean productivity and paleoproductivity – an overview. in: Productivity in the oceans: present and past, Report of the Dahlem Workshop, Berlin. Wiley, New York, USA.

Broecker, W. S., 1974: "no", a conservative water-mass tracer. Earth and Planetary Science Letters, 23(1), 100–107.

Jenkins, W. J., 1988: Nitrate flux into the euphotic zone near Bermuda. Nature, 331(6156), 521–523.

Lux, M., 1998: Franchissement de l'equateur par les masses d'eau dans le cadre de la circulation thermohaline. PhD thesis, IFREMER, Plouzané, France.

Macdonald, A., 1995: Oceanic fluxes of mass, heat and freshwater: A global estimate and perspective. PhD thesis, Department of Earth, Atmospheric and Planetary Sciences, Massachusetts Institute of Technology, Cambridge, MA , USA.

Macdonald, A. M., and C. Wunsch, 1996: An estimate of global ocean circulation and heat fluxes. Nature, 382.

McDougall, T., 1987: Neutral surfaces. J. Phys. Oceanogr., 17, 1950–1964.

Rintoul, S. R., and C. Wunsch, 1987: Mass, heat, oxygen and nutrient fluxes and budget in the North Atlantic Ocean. Deep-Sea Res., 38, Suppl., 355–377, 1991.

Robbins, P. E., and J. M. Toole, 1997: The dissolved silica budget as a constraint on the meridional overturning circulation in the Indian Ocean. Deep-Sea Res., 44(5), 879–906.

Semtner, Jr., A. J. S., and R. M. Chervin, 1992: Ocean general circulation from a global eddy-resolving model. J. Geophys. Res, 97, 5493–5550.

Spitzer, W. S., and W. J. Jenkins, 1989: Rates of vertical mixing, gas exchange and new production: estimates from seasonal gas cycles in the upper ocean near Bermuda. J. Mar. Res, 47, 169.

Eulerian Measurements of the North Atlantic Deep Water Deep Western Boundary Current at 18°S

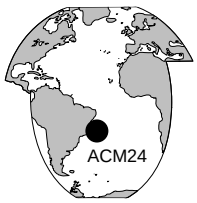

Georges Weatherly and Yoo Yin Kim, Department of Oceanography, Florida State University, USA; and Evgeny A. Kontar, Shirshov Institute of Oceanology, Russian Academy of Sciences, Russia. weatherly@ocean.ocean.fsu.edu

The Deep Basin Experiment (DBE) component of WOCE had as principal objective the improvement of our knowledge of the subthermocline circulation both in a descriptive and dynamic sense (Hogg et al., 1996). For logistic and scientific reasons the DBE was carried out in the Brazil Basin (Fig. 1). This report is concerned with results from the deployment of an array of moored current meters designed to monitor the deep western boundary current (DWBC) of North Atlantic Deep Water (NADW) and the DWBC of Antarctic Bottom Water (AABW) at a mid basin site in the Brazil Basin as part of the DBE. In terms of the WOCE nomenclature, the current meter array is called ACM24.

The array, consisting of ten moorings with a total of thirty-four current meters, was set at about 18°S in the western central Brazil Basin (Fig. 1) in September–October 1993. Eight moorings with a total of twenty-eight current meters were recovered eighteen months later in March 1995 (problems with Brazilian clearance precluded dragging for the two moorings whose releases failed to function properly). Twenty-six of the recovered instruments gave usable data. All moorings set to monitor the Deep Western Boundary Current (DWBC) of North Atlantic Deep Water (NADW) were recovered, and we focus here on the data from these moorings.

NADW is found roughly between 1200 m and 3600 m depths in the Brazil Basin (DeMadron and Weatherly, 1994). The mean currents at 1800 m depth (Fig. 2, page 22) indicate that the NADW DWBC flowed approximately towards the south-east rather than towards the south as expected. The mean currents at 2800 m depth, shown in the data report Harkema and Weatherly (1996) (which can be viewed on the web at http://ocean.ocean.fsu.edu/~georges/cmf/brbamain.htm), also indicate the DWBC flowed towards the south-east at this depth. The DWBC is about 200 km wide (Fig. 2).

The mean velocity component directed towards 140°, the approximate direction the NADW DWBC flowed, is contoured in Fig. 3 (page 23). The locations of the moorings and the depths of the current meters are indicated. Also shown as dashed lines are the upper and lower bounding isopycnals for NADW, $\sigma_2 = 36.7$ and $\sigma_4 = 45.87$, in May 1994 when a WOCE hydrographic survey was made across the mooring array (Smethie and Weatherly, 1996). The NADW DWBC appears imbedded in a flow which extends downward into the underlying AABW (below $\sigma_4 = 45.87$) to the bottom and upward into the overlying Antarctic Intermediate Water (AAIW) (above $\sigma_2 = 36.7$) at least to the level of the uppermost current meters at 900 m depth. The associated transport of the NADW DWBC towards 140° is 36 Sverdrups. Note that the western edge of the other DWBC, the one which flows poleward transporting AABW, can be seen in Fig. 3 about 100 km to the east of the eastern edge of the NADW DWBC.

From velocity sections like Fig. 3 except formed for each day from the eight-day low pass filtered current meter data, we have estimated a time series of the volume transport of the NADW DWBC (Fig. 4). The largest fluctuations in the volume transport evident in this figure have amplitudes comparable to the mean and time scales order about a month. We think these fluctuations are not very well resolved because they appear to be due to mesoscale motions with horizontal dimensions comparable to the mooring separation distance (Weatherly et al., 1998). Nonetheless, a seasonal signal is apparent with larger transport tending to occur around February and minimum around September. The seasonal signal, and its amplitude of about 10 Sverdrups, is more apparent in the six-month running mean curve, the dashed curve, in Fig. 4. The twelve-month running mean curve, the dot-dashed curve, in Fig. 4 is remarkably steady at about 39 Sverdrups. As explained in Weatherly et al.

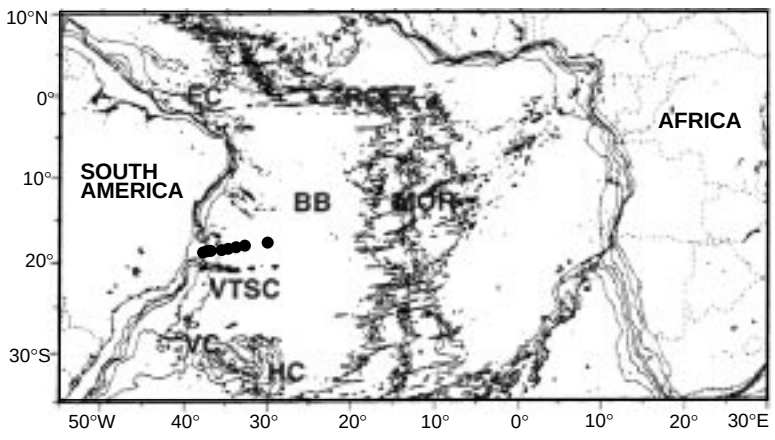

Figure 1. Bathymetric chart of the South Atlantic showing the Brazil Basin (BB), which is bounded to the east by the Mid-Ocean Ridge (MOR) and South America to the west. The deep passages connecting this basin to neighboring basins are indicated: the Vema Channel (VC), the Hunter Channel (HC), the Romanche Chain Fracture Zones (RCFZ), and the Equatorial Channel (EC). The current meter mooring locations are the solid circles just to the north of the Vitoria-Trindade Seamount Chain (VTSC). Isobaths indicated are 200 m, 1000 m, 2000 m, 3000 m, and 4000 m.

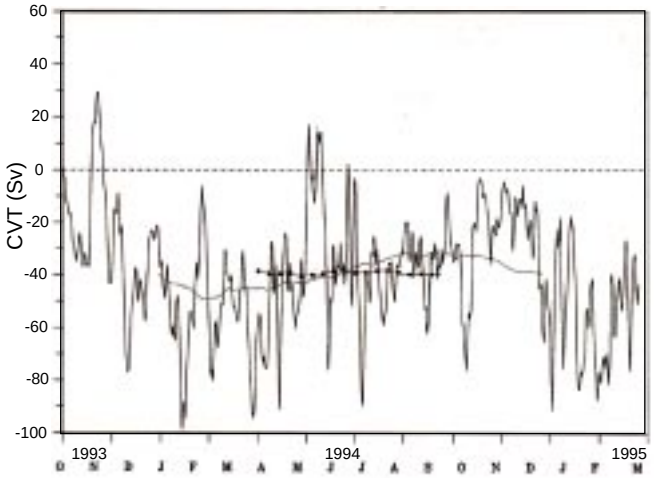

Figure 4. Transport time series (solid curve) formed from daily transport estimates. Negative values denote transport towards 140°. The seasonal variability is better displayed in the six-month running mean dashed curve which indicates maximum flow around February and minimum flow around September with an amplitude of about 10 Sverdrups. The twelve-month running mean dot-dashed curve is remarkably steady with a magnitude of about 39 Sverdrups.

(1998) we think this latter value is a more representative estimate of the mean transport than the 36 Sverdrups inferred from the record mean values shown in Fig. 3. Examining figures comparable to Fig. 3 but for water types (AAIW, lower NADW, middle NADW, lower NADW, and AABW; shown in ibid.) indicates that the seasonal variability is barotropic.

After the results shown in Figs. 3 and 4 were estimated, we became aware of float data obtained in AAIW in the same region of the Brazil Basin (Boebel et al., 1998). Our results for currents in AAIW are more consistent with those of Boebel et al. (1998) if horizontal interpolation rather than vertical extrapolation is used to estimate the missing velocity data value at the 900 m depth level at mooring 3. In particular, the maximum flow towards 140° in Fig. 3 drops from 900 m depth (in AAIW) to about 1800 m depth (in NADW) when we do so, and the velocity core and property core structure of the DWBC essentially coincide (Weatherly et al., 1998) Since this is probably a better representation of the flow field and doing so slightly diminishes the inferred strength of the DWBC, the average transport is probably somewhat less than the 39 Sverdrups estimated from Fig. 4. Weatherly et al. (1998) concluded that the average transport of the NADW DWBC should be revised to about 36 Sverdrups.

In summary, data from ACM24 indicate that the DWBC of NADW at about 18°S in the Brazil Basin flows to the south-east, transports on the average about 36 Sverdrups, is about 200 km wide, is embedded in a flow which extends downward to the bottom and upwards to at least 900 m depth, is seasonally modulated, and is to the west of the poleward flowing DWBC of AABW.

References

Boebel, O., R. E. Davis, M. Ollitrault, R. G. Peterson, P. L. Richardson, S. Schmid, and W. Zenk, 1998: First direct observations of the western South Atlantic circulation at intermediate depth. Submitted to Nature.

DeMadron, X. D., and G. Weatherly, 1994: Circulation, transport and bottom boundary layers in the Brazil Basin. J. Mar. Res., 583–638.

Hogg, N. G., W. B. Owens, G. Siedler, and W. Zenk, 1996: Circulation the deep Brazil Basin. In: Wefer, G., W. H. Berger, and D. J. Webb (Eds.): The South Atlantic: Present and Past Circulation. Springer-Verlag, Berlin, 355–361.

Smethie, W. M., Jr., and G. L. Weatherly, 1996: Scientists report preliminary results from WOCE DBE cruise. WOCE Notes 8(1), 18–22.

Weatherly, G. L., Y. Y. Kim, and E. A. Kontar, 1998: Eulerian measurements of the North Atlantic Deep Water Deep Western Boundary Current at 18°S. Submitted to J. Phys. Oceanogr.

Spanish Edition of WHP Operations and Methods Manual now Available

At the beginning of WOCE, the Hydrographic Programme Office at Woods Hole published a manual on operations and methods to be used during the collection of WOCE hydrographic data. Originally published in 1991, the manual was revised and republished in 1994, and brings together the methodologies used to ensure the high quality of data collected on WOCE hydrographic cruises. It is anticipated that the methodologies in the manual will continue to be of importance during CLIVAR and other programmes during the next decade.

As a result of a co-operative funding effort between the Intergovernmental Oceanographic Commission and the US WOCE Office, we now have available 300 copies of a Spanish version of the 1994 edition of the manual. The translation was done by Alan Cantos of AINCO-Interocean in Madrid. The document is spiral-bound with soft cover, and copies are available on a first come, first served basis, from the US WOCE Office, 305 Arguello Drive, College Station, TX 77840, USA. (fax: 1-409-845-0888; e-mail: uswoce@ocean.tamu.edu).

East Australian Current Volume Transports from PCM3 Array

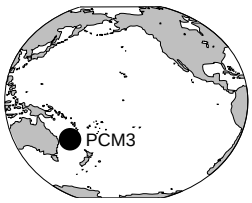

Mauricio M. Mata and Matthias Tomczak, Flinders Institute for Atmospheric and Marine Sciences, Australia; Susan Wijffels and John Church, CSIRO Division of Marine Research, Australia. Mauricio.Mata@es.flinders.edu.au

The WOCE Pacific Current Meter Array 3 (PCM3) was deployed in November 1991 with the main objective of obtaining a direct estimate of volume transport and associated variability of the East Australian Current (EAC) at 30°S. It was serviced in September 1992 and finally recovered in March 1994. The array consisted of six moorings (at 90, 200, 700, 2000, 4400 and 4590 m), with a total of 26 recording current meters (RCM) and 2 upward-looking ADCPs (Fig. 1). Tomczak et al. (1996) made the preliminary assessment for the first 10 months of the data set.

Methods

The raw hourly records were checked individually for bad data, and the resulting gaps filled by interpolation whenever possible. Gaps up to 3 hours were filled linearly. Longer gaps – up to 12 days – were filled spectrally based on Anderson (1974). After this initial treatment the series were low-pass filtered to remove diurnal tides, inertial oscillations and higher frequencies, leaving less than 0.5% of the energy at 25 hours. The filtered series were decimated to a 6 hourly interval. Details of individual current meter series can be found in Mata et al. (1998).

At each time interval, a full depth velocity profile for the deep moorings (4, 5 and 6) was calculated at 25 m resolution using a mooring motion correction scheme based on Hogg (1991). The transports per unit of width time series (around each mooring) were obtained by vertically integrating these profiles. Total transports in the deep moorings were calculated after horizontally interpolating (dx = 1000 m) the meridional component of velocity (v) at each individual 25 m level and then performing the area integral of the $1000 \times 25\,\mathrm{m}$ boxes. The deep mooring records – 5 and 6 – feature strong *knockdowns* associated with bursts of intense northward flow. During these events the top of the mooring had vertical excursions as large as 1200 m. Due to the lack of measurements in the upper water column during these strong events, the vertical transports produced by the scheme were clearly spurious. At these times, the transports were blanked and the resulting gaps filled by spectral interpolation following Anderson (1974).

In the shallow moorings (1, 2 and 3), Hogg (1991) scheme could not be applied, so v values were mapped using optimal interpolation and then integrated to estimate the transports in the area of water depth <1000 metres. All transport series were filtered to remove oscillations less than one week and decimated to daily intervals.

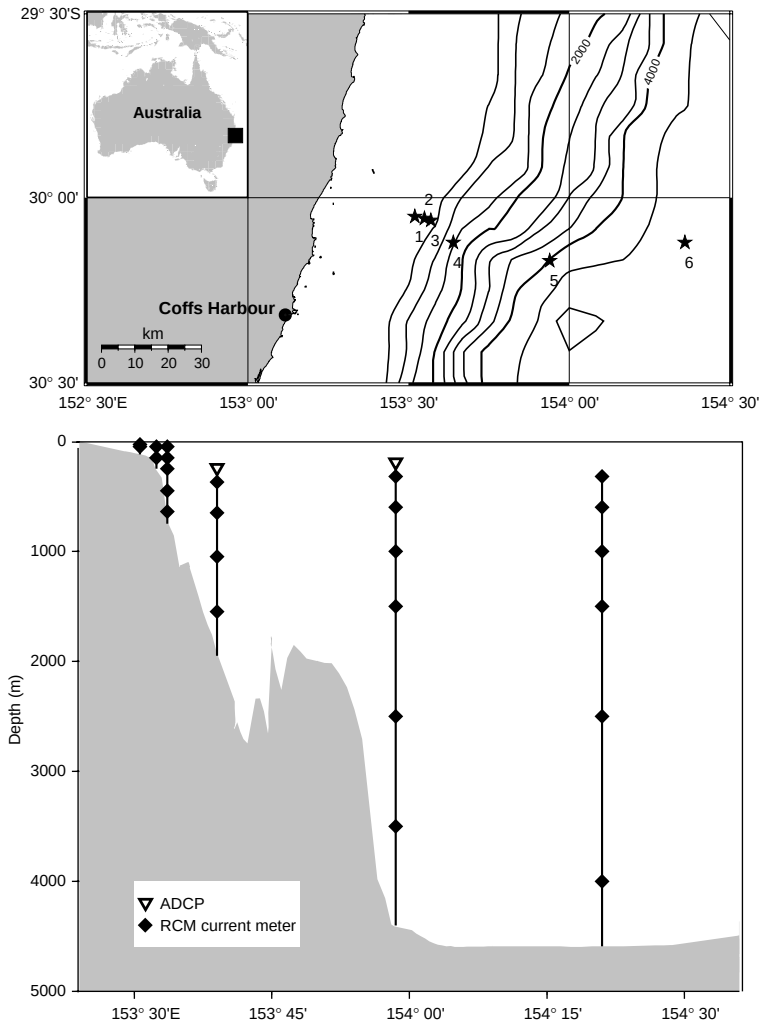

Figure 1. PCM3 mooring sites (top) and instrument distribution (bottom).

Results

The time series of volume transport across the array is shown in Fig. 2.

Despite the dominant direction of the of EAC being poleward it is noticeable that, in some periods, the net integrated transport reverses, reaching values up to 40 Sv northwards. As a result, the mean EAC transport is about half of the value of its standard deviation (see Table 1). The cause of the large reversals is still under investigation. The current meter records point out that they result from a northward intensification of the barotropic component (Mata et al., 1998). Tomczak et al. (1996) suggested that these reversals might also be

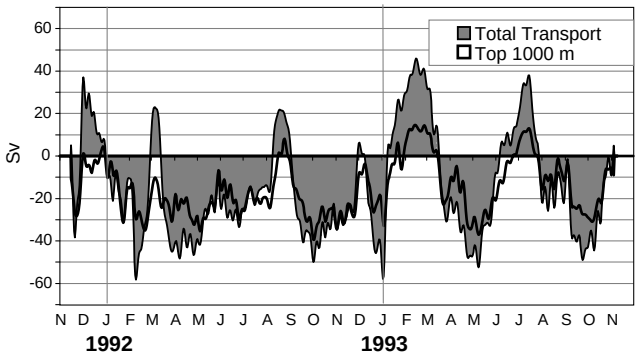

Figure 2. EAC volume transport time series across PCM3 array.

related with the propagation of Rossby waves across the array.

Although it is believed that the EAC has a very well defined annual cycle, with its maximum in the austral summer (e.g. Godfrey, 1973), this is not evident in the PCM3 results. Despite the short time series, we can safely point out that during the sampling period the annual component had a very small overall contribution, with the periods between 180 and 30 days containing most of the variance of the series (Fig. 2). In addition, it is likely that the largest events are underestimated due to the mooring *knockdowns* and associated interpolation errors.

The variance-preserving spectrum for the total transport series shows two major peaks at 144 days and 45 days (Fig. 3). Using ship drift data in the same region, Hamon et al. (1975) obtained similar results with the

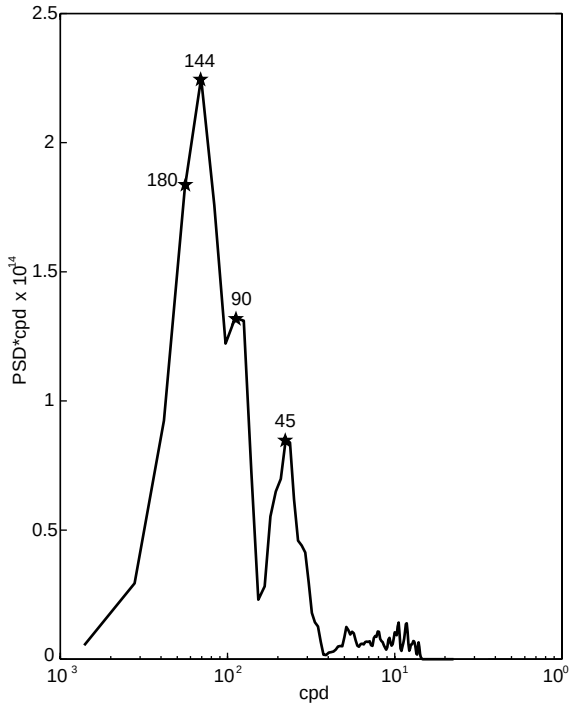

Figure 3. Variance preserving spectra for the transport time series. The numbers within the graph correspond to the periods (in days) of the peaks underneath.

spectrum being dominated by periods ranging from 170 to 50 days. More recently, Ridgway and Godfrey (1997) found a strong localised dominance of the semi-annual component of steric height variability around 30°S, which may suggest a weak seasonal phase locking of the variability.

Fig. 4 (page 21) shows the spatial structure of the mean and standard deviation of meridional velocity across the array. The mean position of the core of the EAC was over mooring 4 (2000 m; ~44 km from the coast), with mean surface values reaching up to $0.5\,\mathrm{m\,s^{-1}}$ southwards. The current deepens offshore with mooring 5 (4400 m) making the biggest contribution to poleward transport in the array. Despite mooring 6 (4590 m) being located at ~115 km from the coast, the presence of the EAC is still evident above 1000 m suggesting that the array was not long enough to sample the entire zonal extent of the current.

Table 1. Simple statistics of the EAC transports series (Sv).

	Mean	St. Dev.	Min	Max
Shallow water (water depth <1000 m)	-0.6	1.5	-4.1	3.8
Top 1000 m	-15.2	12.9	-39.3	14.7
Total	-14.4	24.8	-58.3	45.9

Fig. 4 reveals the presence of an equatorward undercurrent that is intensified along the slope. This current is associated with small low-frequency variability suggesting it is a persistent feature. Beal and Bryden (1997) reported a very similar feature in the Agulhas region, suggesting it may be a common characteristic of deep western boundary dynamics. Future analysis includes a combination of the current meter data with repeat WOCE hydrographic sections and shipborne ADCP along 30°S and will help improve the understanding of these dynamics.

References

Anderson, N., 1974: On the calculation of filter coefficients for maximum entropy spectral analysis. Geophys., 39, 69–72.

Beal, L. M., and H. L. Bryden, 1997: Observations of an Agulhas Undercurrent. Deep-Sea Res., 44, 1715–1724.

Godfrey, J. S., 1973: Comparison of the East Australian Current with the western boundary flow in the Bryan and Cox (1968) numerical ocean model. Deep-Sea Res., 20, 1059–1076.

Hamon, B. V., J. S. Godfrey, and M. A. Greig, 1975: Relation between Mean Sea Level, Current and Wind Stress on the East Coast of Australia. Aust. J. Mar. Freshwater Res., 26, 389–403.

Hogg, N., 1991: Mooring motion correction revisited. J. Atmos. Ocean. Technol., 42(5), 507–518.

Mata, M. M., S. Wijffels, M. Tomczak, and J. A. Church, 1998: Direct measurements of the Transport of the East Australian Current: A Data Report from the WOCE Pacific Current Meter Array 3. CSIRO Marine Research Report Series/ FIAMS Tech. Report, 234/16, 48pp.

Ridgway, K. R., and J. S. Godfrey, 1997: Seasonal cycle of the East Australian Current. J. Geophys. Res., 102 (C10), 22921–22936.

Tomczak, M., P. Otto, J. A. Church, and F. Boland, 1996: Transport estimates for the East Australian Current from PCM3 Mooring Array. Int. WOCE Newsletter, 23, 29–30.

A New Satellite-Derived Freshwater Flux Climatology (Hamburg Ocean Atmosphere Parameters and Fluxes from Satellite Data)

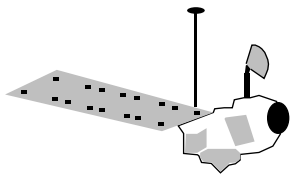

Jörg Schulz, Deutsches Zentrum für Luft- und Raumfahrt, Germany; Volker Jost, Meteorologisches Institut der Universität Hamburg, Germany; Stephan Bakan, Max-Planck-Institut für Meteorologie, Germany. joerg.schulz@dlr.de

The freshwater flux and the connected energy fluxes at the air sea interface are the most challenging parameters that have ever been derived from satellite measurements. The knowledge of turbulent fluxes between the ocean and atmosphere is along with radiative fluxes of large importance to increase our understanding of the large scale climate system. Accurate fields of these fluxes can be used for a direct forcing of ocean circulation models or just for evaluating the results of coupled climate models that have problems at the air-sea interface.

Conventional estimates of global fields of freshwater flux between ocean and atmosphere suffer from the inadequate spatial and time sampling with the exception of the North Atlantic. Additionally, the parameters that determine the freshwater flux are very difficult to measure on buoys or ships. Satellite measurements probably offer a possibility to circumvent some of these difficulties. In the last two decades many efforts have been spend in developing methods to derive geophysical parameters like water vapour content, radiative fluxes, etc. from geostationary and polar orbiting satellites. Retrievals developed for radiometers on polar orbiting satellites like the AVHRR (Advanced Very High Resolution Radiometer) on the NOAA series or the SSM/I (Special Sensor Microwave/Imager) on the DMSP programme are distinguished by accuracies that are competitive to in situ measurements or even better.

Methodology

This section describes the satellite retrievals, parameterisations, and empirical assumptions that are necessary to determine the freshwater flux at the air-sea interface.

Parameterisations and retrievals

The evaporation at the sea surface is parameterised using the bulk approach. The wind speed u, the saturation specific humidity at the sea surface q_s, and the atmospheric specific humidity q are determined from satellite measurements. For u a retrieval of Schlüssel and Luthardt (1991) is used that determines the wind speed at a level of 10 m mainly from the brightness temperature difference between horizontally and vertically polarised components at frequencies of 19 and 37 GHz from SSM/I data. Intercomparison to buoy and ship measurements revealed an r.m.s. error of approximately $2\,\mathrm{ms}^{-1}$ with no bias. Other retrievals also used in the intercomparison show an almost competitive behaviour.

The most difficult part of the story on the microwave side was the determination of q. Different authors have developed retrievals to determine the total precipitable water of the atmosphere (W), e.g. Schlüssel and Emery (1990) and Wentz (1994). This kind of retrieval had first been used to compute monthly mean values of the atmospheric humidity near the surface (Liu, 1986). In the beginning of the nineties it was realised that it could be possible to retrieve not only the total precipitable water but also the boundary layer water vapour content from SSM/I data. A first retrieval was realised by Schulz et al. (1993) that delivers the integrated water vapour content of the lowest – 500 m of the atmosphere (w). This quantity is highly correlated ($r > 0.9$) and linearly related to the specific humidity near the ocean's surface. Chou et al. (1995, 1997) have used both retrievals (W and w) within an EOF method to compute global fields of atmospheric specific humidity. The currently used method of Schlüssel (1996) has corrected the technique of Schulz et al. (1993) concerning some biases in polar ocean basins.

The saturation specific humidity at the sea surface is essentially a function of the sea surface temperature. Since the continuous handling of such large data sets like the AVHRR raw data requires large amounts of computer and man power it was decided to use the NOAA/NASA Oceans Pathfinder Sea Surface Temperature product. These products are available as daily fields with a spatial resolution of 9 km at its best. The daily fields are combined with the instantaneous retrievals of u and q on a rectangular grid.

Lastly, some empirical assumptions have to be incorporated in the computations. The most important is an assumption about the atmospheric stability to compute the transfer coefficient. Within the scheme of Smith (1988) it is assumed that the atmosphere has a relative humidity of 80% at any time. With that assumption the air temperature can be computed from the measured q. The errors in the transfer coefficient that occur if this assumption is wrong are between 2% at high wind speeds and strong unstable conditions and 50% at low wind speeds and strong stable conditions (Schulz et al., 1997). Fortunately, areas with a stable temperature stratification are not very large compared to the global ocean and don't occur too often so that the described errors in the transfer coefficients don't affect monthly or annual time averages for ocean basins too much. Other assumptions concerning the surface pressure or air density are not of great importance for the present climatology.

Measurements of rainfall at the sea surface with radiometers in space have been the topic of many studies in

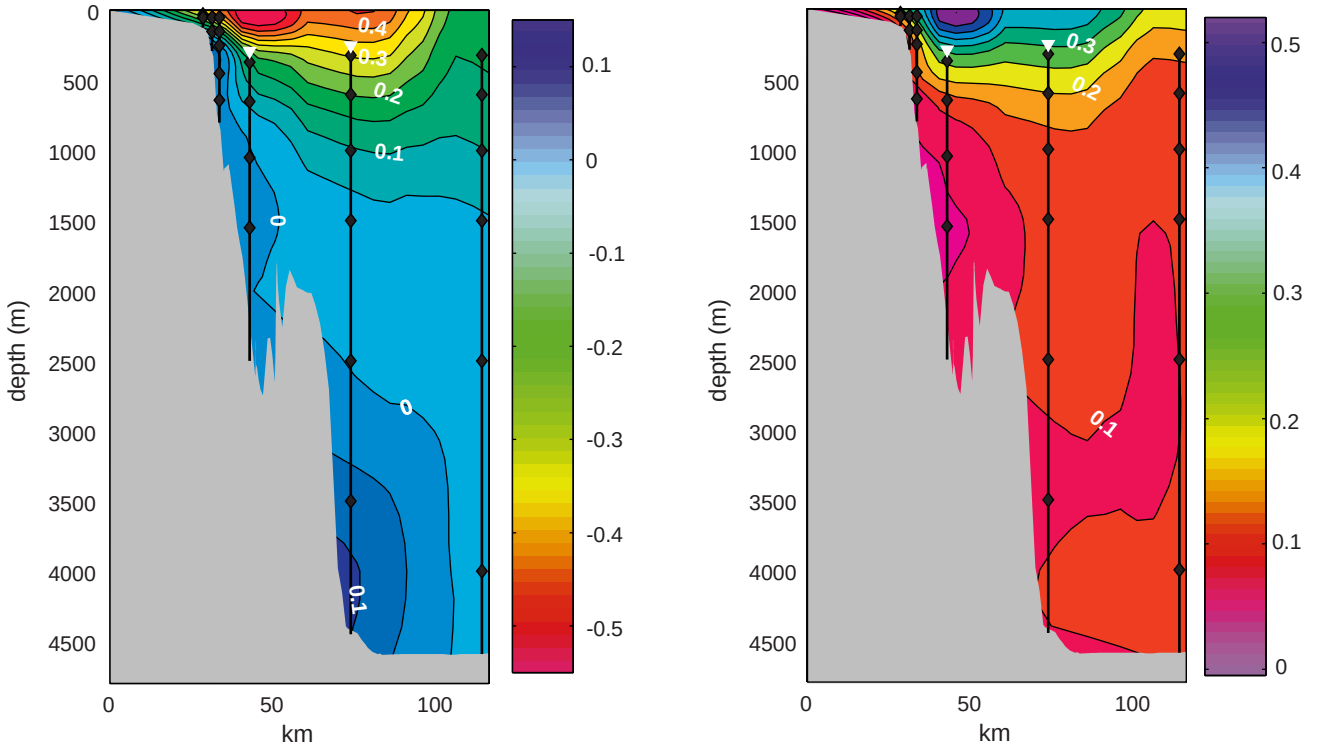

Mata et al., page 18, *Figure 4. Mean meridional velocity (left) and standard deviation (right). In the left picture, negative values indicate southward flow. All units in* $m\,s^{-1}$.

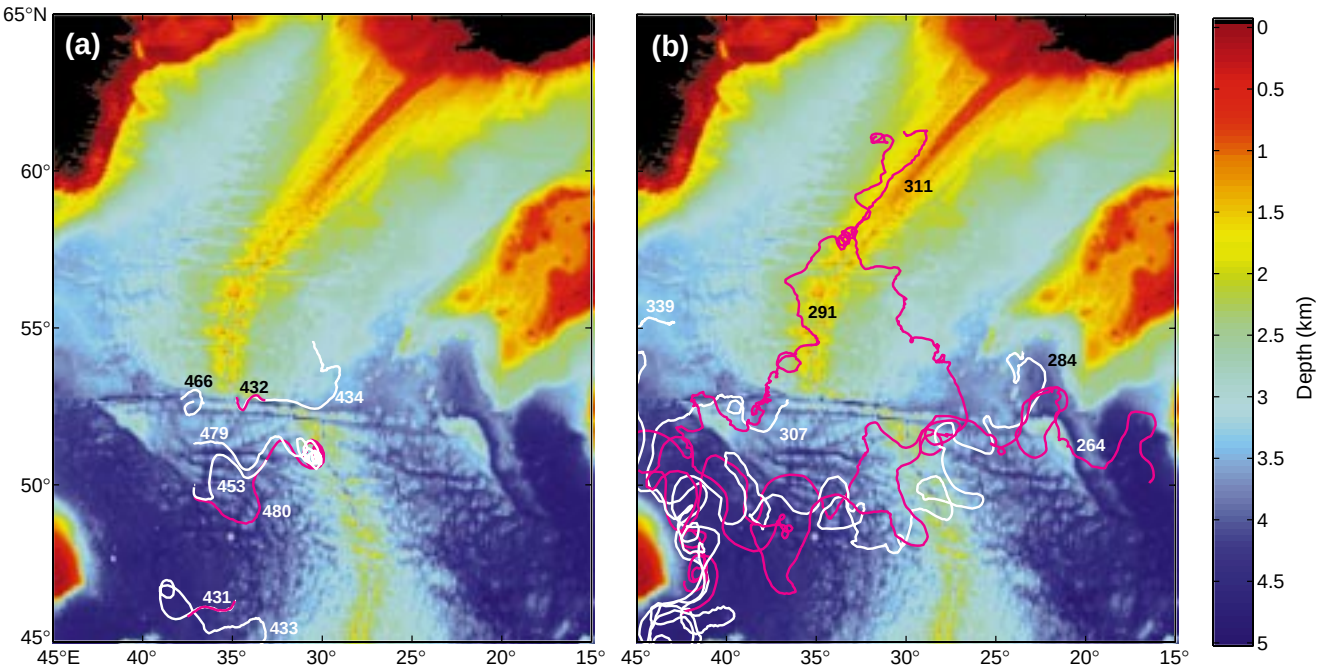

Rossby, et al., page 32, *Figure 2. Selected ACCE (a) and NAC (b) float trajectories. Background and colour bars represent the bathymetry depths. Colour trajectories are used for easy reading in the colour background. Float mission lengths are: 300 days for floats 291, 311, 264, 284; 180 days for float 307; 240 days for float 339; 30 days for floats 431 and 432; 120 days for floats 433 and 434; 45 days for floats 453 and 466; and 150 days for floats 479 and 480.*

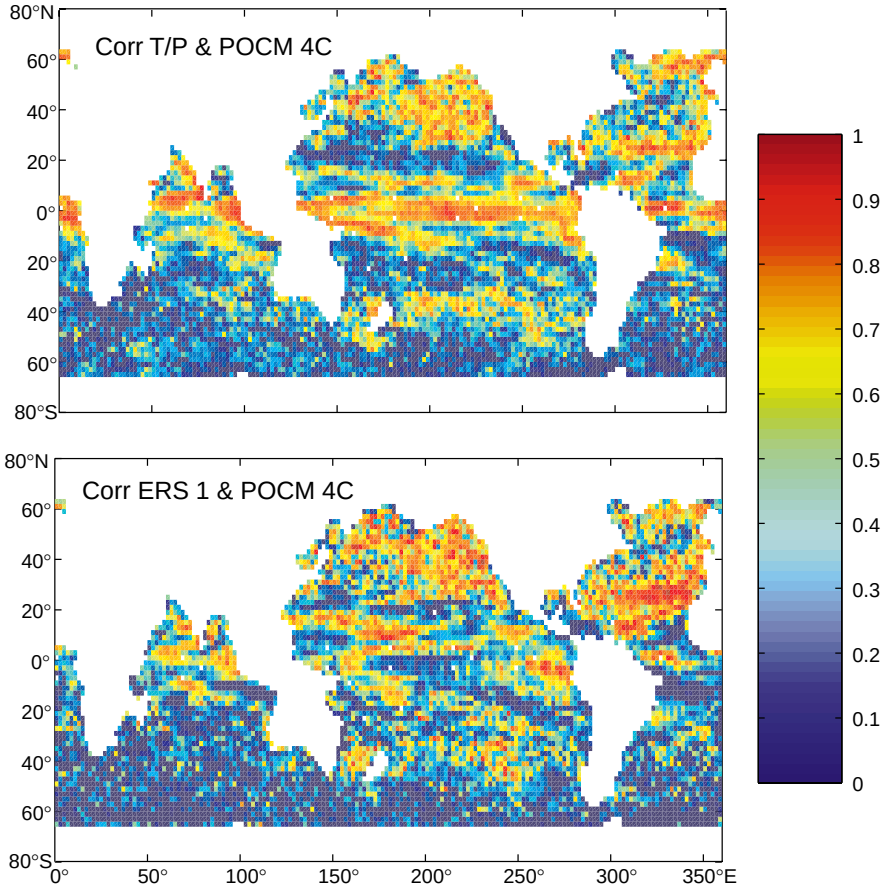

Tokmakian, page 26, *Figure 1. Correlation maps between model and TOPEX/ POSEIDON altimeter data from October 1992 to 1996 (upper). Same except with ERS-1 data for April 1992 through 1995 (lower).*

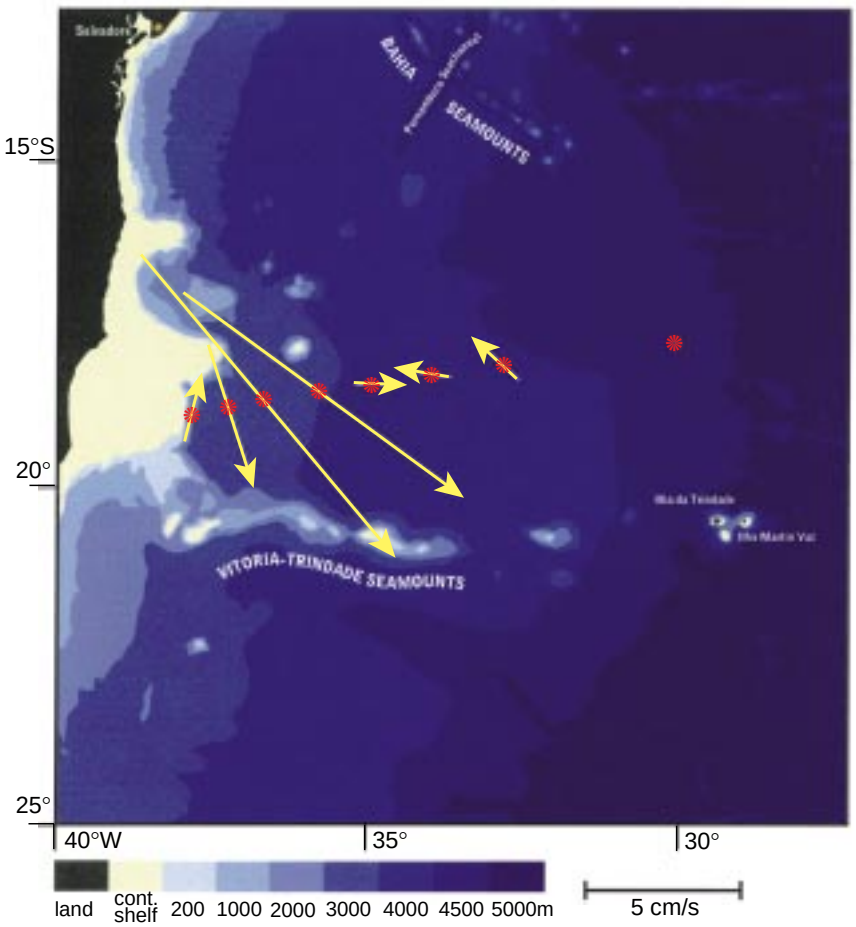

Weatherly et al., page 16, *Figure 2. Average velocity vectors for the current meters at 1800 m depth. The red asterisks are the moorings. The DWBC is indicated as flowing to the southeast and being about 200 km wide.*

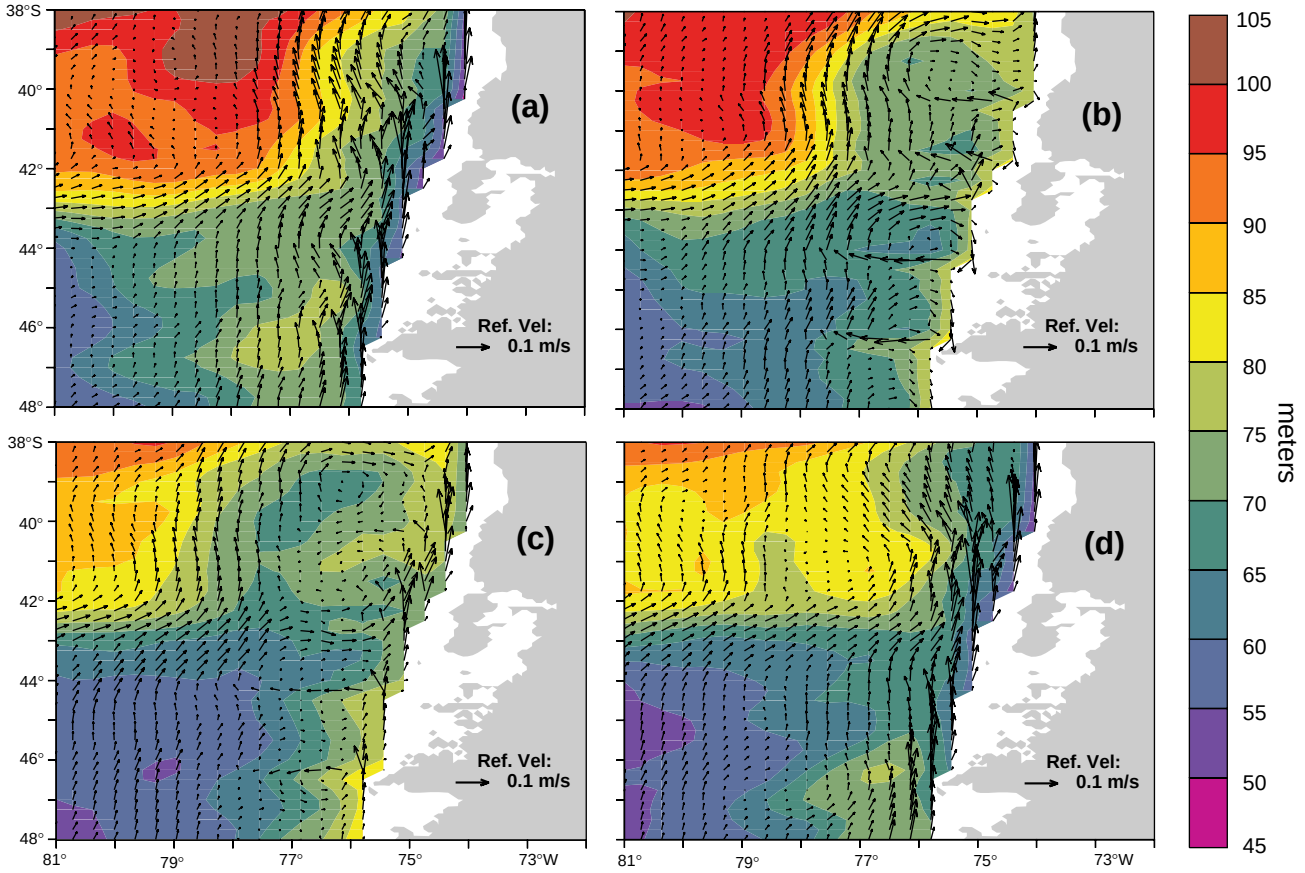

Nuñez and Rojas, page 40, *Figure 5. Finite depth model results for WOCE PR14 sampling area. Averaged flow (vectors) and interface depth (colour contours) field between 1984–1994 are shown for (a) January–February–March, (b) April–May–June, (c) July–August–September, and (d) October–November–December.*

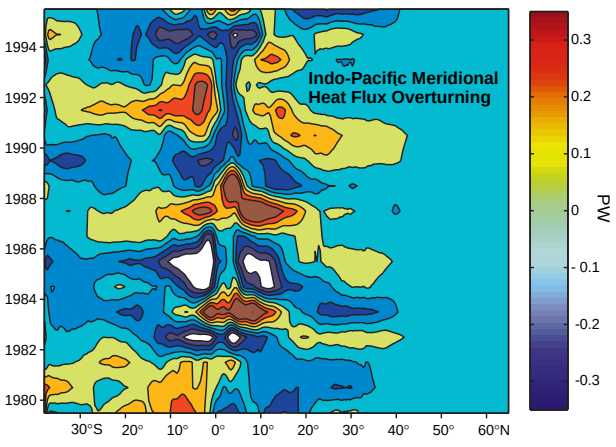

Tokmakian, page 26, *Figure 4. Meridional heat flux computed from model over 17 years for the Indo-Pacific region, annual and semi-annual signals removed.*

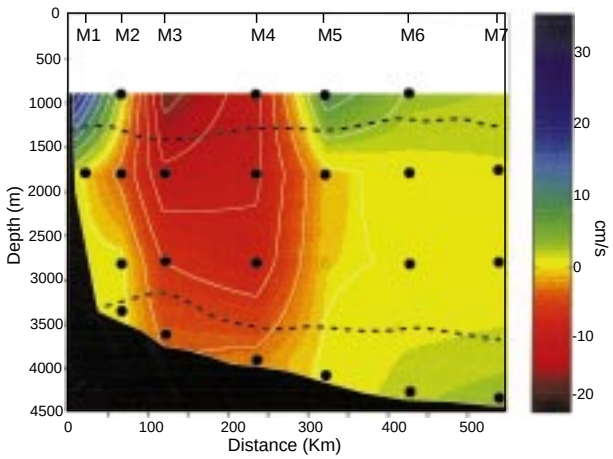

Weatherly et al., page 16, *Figure 3. Contours of the record mean current component oriented along 320°–140°; negative values denote flow towards 140°. Mooring numbers are given at the top, and current meter locations are indicated by solid circles. The bounding isopycnals for NADW, $\sigma_2 = 36.7$ and $\sigma_4 = 45.87$, are indicated by the dashed curves and are taken from data discussed in Smethie and Weatherly (1996).*

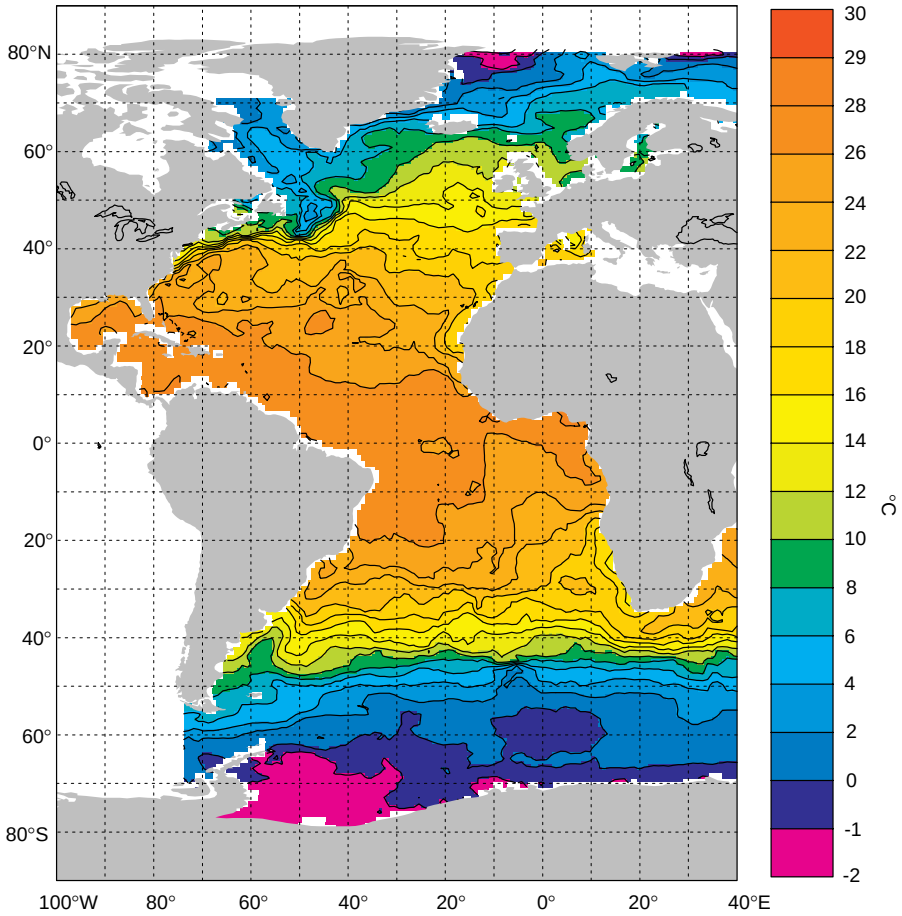

Reynaud et al., page 29, *Figure 2. Annual mean surface potential temperature (°C).*

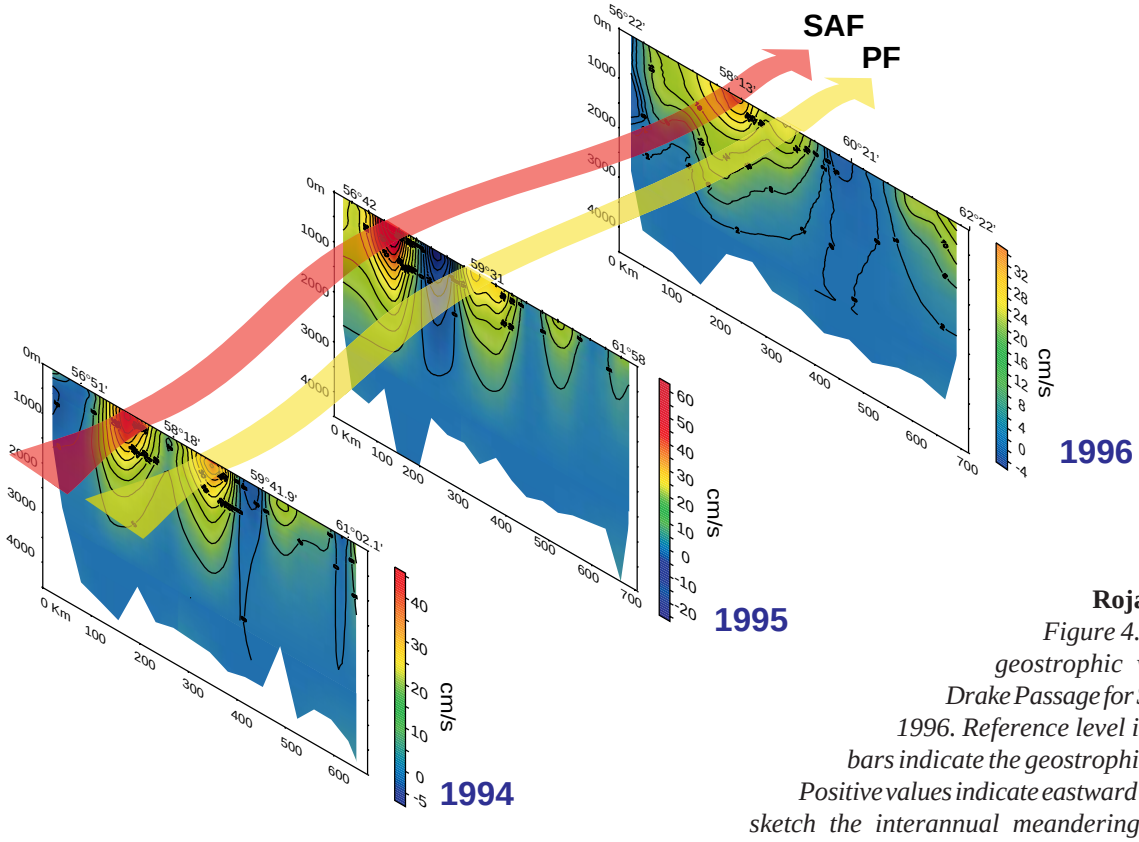

Rojas et al., page 38, *Figure 4. Yearly section of geostrophic velocities across Drake Passage for SR1 cruises 1994–1996. Reference level is 3000 m. Colour bars indicate the geostrophic velocity in cm/s. Positive values indicate eastward velocities. Arrows sketch the interannual meandering of Subantarctic Front (SAF) and Polar Front (PF).*

recent years. In an early stage of the preparation of the climatology it has been decided to use the rain algorithm of Bauer and Schlüssel (1993). This algorithm has been successfully tested within the Precipitation Intercomparison Project (PIP) and the Algorithm Intercomparison Projects (AIP).

Additionally, to the variables needed for computations of *E-P* the radiative longwave net flux has been included in the climatology. The longwave net flux is computed by a scheme described in Schlüssel et al. (1995).

Example

To demonstrate the ability of the climatology to monitor climatic features like the onset of the Indian summer monsoon Fig. 1 shows a one year time series of monthly averages during 1993 for a 2° by 2° grid box. The onset can clearly be identified in June 1993 by a sharp increase of the precipitation curve. This is accompanied by a slight increase in wind speed and a larger decrease in $q_s - q$ during the whole northern summer. Hence, the freshwater flux (*E-P*) is positive throughout the winter and spring, negative during the summer months, and near zero after the monsoon phase. More advantageous in determining the onset date of the monsoon is the use of the available daily fields. It should be noted that the precipitation value of zero from December 1992 to May 1993 indicates a severe drought that is not unlikely but it should be kept in mind that this might be a consequence of the inadequate sampling through the use of only one satellite.

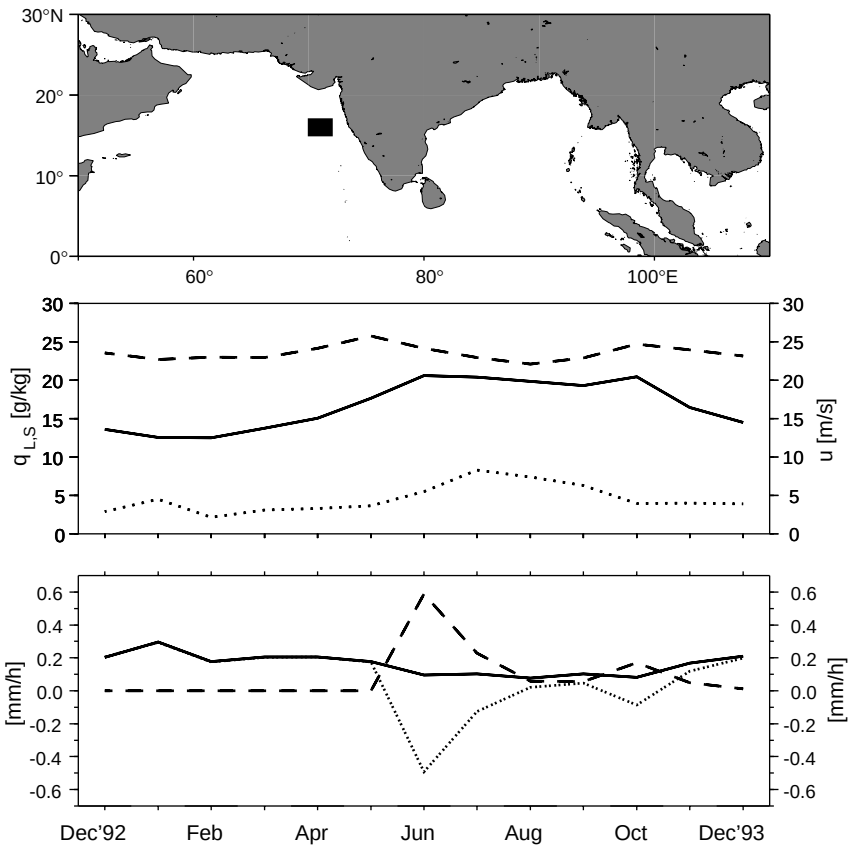

Figure 1. Local case study in a $2° \times 2°$ region during 1993 in the northern Indian Ocean. The upper panel time series represent the monthly means of surface wind speed (dotted line), near-surface humidity (solid line) and the specific humidity of the sea surface (dashed line), whereas the lower time series represent the monthly means of evaporation (solid line), precipitation (dashed line) and the water balance (dotted line).

Limitations

Obviously, the present satellite-derived climatology has limitations. Since large parts of the climatology are based on only one satellite at a time a serious sampling error mostly concerning precipitation could be expected. A case study with data gained during the TOGA COARE campaign showed that the sampling error for grid resolutions of 2° by 3° and a sampling time of 3 weeks can be as high as 20% if only one satellite overpass per day was available. If two SSM/Is were used this error is diminished to less than 4%. So a recomputing of the time series using all available satellite data is a major task for the future.

Another systematic error that is not fully explored today is caused by the use of radiometers on different platforms (AVHRR on NOAA and SSM/I on DMSP). It is expected that this error is rather small because the sea surface temperature gained from AVHRR data is a relative stable quantity compared to the atmospheric variables gained from SSM/I measurements. But this argument holds only if the measurements of sea surface temperature is not hampered for weeks by persistent cloudiness or long periods of darkness as over polar regions when the sea surface temperature could be biased through the more difficult cloud detection in the infrared range.

Additionally, the climatology is limited by the fact that the river runoff into the ocean is not implemented. The observed monthly averages of runoff for several rivers are available (Dümenil et al., 1993) and there is no principle obstacle to use them to check the long term mean of the *P-E* fields.

Availability

The HOAPS data set covers at the moment a time period of 10.5 years (July 1987–December 1996), is freely available for the use by other scientific groups, and will be continued in the future. The following satellite-derived parameters were sampled onto a global grid with three different spatial resolutions (0.5°, 1°, 2.5°) and averaged for three different time resolutions (day, pentad, month):

latent heat flux [$W\,m^{-2}$]
evaporation [$mm\,h^{-1}$]
precipitation [$mm\,h^{-1}$]
water balance [$mm\,h^{-1}$]
near surface humidity [$g\,kg^{-1}$]
specific humidity of the surface [$g\,kg^{-1}$]
wind speed [$m\,s^{-1}$]
sensible heat flux [$W\,m^{-2}$]
longwave net radiation [$W\,m^{-2}$]

The data are available on anonymous ftp on request. A World Wide Web page is under construction and will be available in fall 1998.

The poster that was shown on the 1998 conference of the World Ocean Circulation Experiment in Halifax, Canada, can be downloaded as a postscript file at http://www.dfd.dlr.de/papers/SchulzJ98a or http://sop.dkrz.de/jost/papers/WOCE98_A0.ps.gz.

References

Bauer, P., and P. Schlüssel, 1993: Rainfall, total water, ice water, and water vapor over sea from polarized microwave simulations and Special Sensor Microwave/Imager data. J. Geophys. Res., 98, 20737–20759.

Chou, S.-H., R. M. Atlas, C.-L. Shie, and J. Ardizzone, 1995: Estimates of surface humidity and latent heat fluxes over oceans from SSM/I data. Mon. Wea. Rev., 123, 2405–2425.

Chou, S.-H., C.-L. Shie, R. M. Atlas, and J. Ardizzone, 1997: Air-sea fluxes retrieved from special sensor microwave imager data. J. Geophys. Res., 102, 12705–12726.

Dümenil, L., K. Isele, H.-J. Liebscher, U. Schröder, M. Schumacher, and K. Wilke, 1993: Discharge data from 50 selected rivers for GCM validation. Max-Planck-Institut für Meteorologie, Tech. Rep., 100, Hamburg.

Liu, W. T., 1986: Statistical relation between monthly mean precipitable water and surface-level humidity over global oceans. Mon. Wea. Rev., 114, 1591–1602.

Schlüssel, P., 1996: Satellite remote sensing of evaporation over sea. Radiation and water in the climate system: Remote measurements, edited by Erhard Raschke, NATO ASI Series, Vol. 145, Springer Verlag, Heidelberg, 431–461.

Schlüssel, P., and W. J. Emery, 1990: Atmospheric water vapour over oceans from SSM/I measurements. Int. J. Remote Sensing, 11, 753–766.

Schlüssel, P., and H. Luthardt, 1991: Surface wind speeds over the North Sea from Special Sensor Microwave/Imager observations. J. Geophys. Res., 96, 4845–4853.

Schlüssel, P., L. Schanz, and G. Englisch, 1995: Retrieval of latent heat fluxes and longwave irradiance at the sea surface from SSM/I and AVHRR measurements. Adv. Space Res., 16, 107–116.

Schulz, J., P. Schlüssel, and H. Graβl, 1993: Water vapour in the atmospheric boundary layer over oceans from SSM/I measurements. Int. J. Remote Sensing, 14, 2773–2789.

Schulz, J., J. Meywerk, S. Ewald, and P. Schlüssel, 1997: Evaluation of satellite-derived latent heat fluxes. J. Climate, 10, 2782–2795.

Smith, S. D., 1988: Coefficients for sea surface wind stress, heat flux, and wind profiles as a function of wind speed and temperature. J. Geophys. Res., 93, 2859–2874.

Wentz, F. J., 1994: User's manual SSM/I-2 geophysical tapes. Tech. Rep. 070194, 20pp. [Available from Remote Sensing Systems, Santa Rosa, CA, USA.]

A High Resolution Ocean Model with Variable Forcing of Wind, Heat, and Freshwater: Initial Evaluation

Robin Tokmakian, Naval Postgraduate School, USA. robint@ucar.edu

A new model (POCM_4C) run of the high resolution ($^1/_4°$ Semtner/Chervin Parallel Ocean Climate Model) has been completed which incorporates the use of daily varying surface fluxes of momentum, heat, and freshwater over a period of 18 years from 1979 though 1996 (soon to be through 1998). The basic formulation of the model is described in Semtner and Chervin, 1992. The model run differs from the previous run (POCM 4B Stammer et al., 1996) by the modification of the tracer equations for temperature and salinity to incorporate realistic time varying fluxes. The previous model run included only time varying winds with a monthly heat and freshwater climatology applied. The fluxes used to force the current simulation are computed from the ECMWF reanalysis data set for the period of 1979 to 1993; after which the operational fields from ECMWF are used for the forcing (1994–present). Part of the goal of these model runs is to attempt to understand the intrinsic variability in the model versus that which is forced from the variable surface conditions on time scales longer than annual. It is a further goal of this research to examine which surface signals can be used to monitor subsurface changes related to the various climate indices (e.g. North Atlantic Oscillation or North Pacific Indices).

Comparison of surface fields to observational time series

To establish the realism of the circulation present in the model, it is necessary to quantify the circulation using observations. Comparisons are shown below using time series from tide gauges, altimetric data, and ocean weather station data. Similar comparisons have been made using the TOGA/TOA measurements.

Variability of sea surface height

Several data sets are available to evaluate the realism of the sea surface height estimates made by the model. The only near global data sets are those that are sampled by satellite instruments such as altimeters. Fig. 1 (page 22) shows a map of correlation coefficients of the model's SSH field with that of T/P and ERS-1 (Koblinsky et al., 1998). The model is forced with a consistent data set (ECMWF reanalysis) and assuming its own intrinsic errors are constant over the model run, the model itself can be used to provide a connection between different altimeter data sets from GEOSAT through the TOPEX/POSEIDON and ERS-1/2.

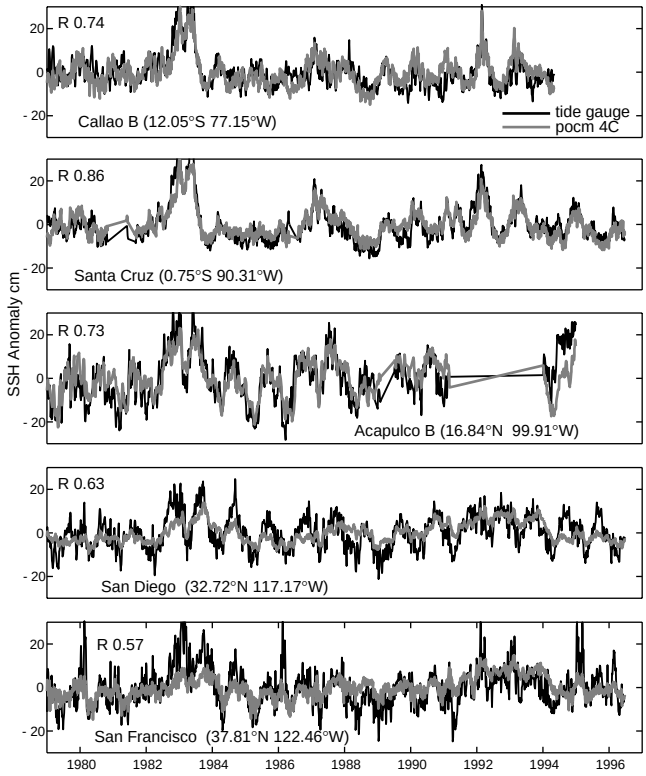

Figure 2. Tide gauge and model comparison of SSH anomalies along the west coast of the Americas.

The correlation maps (data and model output binned $2° \times 2° \times 1\text{month}$) show similar patterns such as the high correlations in the northern hemisphere over those in the southern hemisphere. This hemispheric difference is possibly due to a less accurate wind field forcing the model in the southern hemisphere over that used in the north (fewer observations contribute to the wind product). Significant differences between the two maps can be seen in the tropical region. This is due to the different sampling characteristics of the satellites, T/P samples the tropical ocean every ten days while ERS-1 has a repeat cycle of 35 days. It is also interesting to note that the correlations with ERS-1 are higher than when the model is correlated with T/P in the subtropical region of the North Atlantic. Time series from this region show that ERS-1 and the model have relatively smooth variations in time, while T/P data contains a high frequency signal not seen in ERS-1 data or the model.

Likewise, long term measurements (20 years) of sea level made by tide gauges can be used to evaluate the model's SSH field. Using the time series of sea level measurements available through the Joint Archive for Sea Level at the University of Hawaii, comparisons of the time series to the model's SSH estimates show a remarkable agreement between the in situ SSH and the model's SSH, especially in the tropical region and up the coast of the Americas (Fig. 2).

These two different data sets of SSH quantify the accuracy of the model in two different ways. The tide gauges give a measure of the model's accuracy from the beginning of the model run through the present, but only at coast or island locations. By comparison, the altimeter spatially quantifies the SSH field globally, but only over a short period of time (5 years). By using these fields together, the model's SSH field is quite realistic in time in the northern hemisphere except between 20° to 30°N, the Gulf Stream area and the Kuroshio Extension.

Variability of temperature and salinity

Long in situ time series of temperature and salinity are more difficult to locate for comparison to the surface or subsurface fields of the model. Ocean Weather Station (OWS) data, although not ideal, can help to quantify the realism of the top layers of the model. Fig. 3a and b show times series of the model's surface salinity and temperature fields at OWS Papa as compared to observations. The model is reproducing the annual cycle of the temperature field. However, the amplitude appears to be somewhat too high. The salinity data is more sparse, but does resemble the in situ measurements.

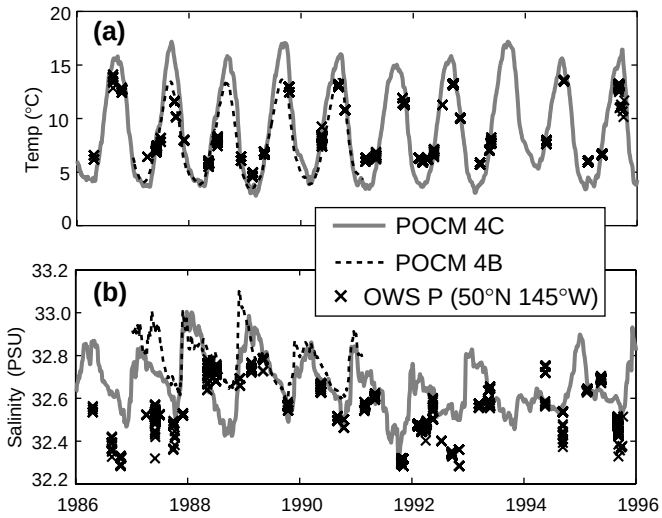

Figure 3. (a) Sea surface temperature measurements from Ocean Weather Station Papa and model. (b) Same except for sea surface salinity.

Variability of heat and freshwater transports

Integrated quantities, such as meridional heat and freshwater fluxes, are useful to examine the large scale, low frequency variability of the model. The heat flux can be broken into the components of overturning, gyre, and Ekman in order to look at the influence each has on the variability of the total meridional heat flux. Fig. 4 (page 23, annual and semi-annual cycles have been removed) shows a latitude-time plot for the Indo-Pacific for the sum of the Ekman and overturning components computed from monthly values

over 17 years of the model run. The gyre component is much smaller than the overturning and most of the overturning is related to the Ekman component of the flow. If the overturning component is correlated with the North Pacific Index (Trenberth and Hurrell, 1994; mean sea level pressure 30°N–65°N, 160°E–140°W), the highest correlation is around 35°–40°N and falls off to on either side with latitude (O(0.7)). With the removal of the Ekman portion, the correlation drops to O(0.4). This implies that the model's low frequency variability in the North Pacific is largely due the Ekman transport associated with the wind field.

A time series (Fig. 5) of monthly values of the overturning heat flux (annual and semi-annual signals removed) at 24°N in the Pacific shows high variability with a standard deviation of ±0.31 PW. The long term mean of the heat flux (0.48 PW) is within the range estimated from observations (0.45±0.26 PW Macdonald and Wunsch, 1996): 0.38 PW supplied by Ekman transport, 2.4 PW transported northward by the Kuroshio and a southward flux of 2.24 PW by the mid-ocean overturning, with the remaining contribution from the gyre circulation.

A similar decomposition of the heat flux can be applied to the Atlantic. The Ekman contribution to the total overturning is not as significant as in the Pacific (figure not shown). Further analysis of the model output should help in the understanding what causes the variability seen in the Atlantic heat flux overturning in the model.

Fig. 6 shows the total freshwater flux over 17 years. The curves for the Indo-Pacific and the Atlantic have been adjusted to include the flow into or out of the Arctic Ocean (Wijffels, 1992). With the adjustment, the model's freshwater flux resembles the values computed from observations, except in the South Atlantic where the model has either too much southward flow of freshwater or too little freshwater going northward.

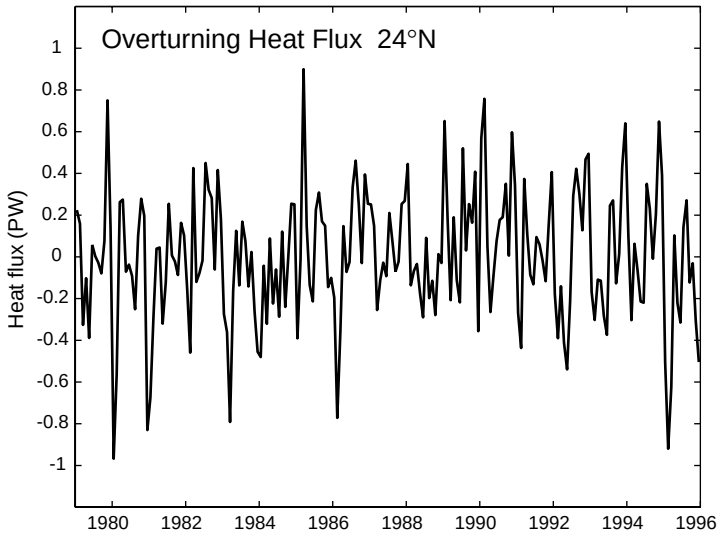

Figure 5. Monthly values of heat flux at 24°N in the Pacific (PW).

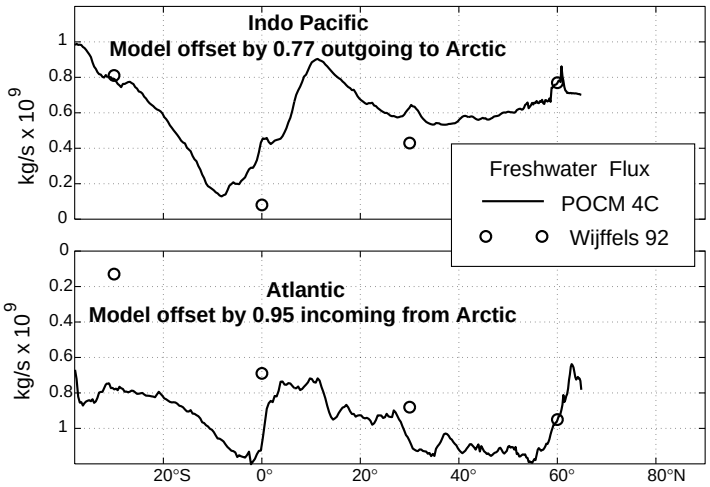

Figure 6. Mean total freshwater flux from the model and data (Wijffels et al., 1992). Units are $kg/s \times 10^9$.

Summary

The new model shows increased variability in temperature and salinity in the upper levels of the model. Further analysis of this model run and its predecessor (POCM 4B) will help in the understanding of the importance of variable heat and freshwater forcing at the surface and the role of the variable wind forcing of the low frequency variations of the model. The output from the model runs are available to the community and further information about accessing the output can be found at **www.scivis.nps.navy.mil/~rtt**. The model provides an opportunity to understand one-time sampled WOCE sections in the context of a variable ocean.

Acknowledgement

Funding provided by NSF under WOCE, DOE funding provided under CHAMMP programme, NCAR for use of computer facilities, OWS-Papa data from H. Freeland, tide gauge data from M. Merrifield, University of Hawaii, H. Bryden for input on the heat fluxes.

References

Koblinsky, C., et al., 1998: NASA/GSFC Ocean Pathfinder, http://neptune.gsfc.nasa.gov/ocean.html.

Macdonald, A., and C. Wunsch, 1996: Oceanic estimates of global heat transport. Int. WOCE Newsletter, 24, 5–6.

Semtner, A. J., and R. M. Chervin, 1992: Ocean general circulation from a global eddy-resolving model. J. Geophys. Res., 97, 5493–5550.

Stammer, D., R. Tokmakian, A. J. Semtner, and C. Wunsch, 1996: How well does a $^1/_4°$ global ocean model simulate large-scale observations? J. Geophys. Res., 101, 25779–25811.

Trenberth, K., and J. W. Hurrell, 1994: Decadal atmosphere-ocean variations in the Pacific. Climate Dynamics, 9, 303–319.

Wijffels, S. E., R. W. Schmitt, H. L. Bryden, and A. Stigebrandt, 1992: Transport of freshwater by the oceans. J. Phys. Oceanogr., 22, 155–162.

A New Analysis of Hydrographic Data in the Atlantic and its Application to an Inverse Modelling Study

T. Reynaud, Laboratoire des Écoulements Géophysiques et Industriels, IMG, France; P. LeGrand and H. Mercier, Laboratoire de Physique des Océans, IFREMER (Centre de Brest), France; and B. Barnier, Laboratoire des Écoulements Géophysiques et Industriels, IMG, France. treynaud@hmg.inpg.fr

In the late 70's climatologies of ocean properties have been produced by several authors (Levitus and Oort, 1977; Reid, 1978; and Levitus, 1982) from analyses of temperature and salinity measurements collected since the beginning of this century. The climatology of Levitus (1982) is traditionally used by the modelling community. Although this climatology has been and still is of great help to the scientific community it also has been criticised because important frontal structures have been smoothed out: nearly no North Atlantic Current (NAC), no Deep Western Boundary Current (DWBC). The absence of these structures restricted the use of this climatology in diagnostic studies. Recently, Lozier et al. (1995) carried out an analysis along isopycnal surfaces over the North Atlantic domain which was found to improve significantly the water mass distribution because their analysis scheme preserves density fronts. However, their *along isopycnal* binning procedure does not directly provide values at depth level and requires a subsequent vertical interpolation procedure for modelling applications.

The climatology presented here for the Atlantic Ocean is based on a simple isobaric averaging scheme similar to that used by Levitus but with a higher vertical resolution and a smaller horizontal radii of correlation. This analysis is seen as an improvement because important observed frontal structures are well represented on the gridded fields.

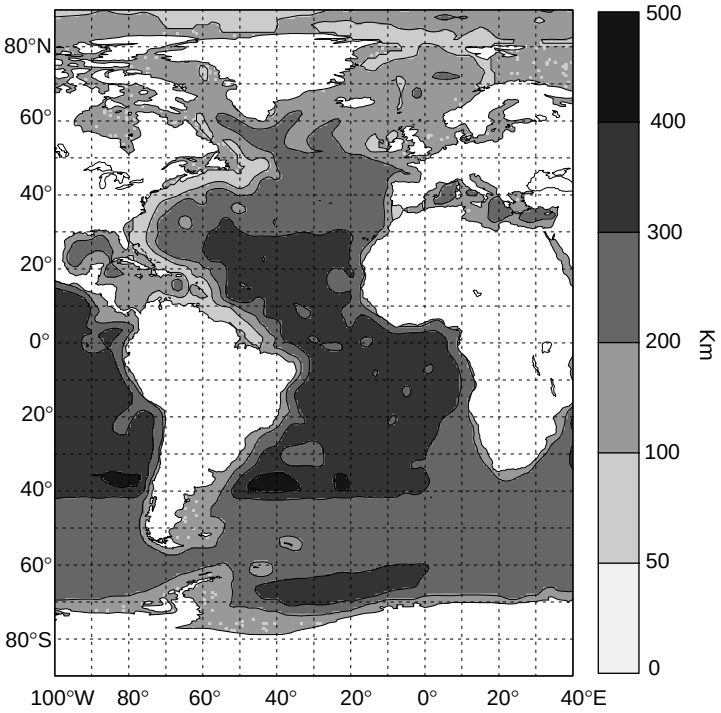

Figure 1. Radius of influence (km).

Table 1. Data set composition before and after the quality control procedure.

Origin	Initial	Final
NODC Bottle	519,016	384,304
NODC CTD (C022)	37,698	26,548
NODC CTD (F022)	38,948	21,054
CTD Brest (WOCE+other)	1,632	1,614
CTD Bremerhaven	1,421	1,294
CTD Scripps	2,763	2,328
CTD US Navy	312	162
CTD WOCE	1,465 +295	1,096 +237
Bottle MEDS	37,416	7,522
CTD Reid	958	910
Bottle WOCE	111	111
Total	642,035	447,180

Data set composition

The data set used in this analysis contains nearly 640,000 hydrographic stations coming mostly from the NODC archive. Some problems were found while processing the NODC data: truncated CTD profiles, double stations, incomplete sections, etc. Consequently, it was found necessary to complete the NODC data set by all available hydrographic stations including the following recent WOCE sections:

Atlantic One-time sections:

A1E, I6, A5, A6-A7-A13-A14-A17, Romanche1 and 3, A9, A10, A11, A12, A15, A21 and S4.

Atlantic WOCE Repeated sections:

AR7E(90-92), AR7W(90-92-93), AR15(90-91-92), AR15(95-96, ETAMBOT 1-2), AR18(92), SR01(92), SR02(90) and SR4(89-90-92).

The description of the composite data set is summarised in Table 1.

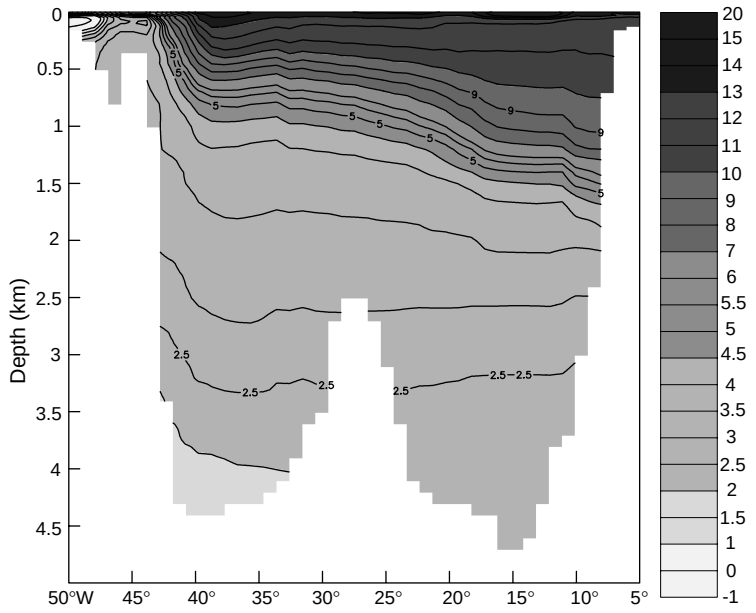

Figure 3. Potential temperature (°C) along section 48°N.

The horizontal domain of this study extended from 100°W–40°E and from 90°S–90°N. The horizontal resolution used is 1° in latitude by 1° in longitude. The vertical resolution is given by the 72 standard levels chosen. The gridded fields are obtained by simply averaging for each grid points all observations located within a prescribed distance. This distance will be referred to as the *radius of influence*, following Levitus (1982).

In contrast with Levitus (1982) and Levitus et al. (1994), this radius is not constant; it is determined as a function of both the bottom topography and data distribution. Its ranges from 50–100 km near coastal regions, to 200–450 km in offshore regions (Fig. 1). The validation of the produced gridded fields is an iterative procedure which consists in finding spurious structures. The responsible hydrographic stations must be identified, problematic values flagged and the procedure restarted. The validation of the oxygen fields is yet not done.

Data process

This composite data set cannot be used directly and must be first quality checked because it contains double stations and suspicious values. The first step of the quality control procedure is to interpolate all the profiles, *temperature*, *salinity and oxygen*, onto 72 defined standard levels. Notice that the maximum vertical spacing used in this study is 100 m. The interpolation scheme used for bottle and low resolution NODC CTD data is such that the interpolation is proceeded onto the closest standard levels to observation depth to avoid the creation of spurious values. The second step of the quality control procedure consists of eliminating double stations and in detecting/correcting anomalies in profiles. This procedure requires to *range check* all the values and to detect spikes and density inversions. It should be noticed that Russian salinities have been carefully treated.

The detailed composition of the final data set is described in Table 1. It was found that nearly 17% of the original data set is made of double-stations. This figure which occurs mainly in coastal regions is likely over-estimated because of the limit of the programme to distinguish between 2 closed stations taken the same day.

The gridding procedure

At this point of the analysis a relatively reliable validated data set has been obtained, the next step will be to analyse it for producing climatological mean fields for temperature, salinity and oxygen. The above quality checked procedure was not fully able to remove all gross errors. Furthermore, the final validated data set contains dedicated experiment profiles like those for the study of *meddies* in the North Atlantic. Such data are not representative of a climatological mean situation and thus are filtered out in the analysis.

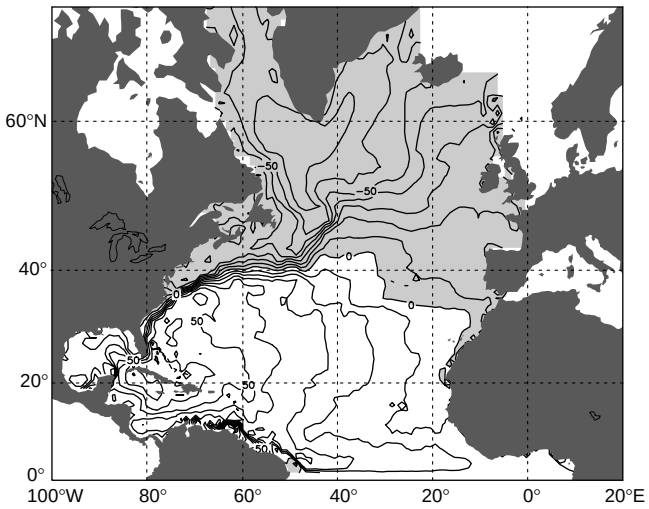

Figure 4. Dynamic topography (cm) from the inverse model. Notice that the basin averaged mean is removed.

In contrast with Levitus (1982) and Levitus et al. (1994) regions with insufficient observations are left flagged. The last step of this gridding procedure is to fill-up these regions. A vertical interpolation is first proceeded when surroundings neighbours are available, a cubic spline is used for that purpose. An objective analysis scheme (De Mey and Menard, 1989) is then applied with correlation radius of 50 to 500 km.

A first look at the annual mean fields

A general statement about this new climatology is that all frontal structures such as the NAC, the Benguela Current or the Antarctic Circumpolar Current, are intensified compared to Levitus et al. (1994). The eastward shift of the NAC near 50°N is also well defined (Fig. 2, page 24) as well as the cyclonic circulation around the Labrador Sea associated

with the West Greenland Current and the Labrador Current.

Another important feature is the DWBC which is observed from the Labrador Sea/Irminger Sea to 30°N along the North American coast (Fig. 3). In offshore regions our climatology is similar to Levitus because respective radii of influence are getting closer. An analysis of the water masses found in this study shows a general agreement with literature. A comparison with Lozier et al. (1995) shows many similarities between their work for the North Atlantic and our gridded fields and indicates that the present procedure is performing despite its simplicity.

An inverse modelling comparison

The geostrophic circulation associated with the present climatology is estimated using the finite-difference inverse model of the Laboratoire de Physique des Océans over the North Atlantic domain. The inverse calculation produces an estimate of the absolute geostrophic velocity over a one-degree grid that is consistent with the climatology density field, large-scale mass and heat conservation, Ekman transports calculated using the ERS wind field products, and the thermal wind balance. The mean dynamic topography estimated by the inverse model (Fig. 4) captures the major fronts associated with the Gulf Stream system, the Azores Current, and the Loop Current in the Gulf of Mexico. A comparison of estimates of the circulation at 250 m depth based on the present climatology (Fig. 5a) and the Levitus climatology (Fig. 5b) shows that the present climatology better resolves the main currents and illustrates the benefit of using a mapping procedure that does not overly smooth property fields. This work is still under progress because problems in the continuity of the DWBC have been encountered south of 30°N.

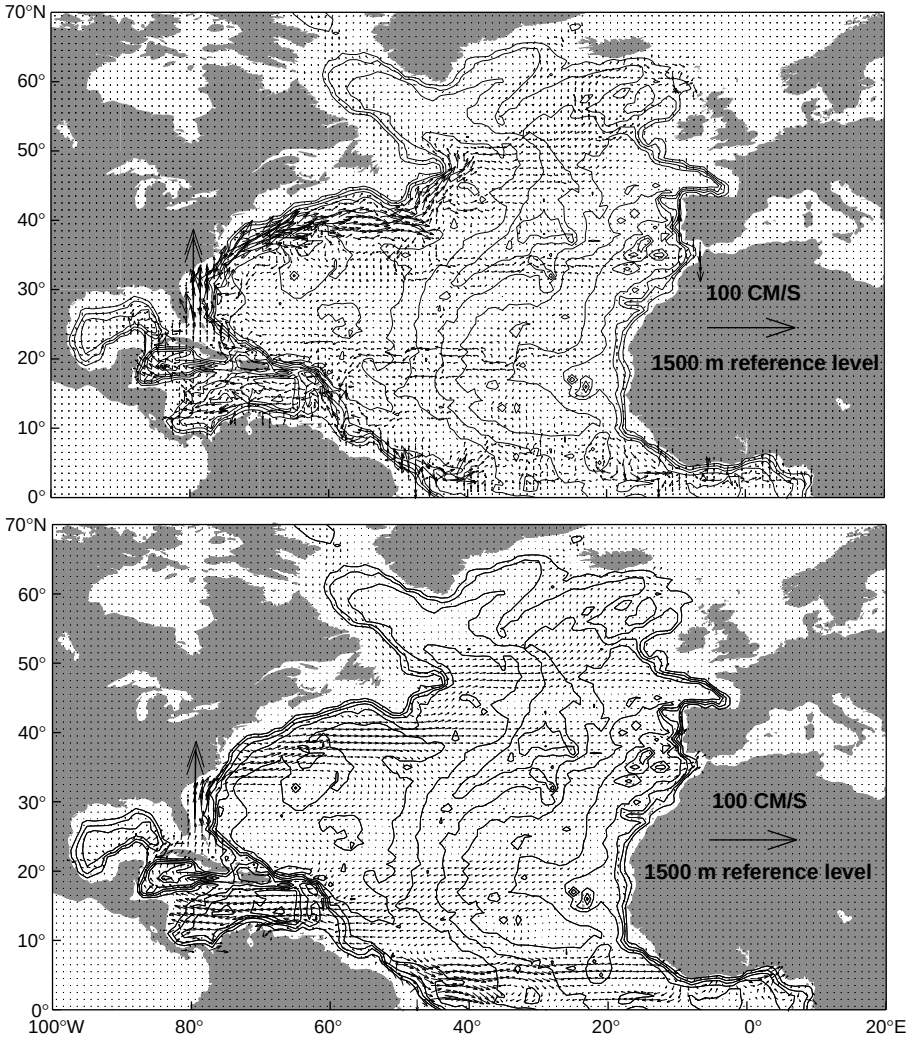

Figure 5. Current at 250 m from the inverse model. Contours indicate bathymetry at 1000 km intervals. Upper: New Climatology. Lower: Levitus et al., 1994.

Conclusion

This climatology has been produced for the needs of the French Clipper modelling experiment. A seasonal analysis has also been proceeded but large holes are found because of the seasonal data distribution which is very poor in some regions (e.g. July–September in the South Atlantic). The winter climatology (January–February–March) was chosen as the most reliable season for initialising the Clipper Experiment. The inverse calculation over the North-Atlantic domain is nearly completed.

Acknowledgements

The authors thank Michel Arhan, E. Fahrbach, Y. Gouriou, Y. Park, A. Poisson, G. Siedler, and W. Smethie for providing access to their data.

References

De Mey, P., and Y. Ménard, 1989: Synoptic analysis and dynamical adjustment of Geos-3 and Seasat altimeter eddy field in the North West Atlantic. J. Geophys. Res., 94, 6221–6231.

Levitus, S., and A. Oort, 1977: Global analysis of oceanographic data. Bull. Amer. Meteor. Soc., 58, 1270–1284.

Levitus, S., 1982: Climatological Atlas of the World Ocean. NOAA Prof. Paper, 13, NOAA, Washington, DC, USA.

Levitus, S., R. Burgett, and T. P. Boyer, 1994: World Ocean Atlas NESDIS, Volume 3-4: Salinity.

Lozier, M. S., W. B. Owens, and R. G. Curry, 1995: The climatology of the North Atlantic. Progr. Oceanogr., 36, 1–44.

Reid, J. L., 1978: On the mid-depth circulation and salinity fields in the North Atlantic Ocean. J. Geophys. Res., 83, 5063–5067.

Isopycnal Float Studies of the Subpolar Front: Preliminary Results

Tom Rossby, Mark Prater, Huai-Min Zhang, Peter Lazarevich, and Paula Perez-Brunius, Graduate School of Oceanography University of Rhode Island, USA.
hzhang@gsosun1.gso.uri.edu

As part of the Atlantic Climate Change Experiment (ACCE) of WOCE, we are deploying isopycnal floats in the Subpolar Front (SPF) just west of the Charlie-Gibbs Fracture Zone (CGFZ) to study pathways of the mean flow and processes of cross-frontal exchange. This region is of particular interest for the Subpolar Front has traditionally been characterised as a zonal flow across the Mid-Atlantic Ridge (MAR), then branching to feed the thermohaline circulation to the north and the wind-driven circulation to the south. Yet the distinct patterns of temperature and salinity on isopycnal surfaces throughout the region indicate that some waters retroflect to the north-west just east of the CGFZ and flow along the Reykjanes Ridge towards Iceland.

Our programme is designed to address the nature and degree of the organised flow over the ridge and the subsequent splitting of waters. We are using unique, oxygen-measuring isopycnal RAFOS floats ballasted for the $27.5\sigma_\theta$ surface.

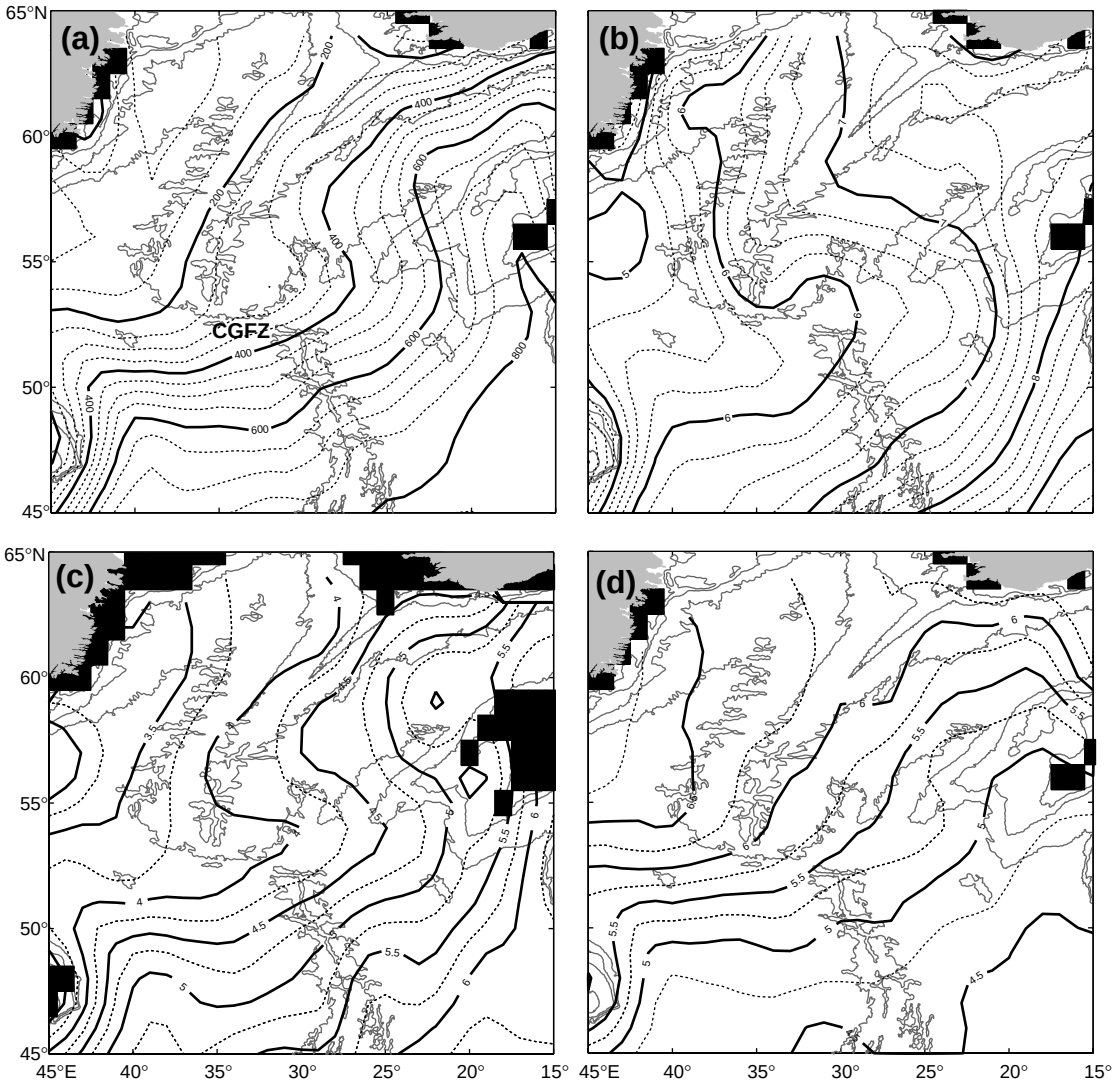

Figure 1. Mean hydrography on $27.5\sigma_\theta$ from forty years of bottle data from NODC. (a) Depth; (b) Potential temperature; (c) Streamfunction relative to $27.8\sigma_\theta$; and (d) Oxygen. Black areas indicate where the $27.5\sigma_\theta$ (1a, 1b and 1d) and $27.8\sigma_\theta$ (1c) do not exist. Thin grey lines indicate the bathymetry contour lines of 1000, 2000, 3000 and 4000 m depths. CGFZ = Charlie-Gibbs Fracture Zone.

Hydrography background

The SPF is a zonally oriented front meandering between 48°N and 52°N, crossing the MAR near the CGFZ (Sy, 1988; Arhan, 1990). The climatological mean potential temperature at $27.5\sigma_\theta$ (with mean depth shown in Fig. 1a) computed from the NODC data set shows how the upper-layer warm waters from the subtropics spread towards the northeast, partly advected by the currents of the NAC (North Atlantic Current) and SPF (Fig. 1b). The salinity field shows a similar pattern. Notice how successive isotherms peel off to the north, going from west to east across the MAR. East of the CGFZ isotherms fan out more broadly, suggesting a more diffuse flow. Some of the warm water turns northeast and some eastward towards Ireland. An interesting question is to what extent these reflect advective processes in the ocean vs. losses of heat to the atmosphere.

Notice the sharp turn to the west-northwest of the isotherms east of the CGFZ and north of 54°N, suggesting an intrusion of warm and salty waters into the Irminger Basin. This results in a nearly congruent retroflection of the acceleration potential contours toward the MAR (Fig. 1c), indicating a flow aligned with the ridge towards Iceland (the Irminger Current) and a weaker flow in the Iceland Basin towards the Nordic Seas. In striking contrast, the oxygen field (Fig. 1d) does not show the intrusion of high oxygen waters into the eastern basin nor the penetration of low oxygen waters into the Irminger Basin. In other words, ψ, θ, and O_2 follow each other closely to 52°N where the flow and temperature fields turn west-northwest, but oxygen contours continue northeast. This disparity raises the question of possible diapycnal fluxes (perhaps due to double diffusion) and of the relative role of advection and diffusion in the area. Our new RAFOS floats are equipped with O_2 sensors, and the combination of oxygen, temperature, and pressure measurements from the floats will help us to address the above questions in better detail.

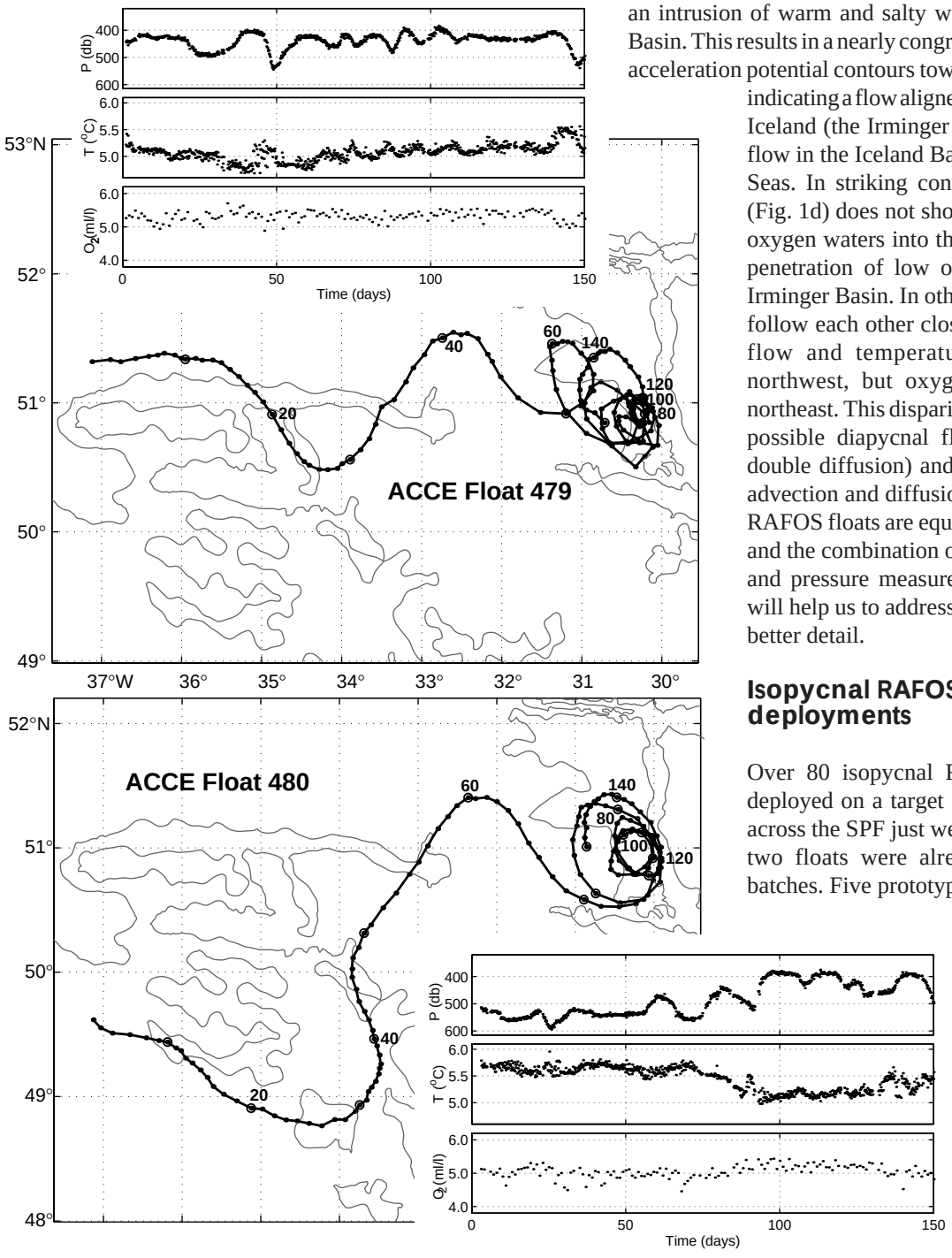

Figure 3. Time series (in float days) of pressure, temperature, and oxygen measurements along the tracks of float 479 (top) and 480 (bottom). Dotted lines in the side panels represent topographic features.

Isopycnal RAFOS float deployments

Over 80 isopycnal RAFOS floats will be deployed on a target surface of $27.5\sigma_\theta$ and across the SPF just west of the CGFZ. Forty-two floats were already deployed in two batches. Five prototype floats were launched in the spring of 1997 during the sound source deployment cruise on the RV Knorr, and 37 floats were deployed in November of 1997 from a cruise on the RV Håkon Mosby. The floats were deployed along 37°W between 49°N and 53°N, at 13 evenly spaced

stations at which CTD-O_2 and water samples were taken. The RV Håkon Mosby then steamed back to Bergen, with XBT measurements taken along the way. The rest of the floats will be deployed at the same stations on a cruise on the RV Knorr from Iceland to Woods Hole in July 1998.

Selected isopycnal RAFOS float trajectories

Shown in Fig. 2a (page 21) are some of the short mission ACCE float trajectories. Prototype float pair 432–434 and pair 431–433 stayed together as pairs for 30 days when one float from each pair surfaced at the end of its mission. The other trajectories are from four of the 1997 fall floats. The meandering trough at 51°N and 35°W is consistent with the mean velocity structure from the NAC floats released 4 to 5 years before. Although float 479 and 480 were released about 190 km apart, they eventually ended up in the same eddy at 51°N but at different times. Their details will be shown in the next section.

Although the ACCE floats surfaced thus far were too few and had too short missions to make a statistical statement about the SPF behaviour after crossing the CGFZ, float 434 did indicate the north-west retroflection of some warm waters. Floats from a previous NAC experiment (Fig. 2b) also revealed such flow patterns. In the NAC experiment, 100 isopycnal RAFOS floats were released in the Newfoundland Basin to both 27.2 and $27.5\sigma_\theta$ surfaces in 1993 and 1994 to study the NAC structure and cross-frontal processes (Rossby, 1996; Anderson-Fontana et al., 1996; Carr et al., 1997). Riding the meandering SPF current and

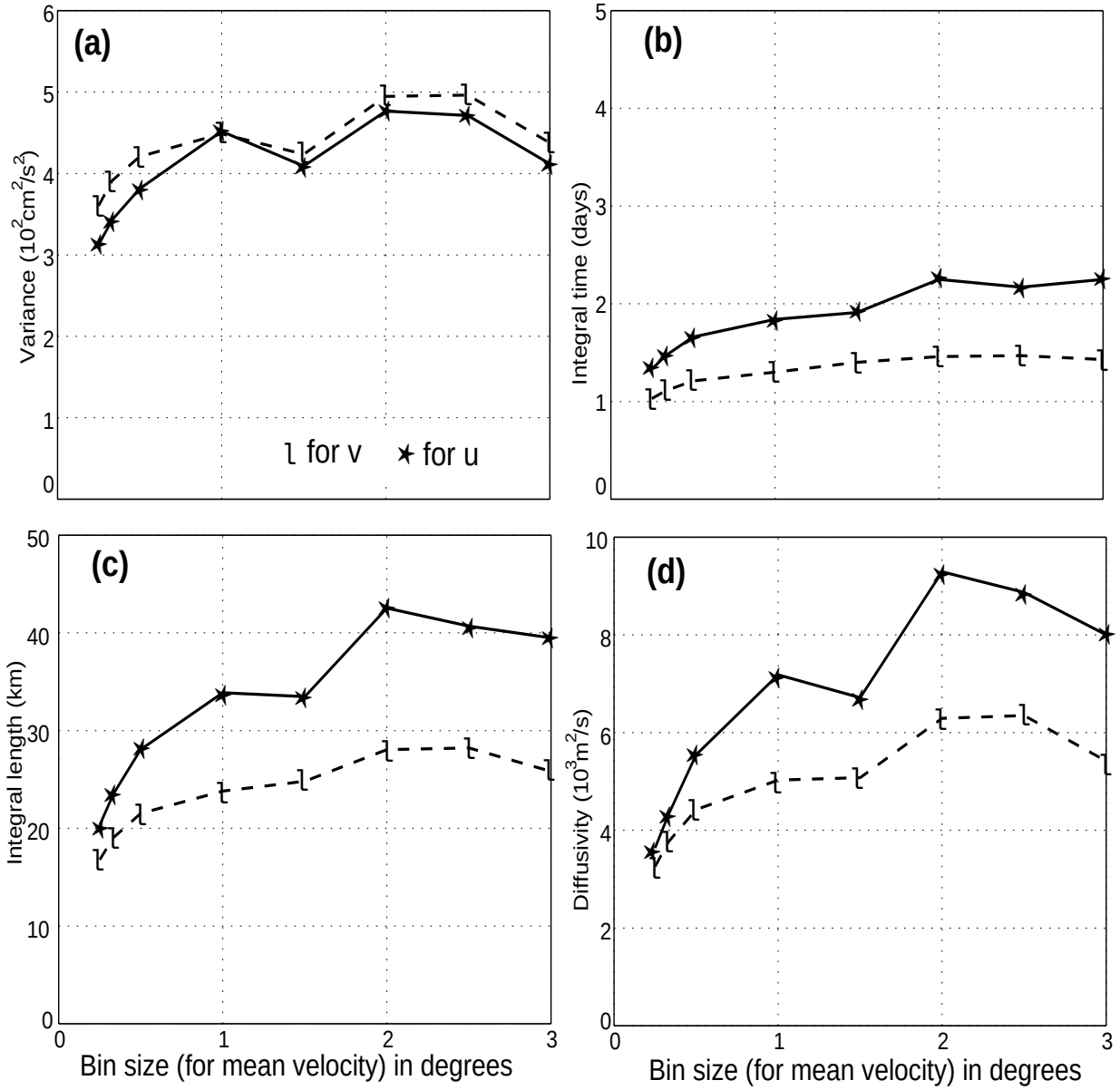

Figure 4. Lagrangian statistics in the SPF region as functions of bin size in resolving the background mean velocity. (a) Variance; (b) Integral time scale; (c) Integral length scale; and (d) Isopycnal diffusivity.

passing the MAR near the CGFZ, float 311 turned north-westward to the southern tip of the Reykjanes Ridge (RR), and then drifted along the western side of the RR. Taking a different path, float 291 slowly crossed the SPF at 38°W and drifted slowly along the RR. However, float 264 drifted zonally toward the Rockall Trough. The assembly of the float trajectories supports the fanning out picture in the temperature and salinity fields (Fig. 1b).

Float measurements of T, P, and O_2

To better aid our study of water-mass exchange along the SPF, we added an oxygen sensor to the RAFOS float. A pulsed technique (Langdon, 1984) makes it possible to operate a standard membrane-type sensor over the lifetime of the floats. Along with increased longevity, this technique virtually eliminates the flow-rate dependence (which causes noise in O_2 from the CTD-O_2 sensors). The oxygen measurement consists of 20 one-second pulses with a 4 minute interval between each pulse. The float position and oxygen are determined once a day, while T and P are measured every 4 hours.

We highlight the data from floats 479 and 480 (Figs. 3a and 3b), which were deployed about 190 km apart (Fig. 2a). The southern float (480) was initially deeper yet warmer than the northern float (479), but both moved in parallel to the east-southeast at 8 to 10 cm/s. When float 480 approached the ridge, it turned to the north and moved towards a point where float 479 had been 20 days earlier. From that point both floats made a looping meander (albeit 20 days apart). This meandering is also evident in the pressure records, whereby the floats are deeper and warmer in the trough (subtropical side) and shallower and cooler in the crest (subpolar side). Both floats were then caught in the same cyclonic eddy at 30.5°W and 51°N. Float 480 experienced a drop in T of 0.5°C and an increase in O_2 of 0.3 ml/l when it entered the eddy, matching existing values of float 479. The floats remained in this stationary eddy for 3 months, at times having orbital speed up to 20 cm/s, before surfacing on schedule.

Lagrangian statistics

Combining the surfaced ACCE floats with the 100 NAC floats, a mean velocity field and Lagrangian statistics can be made for the SPF region west of the MAR. The velocity field reveals the meandering SPF jet, which implies strong lateral velocity shears. In computing the Lagrangian statistics, Taylor theory assumes that the background turbulence is homogeneous. The float motion is a combination of background advection and turbulence. In regions of "strong" lateral mean velocity shear, resolving and subtracting the space-dependent mean velocity are very important before computing the statistics. Otherwise the "trend" is not removed thus biasing the statistics. This is illustrated in Fig. 4, where the velocity variances ($< u'^2 >$, $< v'^2 >$), Lagrangian integral time and space scales, and isopycnal diffusivity, are shown as functions of the bin size in computing the mean velocity. Larger bin sizes (e.g., 2°) cannot resolve the shear velocity structures such as the SPF, thus biasing the variance, integral time and space scales and diffusivity to larger values. Computations for other regions show similar values and patterns.

Summary

We completed a preliminary high-resolution analysis of historical hydrographic data in the Subpolar Front region and have examined our Lagrangian RAFOS float data from the previous North Atlantic Current Study and the present Atlantic Climate Change Experiment. Both data sets support the conjecture that at least part of the SPF retroflects in a broad loop to the north-west just east of the Mid-Atlantic Ridge.

We have started making oxygen measurements from the isopycnal Lagrangian floats. This new application is showing much promise, and we will use these data to verify the above hydrographic picture (particularly the non-congruence of T and O_2 north of 54°N) and to examine the relative roles of advection and eddy diffusion processes in maintaining the distributions of T, S, and O_2 in the retroflection region and beyond. We hope this work will contribute to an improved understanding of the factors (local and remote) that determine the distribution of warm water flow along the Reykjanes Ridge and along the eastern boundary toward the Nordic Seas.

Acknowledgements

We first acknowledge the continuing support of Ms Sandra Anderson-Fontana and Mr Jim Fontaine. We thank the Captains and crews on the RV Knorr and the RV Håkon Mosby who made the cruises successful. The professional assistance from Mr John Kemp is greatly appreciated. This research is supported by NSF OCE-9531878, ONR/NSF N0001492J1651, and CONACYT.

References

Anderson-Fontana, S., M. Prater, and H. T. Rossby, 1996: RAFOS Float Data Report of the North Atlantic Current Study 1993–1995. GSO Technical Report No. 96-4, 241pp.

Arhan, M., 1990: The North Atlantic Current and Subarctic Intermediate Water. J. Mar. Res., 48, 109–144.

Carr, M.-E., E. J. Kearns, and H. T. Rossby, 1997: Isopycnal RAFOS floats as roving hydrographers in the North Atlantic Current region. Geophys. Res. Letters, 24, 551–554.

Langdon, C., 1984: Dissolved oxygen monitoring system using a pulsed electrode: design, performance, and evaluation. Deep-Sea Res., 31, 1357–1367.

Rossby, T., 1996: The North Atlantic Current and surrounding waters: At the crossroads. Reviews of Geophysics, 34, 463–481.

Sy, A., 1988: Investigation of large-scale circulation patterns in the central North Atlantic: the North Atlantic Current, the Azores Current, and the Mediterranean Water plume in the area of the Mid-Atlantic Ridge. Deep-Sea Res., 35, 383–413.

Mechanism of Decadal Variability in the Coupled Ocean-Atmosphere System over the North Atlantic

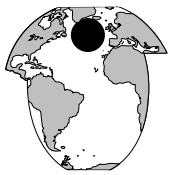

Alexander B. Polonsky, Marine Hydrophysical Institute, Ukraine.
ocean@mhi2.sebastopol.ua

The aim of this note is to continue the discussion of the mechanism of the decadal-scale climate variability in the North Atlantic Ocean initiated by Latif (1997). It is argued that decadal-scale climate variability stems from a coupled ocean-atmosphere mode generated in the North Atlantic. Evaluation of historical observations indicates the importance of changes in the trade winds over the tropical Atlantic and ocean-atmosphere coupling in the entire basin in generating the self-sustained decadal-scale mode. The complete results will be published soon (see Polonsky, 1998).

Ocean variability is a crucial factor in regulating the long-term (interdecadal to multidecadal) changes in the coupled ocean-atmosphere system. The role of the North Atlantic Ocean merits particular attention in this context (Bjerknes, 1964; Deser and Blackmon, 1993; Kushnir, 1994). Changes of the ocean meridional circulation due to variability of high-latitude convection rate in the Atlantic Ocean are a plausible mechanism for generating long-term variability in the coupled ocean-atmosphere system. Concurrently there is a high-amplitude decadal mode in the North Atlantic Ocean. The magnitudes of the decadal and multidecadal modes are of the same order (Deser and Blackmon, 1993; Voskresenskaya and Polonsky, 1993; CLIVAR, 1995).

There are ocean-related candidates for generating low-frequency (including decadal) variability of the coupled system resulting in the climate changes (CLIVAR, 1995):

(a) internal ocean (quasi)-periodical oscillations;
(b) abrupt transitions from one quasi-steady climate state to another;
(c) coupled (including ENSO induced) modes.

Let us consider briefly each of these candidates using selected published results.

(a) According to simulations (Yin and Sarachik, 1995), the oceanic decadal mode is due to inherent feedback between thermohaline advection within the subsurface subtropical layer and convection in the Northern Atlantic Ocean. Chen and Ghil (1995) and Weaver et al. (1994) showed that about 20 year oscillations over the North Atlantic can be generated as a result of feedback between the rate of the high-latitude convection and value of the meridional heat flux (MHF) in the ocean. They point out that these inherent oceanic oscillations can exist without salinity changes and ocean-atmosphere coupling. Philander (1998) argued that the subsurface waters subducted in the subtropical gyre reach the equatorial region in a few years. This means that an anomalous subtropical subduction can modulate the year-to-year variability of the equatorial ocean. The authors of these references emphasise the advective origin of decadal to interdecadal oscillations.

(b) Ruhmstorf (1995) developed Stommel's (1961) idea concerning multi-regime of the oceanic circulation in the scope of the simplified (especially in its atmospheric part) coupled model. He argued that about 20 year oscillation can be a manifestation of the limit cycle during bifurcations of the meridional thermohaline circulation in the North Atlantic Ocean. He believed that even moderate changes in the freshwater input into the high latitudes can induce transitions between different equilibrium states. However, more complete coupled models (e.g., Delworth et al., 1996) show that transitions claim more intense freshwater input anomalies.

(c) The ENSO-induced coupled decadal mode in the Pacific Ocean was analysed by Jacobs et al. (1994). They showed that the planetary waves excited in the ocean by the ENSO-events play the crucial role in the decadal-scale variability of the coupled system (see also Zhang et al., 1997). At the same time Latif and Barnett (1994) argued the importance of the mid-latitude ocean-atmosphere coupling in generating the self-sustained decadal mode over the North Pacific and North Atlantic Ocean. They showed that the period of the oscillations is controlled by the subtropical gyre adjustment which is determined by the speed of the gravest Rossby waves at the coupling latitudes and by the basin geometry. Stochastic atmospheric variability causes the additional red shift in the oceanic spectra with a broad peak at decadal scales superimposed (see, for example, Munnich et al., 1997). Zhang et al. (1995) also emphasised the coupled origin of the decadal mode. They drew attention to the feedback between MHF, ice conditions and sea surface heat fluxes over the Northern Atlantic.

Thus, the most recent results show the crucial role of the meridional oceanic circulation (or MHF) and oceanic planetary waves in generating the decadal mode. The role of coupling and tropical-extratropical connection is not so clear. That is why I would like to summarise below some published results demonstrating the coupled character of the decadal mode and the importance of tropical-extratropical interaction.

1. The mutual compensation of northward Ekman transport and southward flow of the North Atlantic Deep Water (NADW) is a principal mechanism of the quasi-steady overturning over the North equatorial Atlantic (Polonsky, 1985; Kraus and Levitus, 1986; Levitus, 1987). Recently (Dzhiganshin and Polonsky, 1996), we revised published results and confirmed the crucial role of the quasi-steady overturning over the North-western equatorial Atlantic due to northward Ekman/southward NADW in the meridional heat transport. In the subtropical and mid-latitudes, the MHF within the western boundary layer is a crucial share of total oceanic MHF (Bryan, 1982).

Intense decadal-scale variability of the meridional Ekman transport occurs in the North Atlantic Ocean and the temporal range 2–35 years accounts for 40 to 50% of its r.m.s. variability. A typical magnitude of the decadal changes of the meridional Ekman transport in the North tropical and subtropical Atlantic is about 1 Sv. These changes correlate strongly with the low-frequency changes of the Sverdrup transport (especially in the subtropics and mid-latitudes), North Atlantic Oscillation (NAO) index and SST over the North Atlantic Ocean (Polonsky and Voskresenakaya, 1996).

The mutual compensation of the northward Ekman/Gulf Stream transport and southward deep transport in the North Atlantic is expected on a decadal time scale because a typical temporal scale of the baroclinic adjustment of the North Atlantic Ocean due to thermohaline forcing in the Northern latitudes does not exceed one decade (Doscher et al., 1994).

2. Interannual to multidecadal variability of the sea level pressure (SLP) over the Northern Hemisphere is at a maximum in the vicinity of Greenland and in the polar region. In other words, SLP varies strongly over the regions of the NADW origin. The SLP r.m.s. due to these changes exceeds 20 to 25 mb there. The SLP variance tends to be larger also in the vicinity of Iceland Low and Azores High. Decadal variability takes up to 30% of total year-to-year variance over the North Atlantic Ocean in the range of temporal scales from 2 to about 60 years. Low-frequency variability of the oceanic temperature within the upper 1000 m layer is at a maximum in the vicinity of the strong boundary currents and in the region of the NADW sinking (Polonsky and Kazakov, 1995).

3. Decadal meridional Ekman transport and, hence, decadal zonal circulation in the atmosphere boundary layer intensify concurrently over the whole North Atlantic. At that time, the sea surface becomes warmer (cooler) by about 1 to 2°C in the subtropical/mid-latitude (subarctic/equatorial) regions. Advection within the upper mixed layer is a principal cause of these changes in the subtropics/mid-latitudes, while convection is a crucial factor in the subarctic region. Intensified equatorial upwelling causes the sea surface cooling in the vicinity of the equator. During these periods the Azores High becomes deeper and shifts to the north (Voskresenskaya and Polonsky, 1993; Polonsky et al., 1998). In other words there is a positive feedback between SST and SLP anomalies (SSTA and SLPA) (see also Trenberth and Hurrell, 1994). It should be noted that strong positive decadal-scale correlation between subtropical/mid-latitude SSTA and SLPA occurred only during long-term intensification of the zonal atmospheric circulation resulting in deepening of Azores High and Iceland Low. In other words there is an interaction between decadal-scale and multidecadal modes.

So, the above results show the principal importance of coupling and tropical-extratropical interaction in the decadal changes in the North Atlantic Ocean.

A plausible generating mechanism of decadal mode is as follows.

At the first (intense) stage of the decadal oscillation, the positive feedback between SSTA and SLPA in the subtropical/mid latitudes supports this intensification resulting in strong subtropical subduction. Then, the negative SSTA generated over the equatorial Atlantic by intensified trade wind spread over the subtropics and mid-latitudes, while the positive SSTA are advected from the subtropics/mid-latitudes to the high latitudes. This weakens the atmospheric circulation and, hence, reduces the MHF magnitude and subtropical Ekman pumping. As a result, new SSTA are generated over the North Atlantic. They are positive over the equatorial zone and negative over the mid/high latitudes. This again intensifies the atmospheric circulation. Thus, this is a self-sustained coupled oscillation with strong tropical-extratropical interaction.

If the coupling is neglected, decadal-scale oscillations also exist. However, in this case the fast decay of the oscillations occurs as shown by Polonsky et al. (1998) using a simplified box model.

The absence of a robust atmospheric decadal-scale signal associated with extratropical SST fluctuations in some coupled models (e.g., Zorita and Frankignoul, 1997) can be the result (at least, in part) of coarse resolution, poor parameterisation of the convective processes, model drift, etc. It is clear, on the other hand, that different mechanisms are responsible for the long-term variability of the coupled system. The stochastic component of the atmospheric forcing is one of them. It is therefore necessary to perform precise global observations (WOCE/TOGA-TAO-type) during at least a few decades and to develop coupled models with improved parameterisation of the small-scale (sub-grid) processes and using recent techniques (e.g., assimilation, ensemble averaging, etc.). Only in this case, can further progress in study and predictability of long-term climatic variability be expected.

Acknowledgements

I would like to thank Prof. S. Hastenrath for valuable discussion.

References

Bjerknes, J., 1964: Atlantic air-sea interaction. Adv. Geophys., 10, 1–82.

Bryan, K., 1982: Poleward heat transport by the oceans: Observations and models. Ann. Rev. Earth Planet Sci., 10, 15–38.

Chen, F., and M. Ghil, 1995: Interdecadal variability of the thermohaline circulation and high-latitude surface fluxes. J. Phys. Oceanogr., 25, 2547–2568.

CLIVAR Science Plan, 1995: WCRP-89, 200pp.

Delworth, T. S., S. Manabe, and R. J. Stouffer, 1996: Interdecadal variability of the thermohaline circulation in a coupled ocean-atmosphere model. J. Climate, 6, 1993–2011.

Deser, C., and M. L. Blackmon, 1993: Surface climate variations over the North Atlantic Ocean during winter 1900–1989. J. Climate, 6, 1743–1760.

Doscher, R., C. W. Böning, and P. Herrmann, 1994: Response of circulation and heat transport in the North Atlantic to change. J. Phys. Oceanogr., 24, 2306–2320.

Dzhiganshin, G., and A. B. Polonsky, 1996: Seasonal variability of the currents and transports in the N-W Equatorial Atlantic. Mar. Hydrophysical J., 6, 39–55 (in Russian, translated and published in the Netherlands as former Soviet Journal of

Physical Oceanography next year after original paper).
Kraus, E. B., and S. Levitus, 1986: Annual heat flux variations across the tropic circles. J. Phys. Oceanogr., 16, 1479–1486.
Kushnir, J., 1994: Interdecadal variations in the North Atlantic sea-surface temperature and associated atmospheric conditions. J. Climate, 7, 141–160.
Jacobs, G. A., H. E. Hurlburt, J. C. Kindle, E. J. Metzger, J. L. Mitchell, W. J. Teague, and A. J. Wallcraft, 1994: Decadal-scale trans-Pacific propagation and warming effects of an El Niño anomaly. Nature, 370, 360–363.
Latif, M., 1997: Dynamics of interdecadal variability in Coupled Ocean-Atmosphere Models. Int. WOCE Newsletter, 26, 17–20.
Latif, M., and T. Barnett, 1994: Causes of decadal climate variability over the North Pacific and North America. Science, 266, 634–637.
Levitus, S. 1987: Meridional Ekman heat fluxes for the world and individual oceanic basins. J. Phys. Oceanogr., 17, 1484–1492.
Munnich, M., M. Latif, and E. Maier-Reimer, 1997: Decadal scale oscillations in a simple coupled model. Annales Geophysicae, Suppl. II to v.15, P.II, p.475.
Philander, S. G. H. 1998: Tropical-extratropical oceanic exchanges. Talk at WOCE International Meeting (Halifax, 24–29 May 1998).
Polonsky, A., 1985: Circulation in the N-W Tropical Atlantic and meridional heat flux. Marine Hydrophysical J., 2, 58–62 (in Russian).
Polonsky, A., 1998: On an interdecadal variability of the ocean-atmosphere system. Meteorology and Hydrology, 5, (in Russian, translated and published in New York by Allerton Press).
Polonsky, A. B., and S. I. Kazakov, 1995: On a trend in the Coupled System over the North Atlantic and conveyor belt variability. Proceedings of Regional Workshop on Climate Variability and Climate Change Vulnerability and Adaptation (PRAHA, 11–16 September 1995), PRAHA, 54–58.
Polonsky, A., A. Kuzmin, and E.Ostrovsky, 1998: On a decadal variability in the Coupled Ocean-Atmosphere System. K. Fedorov Memorial Symposium, (St. Peterburg, Puskin, 18–22 May 1998), Abstracts, 137–138.
Polonsky, A., and E. Voskresenakaya, 1996: Low-frequency changes of the meridional drift transport in the North Atlantic. Meteorology and Hydrology, 7, 89–99 (in Russian).
Rumstorf, S. 1995: Bifurcations of the Atlantic thermohaline circulation in respons to changes in the hydrological cycle. Nature, 376, 145–149.
Stommel, H. 1961: Thermohaline convection with two stable regimes of flow. Tellus, 13, 224–230.
Trenberth, K. E., and J. W. Hurrell, 1994: Decadal atmosphere-ocean variations in the Pacific. Climate Dyn., 9, 303–319.
Voskresenskaya, E. N., and A. B. Polonsky, 1993: Trends and interannual variability of the parameters of coupled system in the North Atlantic. Meteorology and Hydrology, 11, 73–81 (in Russian).
Weaver, A., S. M. Aura, and P. G. Myers, 1994: Interdecadal variability in an idealized model of the North Atlantic. J. Geophys. Res., 99, 12423–12442.
Yin, F. L., and E. S. Sarachik, 1995: Interdecadal thermohaline oscillations in a sector ocean general circulation model: Advective and convective processes. J. Phys. Oceanogr., 25, 2465–2484.
Zhang, S., C.A. Lin, and R. Greatbatch, 1995: A decadal oscillation in the ocean model coupled to a thermodynamic sea ice mode. J. Marine Res., 53, 79–92.
Zhang, Y., J. M. Wallace, and D. S. Battisti, 1997: ENSO-like interdecadal variability: 1990–93. J. Climate, 10, 1004–1020.
Zorita, E., and N. Frankignoul, 1997: Modes of North Atlantic decadal variability in the ECHAM1/LSG Coupled Ocean-Atmosphere General Circulation Model. J. Climate, 10, 183–200.

WHP Repeated Hydrography Section SR1, Drake Passage

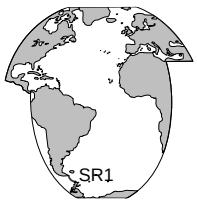

Ricardo Rojas, Yenny Guerrero, Teresa Calvete and Wanda Garcia, Servicio Hidrografico y Oceanografico de la Armada (SHOA), Chile. rrojas@shoa.cl

The Southern Ocean Circulation is dominated by a continuous eastward flow known as the Antarctic Circumpolar Current (ACC), which is essentially wind-driven. Waters with diverse properties are entrained into the ACC along its path and are subsequently blended into a more uniform flow. The study of the ACC at Drake Passage has brought numerous efforts from the scientific community for at least the last 50 years, but the most concentrated efforts came during the mid-1970s to the early 1980s, when various field experiments were conducted at Drake Passage during the International Southern Ocean Studies (ISOS) programme.

More recently and according to the WOCE Implementation Programme, the major justification for having a Southern Ocean project within the WOCE Goals is to improve the description of its role "both as a pipeline for mass transfer between the other oceans and, on the zonal average, as a region where heat supply at low latitudes is lost to the atmosphere". From the various goals of WOCE for the Southern Ocean, the Chilean Navy has given attention to the following:

(1) To monitor the thermohaline structure and variability of the ACC and associated fronts at Drake Passage. This area is also known as the Southern Ocean choke point.

(2) To monitor the low frequency variability of water masses and baroclinic structure.

WOCE cruise SR1 was planned and designed to accomplish those objectives by taking advantage of the crossings of the Drake Passage by the Chilean supplies vessels to Antarctic Bases at least once a year. Since 1993, four cruises have been performed in the area aboard AGOR 60 Vidal Gormaz of the Chilean Navy. Two of them have been carried out during the austral spring season (November) 1993 and 1994, and the other two during the summer season (December) 1995 and 1996. CTD data collected in these cruises were measured with a Sea-Bird SEACAT SBE-19 CTD and a Sea-Bird SEACAT SBE 25. Standard procedures for data reduction have been applied by the Chilean National Data Center (CENDOC) located at SHOA. In the following paragraphs we summarise some results for the last three cruises.

The tracks for the SR1 section for 1994 to 1996 are presented in Fig. 1. It basically corresponds to a line of hydrographic stations spanning Cape Horn and Shetland Islands. The vertical sampling reached at least 3000 metres for these three cruises.

Figs. 2a and b show the potential temperature and salinity sections for the 1996 cruise. The potential tem-

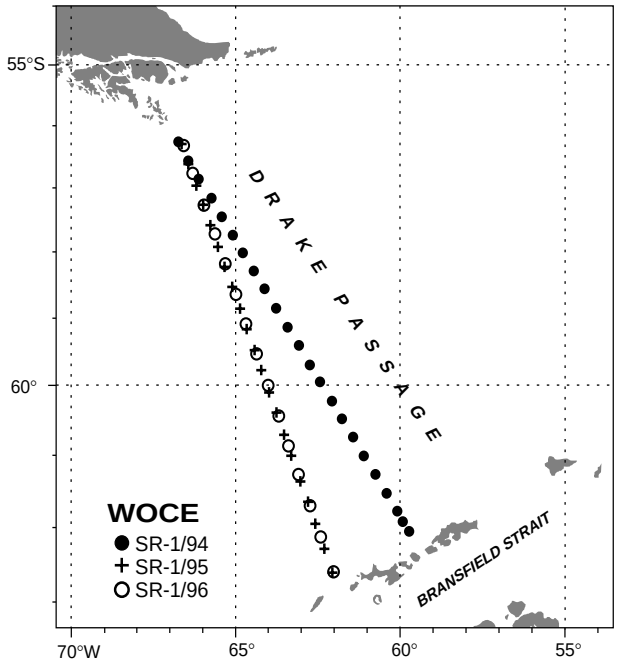

Figure 1. Position of stations during WOCE SR1 - 1994, 1995 and 1996 cruises onboard Chilean RV AGOR 60 Vidal Gormaz.

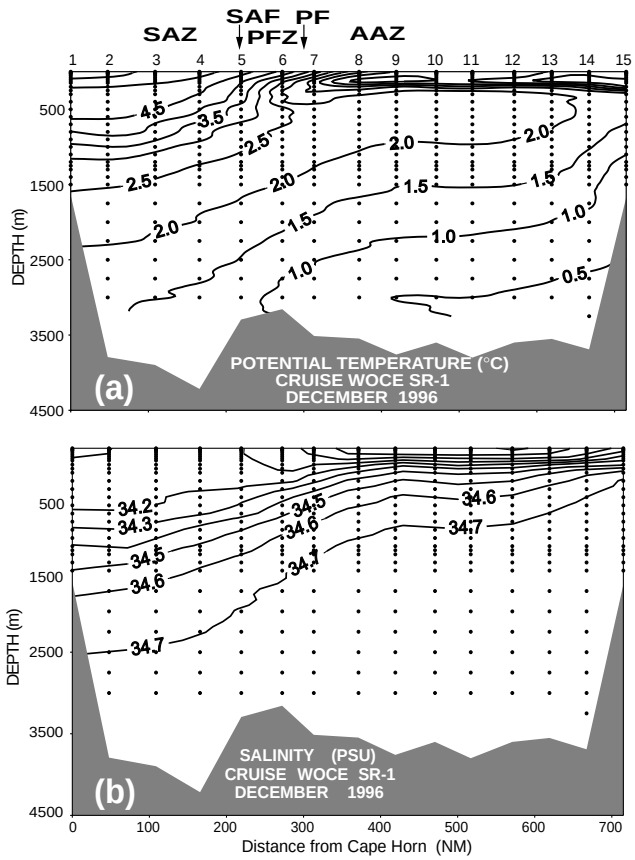

Figure 2. Potential temperature (a) and salinity (b) of WOCE SR1 section in 1996. The Subantarctic Front (SAF) and the Polar Front (PF) separate the Subantarctic Zone (SAZ), the Polar Frontal Zone (PFZ) and the Antarctic Zone (AAZ).

perature plots for 1993 and 1995 show a remarkable similarity to the one shown in Fig. 2a. This pattern of sharp temperature gradients, as the result of the rising of the Circumpolar Deep Water (CDW) in steps towards the south, is related to the zonation of the water masses in the area (Whitworth, 1980; Peterson and Whitworth, 1989). The four zones are from north to south: the Subantarctic Zone (SAZ), the Polar Frontal Zone (PFZ), the Antarctic Zone (AAZ) and the Continental Zone (CZ). These zones are separated by the Subantarctic Front (SAF), the Polar Front (PF) and the Continental Water Boundary (CWB) respectively. The latter front has been referred also as the ACC Southern Front (Sprintall et al., 1997). In Figs. 2a and b, both the zones and the fronts present in 1996 are shown. It is interesting to mention that in February of 1995 and 1996 two cruises were occupied by the BIO Hesperides at the nominated SR1b track (across the Scotia Sea, eastward of the ones made by the Chilean Navy). Garcia et al (1997) present the results and find almost the same features as we found.

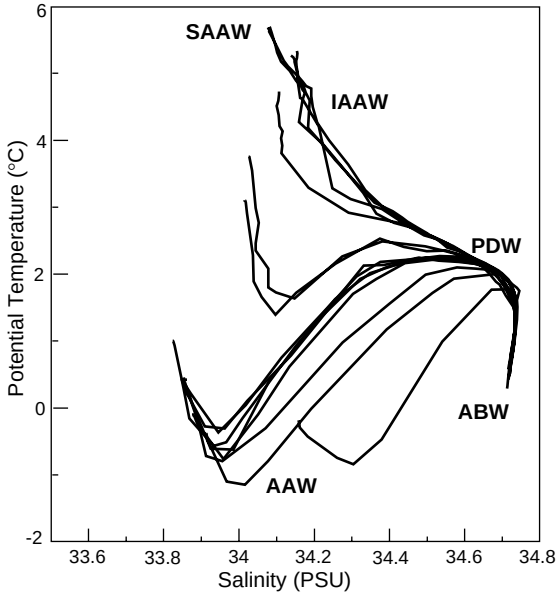

Figure 3. T-S diagram for all CTD casts in SR1 1996. SAAW (Subantarctic Water), AAW (Antarctic Water), IAAW (Intermediate Antarctic Water), PDW (Pacific Deep Water) and ABW (Antarctic Bottom Water).

With regard to water masses present at Drake Passage, Fig. 3 shows the T-S curves for the WOCE-SR1 cruise in 1996. Five water masses can be identified; the SubAntarctic Water (SAAW), Intermediate Antarctic Water (IAAW), Antarctic Water (AAW), Pacific Deep Water (PDW) and the Antarctic Bottom Water (ABW).

In regard to geostrophic velocities, Fig. 4 (page 24) shows a composite of the geostrophic velocities for the three years. In this figure, as a way to show the interannual variability of the fronts, which are recognised as jet streams, the location of the SAF and the PF are shown, such that it is possible to realise the meridional meandering of the fronts during these years. This feature is characteristic of

the dynamic variability of the ACC at Drake Passage. Sprintall et al. (1997) have shown that the fronts have seasonal changes in position. For the 1994, 1995 and 1996 cruises, transport calculations were done using the geostrophic velocities calculated with a reference level of 3000 metres. The volume transport for these 3 cruises is 106, 113 and 106 Sverdrups respectively. As a whole, the transport values look quite similar to other previous calculations (Whitworth, 1980; Peterson and Whitworth, 1989).

The shifting or meandering of the SAF and PF is a characteristic of the temporal variability at Drake Passage, some of them become cyclonic eddies and are identified in the vertical section of temperature and geostrophic velocities. These features are well known to be a mechanism of exchange for sea water properties in the Southern Ocean. Future works carried out by the Chilean Navy will include ADCP measurements to achieve a better understanding of the dynamics of the ACC at Drake Passage.

Acknowledgements

We would like to thank all the participants involved in PR14 and SR1 cruises, officers and crew from AGOR Vidal Gormaz and also the scientific (principal investigators) and technical personnel of the Department of Oceanography of SHOA who carried out the measurements at sea.

References

Garcia, M., O. Lopez, J. Puig de Fabregas, and J. Sospedra, 1997: Repeated observations of the ACC on WOCE SR1b. Int. WOCE Newsletter, 29, 16–18.

Peterson, R. G., and Whitworth III, T.,1989: The Subantarctic and Polar fronts in relation to deep water masses through the Southwestern Atlantic. J. Geophys. Res., 94, 10817–10838.

Sprintall, J., R. Peterson, D. Roemmich, and J. Gallo, 1997: High resolution XBT/XCTD measurements across Drake Passage. Int. WOCE Newsletter, 29, 18–19.

Whitworth, III, T., 1980: Zonation and geostrophic flow of the Antarctic Circumpolar Current at Drake Passage. Deep-Sea Res., 27, 497–507.

Circulation Offshore Southern Chile, PR14 Repeated Hydrography Section

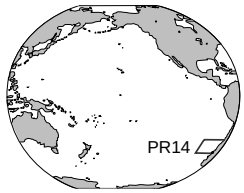

Rodrigo Nuñez and Ricardo Rojas, Servicio Hidrografico y Oceanografico de la Armada (SHOA), Chile. rrojas@shoa.cl

WOCE line PR14 (a repeated hydrographic line) has been planned and designed to study an enclosed area of the south-east Pacific Ocean where the ACC (Antarctic Circumpolar Current) divides upon impinging on the coast of South America and forms the Humbolt Current (HC), flowing northward, and the Cape Horn Current (CHC) flowing to the south.

Since 1993, five cruises have been performed in this area on board AGOR 60 Vidal Gormaz. Two of them have been carried out during the austral fall season 1995 (16 May–23 June) and 1997 (8–25 March), one during the winter season 1996 (14–27 August) and two during the spring season: 1993 (7–16 October) and 1994 (4–25 October). CTD data were collected with a Sea-Bird SBE-09 CTD, a Sea-Bird SEACAT SBE-19 CTD and a Sea-Bird SEACAT SBE 25. Standard procedures for data reduction have been made.

The general track for the PR14 section (Fig. 1) has been composed of 4 east–west oriented legs (the northern-most at 38°S and the southernmost at 48°S), and 1 north–south leg about 82°W. The geographic locations of the hydrographic stations are indicated with symbols on each one of the legs.

T-S characteristics, geostrophic velocity and transport

Rojas et al. (1995) reported preliminary results of T-S characteristics and geostrophic velocities for the 1994 period. In general vertical sections of temperature and salinity show a consistent pattern year after year with changes depending on the season. Figs. 2 and 3 show the potential temperature and salinity sections for leg 1 and leg 4 (latitudes 38° and 48°S) for PR14-1997. Warmer temperatures close to the surface and a coastal upwelling characterises the northern section (leg 1) compared to

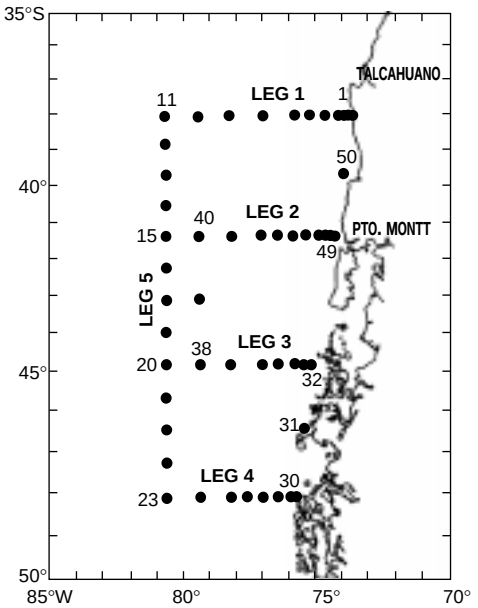

Figure 1. WOCE PR14 cruise tracks for 1994–1997. Symbols drawn on legs indicate the grographic location of each hydrographic station.

southern section (leg 4) where lower temperatures are dominant. In terms of salinity distribution in leg 1 the saltier core, characteristic of the Peru–Chile Undercurrent or Gunther Current (GC), is found attached to the coast at depths of 300 m, while on leg 4 this core is no longer found.

For the 1993, 1994 and 1995 cruises, transport calculations were performed using the geostrophic velocities calculated with a reference level of 1000 m. A least square fitting formulation with side boundary constrains was made in order to adjust the net flow inside the rectangles defined by leg 1, leg 4 and leg 5 equal to zero. The transport along the southern boundary of the rectangles, i.e. the line that joins the southernmost stations of each latitudinal leg, was set to zero. Fig. 4 shows a schematic diagram of the rectangles used in the calculations. Table 1 shows the results.

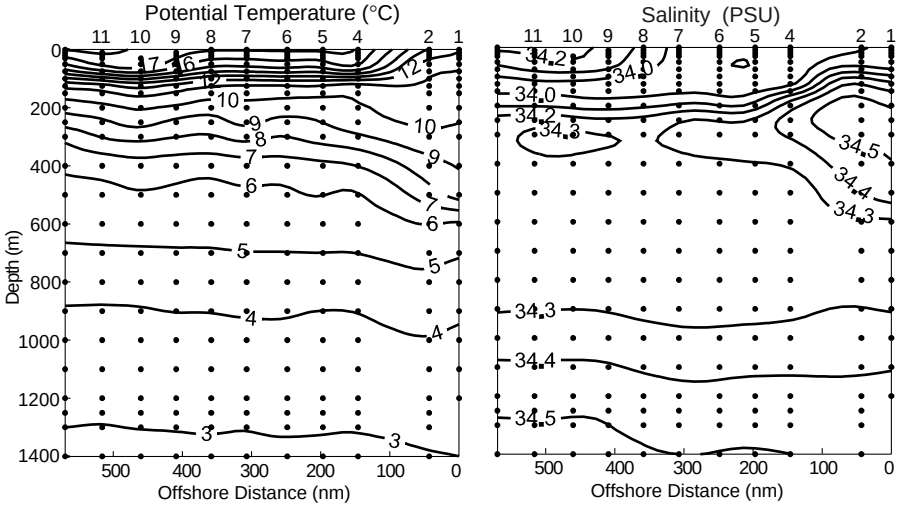

Figure 2. Cross-shelf section of potential temperature and salinity at leg 1 (38°S) during WOCE cruise PR14 in 1997.

Some of the most important characteristics of the transport are:

(1) The net transport along longitude 80°40'W remains almost constant from year to year. The change in transport between spring (1993 and 1994 cruises) and fall (1995 cruise) is less than 10% of the 1994 transport.

(2) Surface transport, in the first 150 m of the water column above the seasonal thermocline, accounts for an average 17% of the total net transport across the north-south leg of the cruises.

(3) In the three cruises the largest part of the eastward transport comes into the region between latitudes 41°30'S and 44°20'S (leg 2 and leg 3, respectively).

(4) The north-south transports have the same directions across each leg during each of the three year periods of the observation.

(5) The results of the transport for the 1993 and 1994 cruises are almost identical. Both cruises were made during the months of October and show remarkably similar characteristics. Eastward transport is found between leg 3 and leg 1 and westward transport is found between leg 3 and leg 4.

(6) In 1995 the transport (still centred between leg 2 and leg 3) moved southward and was found between leg 2 and leg 4. Westward transport is now found in the northern part of the region, between leg 1 and leg 2.

Circulation at the WOCE PR14 sampling area using a numerical model

The model used is the Naval Research Laboratory global ocean model, best known as the NRL model (Wallcraft, 1991). The subregion used for this research corresponds to the South East Pacific Ocean and goes from latitude 5°S to 55°S and from the west coast of South America to longitude 110°W. The atmospheric forcing is introduced into the model through realistic wind stress. The model is spun-up from rest to statistical equilibrium using the Hellerman and Rosenstein (1983) monthly mean wind stress climatology. To drive the model on interannual time scales, 1000 mbar winds from the European Centre for Medium-Range Weather Forecasts (ECMWF) are used. Two versions of the model were used:

(i) a reduced-gravity version with five active upper layers and an infinitely deep at-rest lower layer,

(ii) a six-layer finite-depth version with realistic topography confined to the lowest layer.

A detailed explanation of the application of the model in the PR14 area can be found in a technical report by Nuñez (1996). To study the spatial and temporal variability of the upper circulation in the WOCE PR14 region, monthly average of

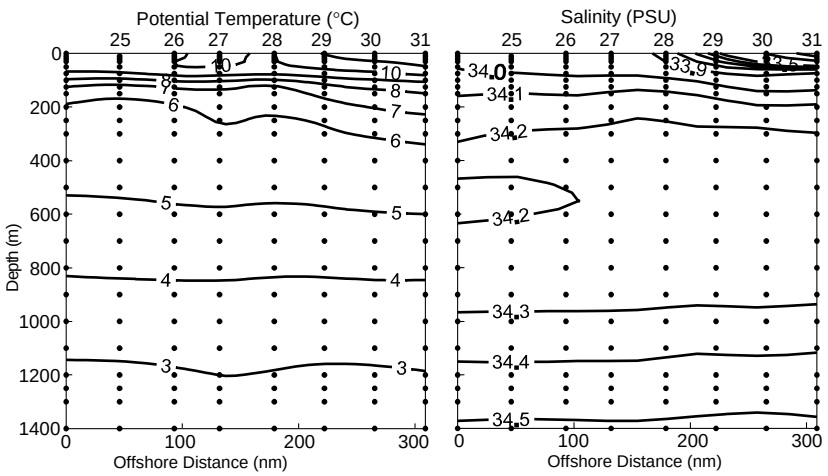

Figure 3. Same as Figure 2 for leg 4 (48°S).

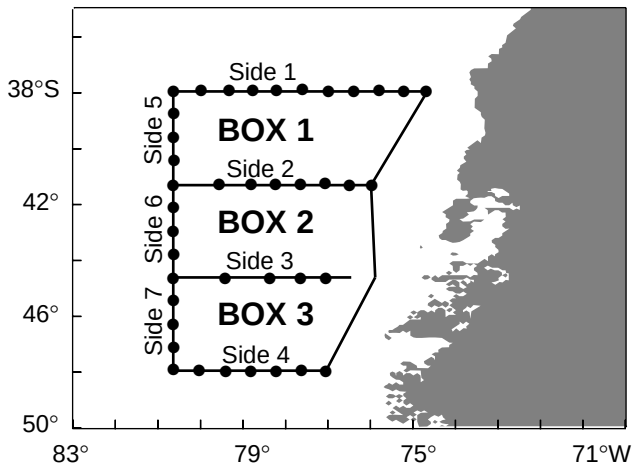

Figure 4. Schematic diagram of the boxes used to calculate the net transport derived from geostrophic velocity fields.

flow fields and layer interface depths were calculated. Figs. 5a–5d (page 23) correspond to the average of three-month periods over eleven years (1984–1994). The results are presented for the months of January–February–March (Fig. 5a), April–May–June (Fig. 5b), July–August–September (Fig. 5c) and October–November–December (Fig. 5d). An important common feature of these plots is that the largest gradient in the interface layer depth is located at 42°S, approximately following the 3600 m isobath. The ACC enters the WOCE PR14 sampling region parallel to these contours and follows the curvature of them until it exits toward the north as the HC. The location of the northward turning point of the ACC shifts seasonally from 75°45'W in October–November–December (OND), to 76°30'W in January-February-March (JFM), to 77°W in April-May-June (AMJ) and to 78°W in July-August-September (JAS). The exiting latitude of the HC from the WOCE PR14 sampling region varies accordingly with the location of the turning point. In JFM, AMJ and JAS the shape of the curvature of the northward HC follows, more or less, the bottom bathymetry. In OND, when the winds are weaker and the northward coastal current is stronger, the shape of the curvature is modified by coastal upwelling (shallower interface depth along the coast) and strong coastal currents. OND and JFM have upwelling along the coast and a well defined northward coastal current. In JAS the coast has upwelling north of latitude 44°S and downwelling south of this latitude. The downwelling in layer 1 is compensated by upwelling of the interface depth between layers 2 and 3, resulting in a northward current in the upper layer. AMJ has a southward current alongshore, south of latitude 40°S, that is related to coastal downwelling.

The NRL finite-depth model has proven to be a valuable tool in the study of temporal and spatial variability of the eastern boundary current system of the south east Pacific Ocean. The knowledge that bottom topography has a considerable steering effect on the currents of this region is important for understanding some main features of the flow described in this chapter. The NRL model does not reproduce the near-shore transport, nor the GC. The lack of accuracy along the coast is assumed to be a result of not having open-boundary sections that could simulate the flow of fresher and colder water from the Chilean Inland Seas into the Pacific Ocean. These fluxes are not known, but they are being measured as part of the Chilean Inland Seas Experiment.

The Cape Horn Current is formed at a higher latitude by the portion of the ACC that does not cross over the Chile Rise and impinges on the coast turning south into the Drake Passage. The model does not show this.

The fact that the ACC enters the WOCE PR14 sampling region around latitude 42°S year round, following the east-west 3600 m isobath, is a very important result. The meridional extension of the ACC across 80°40'W is controlled by local winds generated by the interaction of the South Pacific High (SPH) pressure and the Amundsen Sea Low pressure. The winds change the magnitude and direction of the east-west transport in boxes 1 and 3 (Fig. 4) – lateral transports associated with the ACC transport – creating the impression that the ACC has moved southward or northward, while in reality the main flow has always been centred at 42°–43°S. Another conclusion is the fact that the turning point of the ACC is related to the circulation and density structure induced by winds in the northern part of the WOCE PR14 sampling region (north of 42°S). Several authors had documented the change in position of the centre of the SPH from summer to winter (Strub et al., 1996; Schwerdtfeger, 1976). In winter (June–July–August) the SPH moves about 5° northwest of the summer position, diminishing the effect of the anticyclonic winds on the northern portion of the WOCE PR14 sampling region. The variability in the intensity of the winds in the northern part of the region changes the depth of the mixed layer and therefore, the vertical density structure. Figs. 5b through 5d show the temporal variability of the vertical structure in the northern part of the WOCE PR14 sampling region. Fig. 5c is the result of the SPH at its northern most position; as it

Table 1. Vertically Integrated-Adjusted Transport obtained from the least square fit analysis. Transport is given in Sverdrups (Sv). Arrows after transport values indicate direction of the flow. ↑ = northward, ↓ = southward, → = eastward, and ← = westward. Bold figures are used to indicate a reversal in the flow direction.

WOCE PR14			1993 (Sv)	1994 (Sv)	1995 (Sv)
Box 1		Side I	2.90↑	2.95↑	2.58↑
Box 1		Side V	**0.79**→	**0.54**→	**0.30**←
Box 1	Box 2	Side II	N/A	2.41↑	2.88↑
Box 2		Side VI	3.04→	3.44→	3.29→
Box 2	Box 3	Side III	N/A	1.03↓	0.41↓
Box 3		Side VII	**0.25**←	**0.29**←	**0.35**→
Box 3		Side IV	0.68↓	0.74↓	0.76↓
Net transport across 80°40'W		Side V +VI+VII	3.58→	3.65→	3.34→

moves south-eastward to its summer location the upper layer thickness increases (Fig. 5d) and the deepening effect moves southward; when the SPH reaches its southernmost location the layer thickness is maximum and the deepening effect stops moving southward (Fig. 5b); finally, when the SPH starts retreating north-westward the layer thickness starts decreasing.

Acknowledgements

We would like to thank all the participants involved in PR14 cruises, officers and crew from AGOR Vidal Gormaz and also the scientific (principal investigators) and technical personnel of the Department of Oceanography of SHOA who carried out the measurements at sea. The Chilean Oceanographic Data Center (CENDOC) also contributed with the quality control procedures for data reduction. Part of this investigation was done while the first author was obtaining his PhD at COAPS-FSU. Special thanks to Joseph Metzger from the Naval Research Laboratory, Stennis Space Center, for his support with the results of the NRL model and to Dr James J. O'Brien for his guidance and support while at FSU.

References

Hellerman, S. and M. Rosenstein, 1983: Normal monthly wind stress over the world ocean with error estimates. J. Phys. Oceanogr., 13, 1093–1104.

Nuñez, R., 1996: A study of the ocean circulation off the coast of Chile. Technical Report 96-4. COAPS, Florida State University, 95pp.

Rojas, R., N. Silva, W. Garcia, and Y. Guerrero, 1995: WHP repeated hydrography section PR14, offshore southern Chile. Int. WOCE Newsletter, 20, 31–33.

Schwerdentfeger, W., 1976: Climate of Central and South America. Elsevier Scientific Publishing Co., New York, 532pp.

Strub, T. P., J. Mesías, V. Montecino, J. Rutllant and S. Salinas, 1996. Coastal ocean circulation off western South America. Accepted for publication in The Sea, 10, 34pp.

Wallcraft, A. J., 1991: The Navy Layered Ocean Model User's Guide. NOARL report 35, 21pp. Naval Oceanographic and Atmospheric Research Laboratory, Stennis Space Center, MS, USA.

Global Directory of Marine (and Freshwater) Professionals (GLODIR)

The Global Directory of Marine (and Freshwater) Professionals is a database, developed and maintained by the Intergovernmental Oceanographic Commission of UNESCO (IOC), containing information on individuals involved in all aspects of Marine or Freshwater Research and Management. It is intended to be a tool for scientists, policy makers and anyone who needs to contact a marine or freshwater professional. A Professional is defined as anyone who, through his/her job, has expertise related to the research and management of the aquatic environment. The GLODIR is a product developed under the auspices of the IODE's Group of Experts on Marine Information Management (GE-MIM). GLODIR is a free product but can be used only for non-profit purposes.

How to access GLODIR?

http://ioc.unesco.org:591/glodir

How to enter your own data?

The IOC has made several agreements with national or regional organisations who take responsibility for the collection and management of information on individuals in their country or region. Details on these national and regional arrangements can be obtained from the IOC (see below). However, if you have access to the WWW then you can also submit your own data directly on-line through the URL **http://ioc.unesco.org:591/glodir**

After clicking on 'Create your own Record' in the main menu you will be presented with an on-line form. The first task will be to create your own UserID and Password. These will be needed when you want to edit your record later (they should be considered as your PIN numbers. Don't lose them!). After filling the first form you will also be asked to proceed to a second step where you will select ASFA Subject Descriptors which best describe your subject areas.

How to edit your record?

After clicking on 'Edit Your Record' you will be asked for your UserID and Password. After passing this checkpoint you will be presented with an on-line form containing your record information for editing.

Requirements

Javascript* capable web browser (e.g. Netscape Communicator 4.05, MS Internet Explorer 4.0). Try it with Netscape 3 but it may not always work.

* Netscape: to enable Javascript: go to Preferences, Advanced: select 'enable javascript' or go to Options - Network Preferences - select 'enable javascript'.

More Information

For more information or technical assistance contact: Peter Pissierssens, IOC - e-mail: p.pissierssens@unesco.org or Pauline Simpson, SOC - e-mail: ps@soc.soton.ac.uk.

Note on Copyright

WOCE is a component of the World Climate Research Programme (WCRP), which was established by WMO and ICSU, and is carried out in association with IOC and SCOR. The scientific planning and development of WOCE is under the guidance of the Scientific Steering Group for WOCE, assisted by the WOCE International Project Office.

The International WOCE Newsletter is edited by Roberta Boscolo (roberta.boscolo@soc.soton.ac.uk) at the WOCE IPO at Southampton Oceanography Centre, Empress Dock, Southampton, SO14 3ZH, UK, Tel: 44-1703-596789, Fax: 44-1703-596204, e-mail: woceipo@soc.soton.ac.uk,

http://www.soc.soton.ac.uk/OTHERS/woceipo/ipo.html

We hope that colleagues will see this Newsletter as a means of reporting work in progress related to the Goals of WOCE as described in the Scientific Plan.

The editor will be pleased to send copies of the Newsletter to institutes and research scientists with an interest in WOCE or related research.

Printed by Technart Ltd., Southern Road, Southampton SO15 1HG.